

**Polymerization Kinetics and Structure-Property Relationships of Ethylene/1-Hexene Copolymers**

by

Anuar Alfonso Caldera Palacios

A thesis submitted in partial fulfillment of the requirements for the degree of

Master of Science

in

Chemical Engineering

Department of Chemical and Materials Engineering

University of Alberta

© Anuar Alfonso Caldera Palacios, 2018

## Abstract

Polyethylene accounts for 32% of the world's plastics production and it is continuing to grow for the foreseeable future. Its versatility to modify its molecular structure using different types of catalyst or modifying the reaction conditions makes polyethylene suitable for a wide range of applications resulting in large advantages in plastic production for the last 50 years.

However, polyethylene still faces new challenges. Combining the knowledge of the catalyst package and the production process is required for new breakthroughs to occur for further development and optimization of polyethylene production and quality. In this research project, the polymerization kinetic of metallocene catalyst will be investigated and a model for structure-property relationship will be proposed to contribute with the knowledge of the catalyst package.

The solution polymerization kinetics of ethylene and 1-hexene with the metallocene catalyst Bis(cyclopentadienyl) hafnium(IV) dichloride was investigated in a semi-batch reactor. The polymerization kinetics were studied; modifying the following variables: Hydrogen/ethylene ratio, ethylene/1-hexene ratio, reaction temperature, and ethylene concentration. Later, reaction mechanisms and mathematical models were proposed using the experimental data to explain the uptake ethylene curves and polymer characterization results. The mathematical models developed will help to predict the polymer structure at different reaction conditions.

Additionally, a model to correlate polymer structure with its mechanical properties was proposed. The model includes the Molecular Weight Distribution (MWD) and the Short Chain Branching Distribution (SCBD) of the polymer obtained by Cross Fractionation Chromatography (CFC). The model will predict a Primary Structure Parameter (PSP) that correlates with several mechanical properties of the polymer. Thus, if the polymer structure is known, the mechanical

properties could be estimated or if a specific mechanical property is desired, the possible polymer structure needed can be estimated.

Finally, the kinetic model and the mechanical properties were integrated to predict the mechanical properties of the polymer from reaction conditions. Thus, it can be simulated how the mechanical properties are affected when a variable in the reaction condition changes (i.e. when several catalysts are mixed in the reactor). This integration would help to obtain a starting point in the development of new grades, cutting time and resources.

## **Acknowledgments**

I would like to acknowledge and express my gratitude to my supervisor Prof. João B.P. Soares for his consistent guidance, support and encouragement. He gave me the opportunity to learn more about my passion, Polymers!

Thanks to Chevron Phillips company and Dr. Paul DesLauriers for providing financial support.

I would like to thank my colleagues in the group of applied macromolecular engineering for their support and inspiration. Special thanks to Dr. Saeid Mehdiabadi for his coaching and support throughout my project.

My deepest and lovely gratitude to my wife, thanks to her sacrifice, support and encourage to become this dream possible.

My eternal gratitude to my mom, her courage to pursue my dreams and her love from distance keep me motivate through my studies.

Thanks to my sisters and my dad, their support and motivation were also key to get this Master Degree.

## Table of Contents

Chapter 1 : Introduction .....	1
Chapter 2 : Literature Review .....	3
2.1. Importance of Polyethylene .....	3
2.2. Polyethylene Types .....	4
2.3. Catalysts for Polyethylene Production .....	5
2.4. Polymerization Kinetics and Polyolefin Microstructure .....	12
2.5. Mechanical Properties and Polyolefin Microstructure .....	20
Chapter 3 : Ethylene/1-Hexene Polymerization with Bis(cyclopentadienyl) Hafnium(IV) Dichloride .....	24
3.1 . Introduction .....	24
3.2. Materials .....	24
3.3. Polymerization Procedure .....	26
3.4. Polymer Characterization .....	28
3.4.1. Molecular Weight Distribution .....	28
3.4.2. Comonomer Content .....	29
3.5. Polymerization Kinetics .....	31
3.5.1. Estimation of Ethylene, 1-Hexene and Hydrogen Concentrations in Toluene .....	31
3.5.3. Arrhenius Constant Estimation .....	40
3.5.4. Effect of Hydrogen on the Polymerization Rate of Ethylene .....	44
3.5.5. Ethylene/1-Hexene Copolymerization with $Cp_2HfCl_2$ .....	55
3.5 . Conclusions .....	64
Chapter 4 : Correlating the Microstructure of Linear High-Density Polyethylene with Mechanical Properties using Cross Fractionation Chromatography .....	65
4.1. Introduction .....	65
4.2. Experimental Part .....	67
4.3. PSP2 and PSP2* Calculations .....	67
4.3.1. Density .....	67
4.3.4. Probability of Tie Molecule Formation .....	70
4.4. PSP2 and PSP2* Calculation Methods .....	70
4.4.1. PSP2 Estimation .....	70
4.4.2. PSP2* Estimation .....	71
4.5. Results and Discussion .....	73

4.6. Conclusions .....	85
Chapter 5 : Integration of Polymerization Kinetics with Polymer Mechanical Properties	
Prediction .....	86
5.1. Introduction .....	86
5.2. Virtual Polymerization Reactor Conditions and Modeling Equations.....	86
5.4. Results and Discussion.....	90
5.4.1. Single Catalysts .....	90
5.4.2. Mix of $Cp_2HfCl_2$ , $Cp_2ZrCl_2$ and CGC-Ti catalysts .....	95
5.4.2.1 Ethylene concentration of 0.2 mol/L and 1-hexene concentration of 0.01 mol/L.....	96
5.4.2.3 Ethylene concentration of 0.6 mol/L and 1-hexene concentration of 0.2 mol/L.....	101
5.5. Conclusions .....	103
Chapter 6 : Conclusion and Recommendations .....	
6.1. Conclusions .....	107
6.2. Recommendations .....	108
References.....	113

## List of Figures

<b>Figure 2-1.</b> Plastics demand in the world in 2015.....	3
<b>Figure 2-2.</b> Types of polyethylene .....	4
<b>Figure 2-3.</b> Monochromate chromium catalyst – First generation.....	6
<b>Figure 2-4.</b> Cossee and Arlman mechanism: a) activation, and b) propagation .....	6
<b>Figure 2-5.</b> Typical metallocene catalyst structure .....	7
<b>Figure 2-6.</b> Metallocene catalyst structure for $[(CH_3)_2Si(2-CH_3Ind)_2]ZrCl_2$ .....	7
<b>Figure 2-7.</b> Structure of a constrained geometry catalyst. ....	8
<b>Figure 2-8.</b> A possible MAO structure.....	9
<b>Figure 2-9.</b> Reaction mechanism for metallocene catalysts: a) activation, and b) propagation ....	9
<b>Figure 2-10.</b> Molecular weight and comonomer content for an ethylene/1-olefin copolymer made with a metallocene catalyst. Comonomer content in polyolefins is often expressed as short chain branch frequency (SCB/1000 C). ....	10
<b>Figure 2-11.</b> Molecular weight and comonomer content distribution for a hypothetical bimodal polyolefin. ....	11
<b>Figure 2-12.</b> Late transition metal catalyst.....	11
<b>Figure 2-13.</b> Transfer to hydrogen .....	12
<b>Figure 2-14.</b> Flory distribution for polymer made with Catalyst 1, Catalyst 2, and their 50/50 wt% blend. ....	19
<b>Figure 2-15.</b> Stockmayer distribution for catalyst 1, catalyst 2 and mix. ....	20
<b>Figure 2-16.</b> Solidification model for a semi-crystalline polymer.....	21
<b>Figure 2-17.</b> a) Tie molecules b) Entanglement loose loops.....	22
<b>Figure 3-1.</b> Bis(cyclopentadienyl) hafnium(IV) dichloride. ....	24
<b>Figure 3-2.</b> Toluene purification/storage bottle. ....	25
<b>Figure 3-3.</b> P&D reactor diagram. ....	27
<b>Figure 3-4.</b> Catalyst productivity for the polymerization of ethylene with $Cp_2HfCl_2$ for varying ethylene concentrations.....	33
<b>Figure 3-5.</b> $Cp_2HfCl_2$ productivity as a function of the square of ethylene concentration .....	33
<b>Figure 3-6.</b> Normalized ethylene uptake curves polymerizations with $Cp_2HfCl_2$ . ....	36
<b>Figure 3-7.</b> Smoothed ethylene uptake curves for polymerizations with $Cp_2HfCl_2$ . ....	37

<b>Figure 3-8.</b> Validation experimental ethylene uptake curves versus model: a) Homo_60_1, b) Homo_100_2, c) Homo_120_2, and d) Homo_150_1. ....	38
<b>Figure 3-9:</b> a) experimental vs predicted productivities and b) model limitations for the first 150 s of polymerization. ....	39
<b>Figure 3-10.</b> a) Normalized and, b) moving average uptake ethylene curves polymerizations at 100 °C and 140 °C. ....	41
<b>Figure 3-11.</b> Experimental values versus model predictions for polymerizations with Cp <sub>2</sub> HfCl <sub>2</sub> at 100 °C and 140 °C: a) Homo_100_T100_1, b) Homo_100_T100_2, c) Homo_100_T140_1, and d) Homo_100_T140_2. ....	42
<b>Figure 3-12.</b> Arrhenius plot for: a) $k_p \cdot k_f$ and b) $k_d$ . ....	43
<b>Figure 3-13.</b> Number average molecular weights ( $M_n$ ) of polyethylene made at 100 °C, 120 °C and 140 °C with Cp <sub>2</sub> HfCl <sub>2</sub> . ....	44
<b>Figure 3-14.</b> Relations between $M_n$ and ethylene concentration: a) Non adjusted intercept, and b) intercept set to zero. ....	48
<b>Figure 3-15.</b> Correlation of $(mw/M_n) \cdot M$ versus hydrogen concentration. ....	48
<b>Figure 3-16.</b> Number average molecular weight estimated versus experimental. ....	49
<b>Figure 3-17.</b> a) Normalized and b) moving average uptake ethylene curves polymerizations varying hydrogen concentration. ....	53
<b>Figure 3-18.</b> Ethylene polymerizations with hydrogen versus model .....	54
<b>Figure 3-19.</b> Experimental values versus model predictions for polymerizations with Cp <sub>2</sub> HfCl <sub>2</sub> without hydrogen: a) Homo_60_1, b) Homo_100_2, c) Homo_120_2, and d) Homo_150_1. ..	54
<b>Figure 3-20.</b> Experimental average ethylene content in copolymers vs the Mayo-Lewis equation for Cp <sub>2</sub> HfCl <sub>2</sub> . ....	57
<b>Figure 3-21.</b> Normalize ethylene uptake curve for ethylene/1-hexene copolymerization. ....	61
<b>Figure 3-22.</b> Moving average ethylene uptake curve for ethylene/1-hexene copolymerization..	61
<b>Figure 3-23.</b> Validating experimental ethylene uptake curves versus model predictions: a) Copo_60_1, b) Copo_100_2, and c) Copo_150_4. ....	62
<b>Figure 3-24.</b> Decay constant versus mole fraction of 1-hexene in toluene. ....	63
<b>Figure 4-1.</b> PENT (a) and SP-NCTL (b) versus PSP2. ....	66
<b>Figure 4-2.</b> Correlation of between melting temperature and polyethylene density. ....	68
<b>Figure 4-3.</b> GPC-IR cut in slice by slice basis. ....	71

<b>Figure 4-4.</b> Cross fractional results for an ethylene/1-hexene sample.....	72
<b>Figure 4-5.</b> Continuous raw IR signal (a) and separated chromatograms (b) to process the cross-fractionation raw signals.....	72
<b>Figure 4-6.</b> Polyethylene characterization by GPC-IR and CFC.....	75
<b>Figure 4-7.</b> Primary structural parameters, PSP2 and PSP2*, versus mechanical properties of polyethylenes.....	77
<b>Figure 4-8.</b> SCBD over molecular weight of sample A.....	78
<b>Figure 4-9.</b> Virtual binary polymer blends designed to compare PSP2 and PSP2*: a) Blend 1, b) Blend 2, c) Blend 3, and d) Blend 4.....	78
<b>Figure 4-10.</b> Comparison of PSP2 and PSP2*.....	80
<b>Figure 4-11.</b> Behavior of PSP2*- PSP2 varying ethylene content and chain average length.....	81
<b>Figure 4-12.</b> Comparison of blends with same PSP2* of Blend 3.....	83
<b>Figure 4-13.</b> Molecular weight distribution and short chain branching distributions of blends 3.A (a) and 3.E (b).....	84
<b>Figure 4-14.</b> Distribution of number of blends for PSP2* intervals of 0.1 units.....	84
<b>Figure 5-1.</b> Comparison between the experimental and estimated $M_n$ for a) $Cp_2ZrCl_2$ and b) CGC-Ti.....	89
<b>Figure 5-2.</b> Logic flowchart for integration model.....	90
<b>Figure 5-3.</b> Molecular weight and comonomer content distribution for ethylene/1-hexene copolymers made with $Cp_2HfCl_2$ (a), $Cp_2ZrCl_2$ (b) and CGC-Ti (c).....	91
<b>Figure 5-4.</b> $M_n$ versus ethylene and 1-hexene concentrations for ethylene/1-hexene copolymers made with $Cp_2HfCl_2$ (a), $Cp_2ZrCl_2$ (b) and CGC-Ti (c).....	92
<b>Figure 5-5.</b> $F_{Ethylene}$ versus ethylene and 1-hexene concentrations for ethylene/1-hexene copolymer made with $Cp_2HfCl_2$ (a), $Cp_2ZrCl_2$ (b) and CGC-Ti (c).....	92
<b>Figure 5-6.</b> PSP2* versus ethylene and 1-hexene concentrations for ethylene/1-hexene copolymer made with $Cp_2HfCl_2$ (a), $Cp_2ZrCl_2$ (b) and CGC-Ti (c).....	94
<b>Figure 5-7.</b> Fraction of polymer made with $Cp_2HfCl_2$ (a), $Cp_2ZrCl_2$ (b) and CGC-Ti (c).....	96
<b>Figure 5-8.</b> $M_n$ (a) and $F_{Ethylene}$ (b) for mixing catalyst at ethylene concentration of 0.2 mol/L and 1-hexene concentration of 0.01 mol/L.....	97
<b>Figure 5-9.</b> PDI at ethylene concentration of 0.2 mol/L and 1-hexene concentration of 0.01 mol/L.....	98

<b>Figure 5-10.</b> PSP2* at ethylene concentration 0.2 mol/L and 1-hexene concentration 0.01 mol/L. .....	98
<b>Figure 5-11.</b> Fraction of polymer produce with Cp <sub>2</sub> HfCl <sub>2</sub> (a), Cp <sub>2</sub> ZrCl <sub>2</sub> (b) and CGC-Ti (c). ...	99
<b>Figure 5-12.</b> $M_n$ (a) and $F_{Ethylene}$ (b) for mixing catalyst at ethylene concentration 0.6 mol/L and 1-hexene concentration 0.1 mol/L. ....	100
<b>Figure 5-13.</b> PSP2* at ethylene concentration 0.6 mol/L and 1-hexene concentration 0.1 mol/L. .....	101
<b>Figure 5-14.</b> Fraction of polymer produce with Cp <sub>2</sub> HfCl <sub>2</sub> (a), Cp <sub>2</sub> ZrCl <sub>2</sub> (b) and CGC-Ti (c) ..	101
<b>Figure 5-15.</b> $M_n$ in g/mol and $F_{Ethylene}$ for mixing catalyst at ethylene concentration 0.6 mol/L and 1-hexene concentration 0.2 mol/L.....	102
<b>Figure 5-16.</b> PSP2* at ethylene concentration of 0.6 mol/L and 1-hexene concentration 0.2 of mol/L.....	103
<b>Figure 6-1.</b> Ethylene uptake curves at different catalyst concentration. ....	109
<b>Figure 6-2.</b> Current installation for ethylene pressure control. ....	109
<b>Figure 6-3.</b> Flow data of regulator PCV-2 .....	110
<b>Figure 6-4.</b> Proposal for new ethylene pressure control. ....	111

## List of Tables

<b>Table 2-1.</b> Ethylene polymerization mechanism with a single-site catalyst. ....	12
<b>Table 2-2.</b> Terminal model for copolymerization .....	15
<b>Table 2-3.</b> Kinetic parameters and reaction conditions.....	18
<b>Table 2-4.</b> Polymer structure variables .....	18
<b>Table 3-1.</b> Comparison of method to estimate 1-hexene content in the copolymer.....	30
<b>Table 3-2.</b> Productivity for homopolymer reactions .....	32
<b>Table 3-3.</b> Proposed mechanism for the polymerization of ethylene with $\text{Cp}_2\text{HfCl}_2$ . ....	34
<b>Table 3-4.</b> Ethylene polymerization conditions. ....	36
<b>Table 3-5.</b> Ethylene polymerization kinetic parameters with $\text{Cp}_2\text{HfCl}_2$ . ....	38
<b>Table 3-6.</b> Ethylene polymerization conditions at 100 and 140 °C .....	40
<b>Table 3-7.</b> Ethylene kinetic parameters for polymerization with $\text{Cp}_2\text{HfCl}_2$ at 100 and 140 °C...	41
<b>Table 3-8.</b> Pre-exponential factors and activation energies for propagation and decay constants for the polymerization of ethylene with $\text{Cp}_2\text{ZrCl}_2$ .....	43
<b>Table 3-9.</b> Number and weight average molecular weight at 100 °C, 120 °C and 140 °C.....	44
<b>Table 3-10.</b> Number and weight average molecular weight for polymerization of ethylene reactions with/without hydrogen.....	45
<b>Table 3-11.</b> Proposed mechanism for the polymerization of ethylene including transfer reactions with $\text{Cp}_2\text{HfCl}_2$ . ....	46
<b>Table 3-12.</b> Ratio of transfer constants to propagation constant.....	49
<b>Table 3-13.</b> Proposed mechanism for the polymerization of ethylene with transfer and re- activation reactions with $\text{Cp}_2\text{HfCl}_2$ . ....	50
<b>Table 3-14.</b> Ethylene polymerization conditions varying hydrogen concentration. ....	52
<b>Table 3-15.</b> Kinetic Parameters of ethylene polymerizations with/without hydrogen.....	53
<b>Table 3-16.</b> Ethylene and 1-hexene concentrations for copolymerizations with $\text{Cp}_2\text{HfCl}_2$ and the average 1-Hexene content in the copolymer. ....	56
<b>Table 3-17.</b> Estimated mole fraction of ethylene concentration in toluene for copolymerizations and the average ethylene content in the copolymer. ....	56
<b>Table 3-18.</b> Estimated reactivity ratios for ethylene/1-hexene copolymerizations with $\text{Cp}_2\text{HfCl}_2$ .....	57
<b>Table 3-19.</b> Proposed ethylene/1-hexene copolymerization mechanism with $\text{Cp}_2\text{HfCl}_2$ .....	58

<b>Table 3-20.</b> Ethylene/1-hexene copolymerization conditions.....	60
<b>Table 3-21.</b> Ethylene/1-hexene copolymerization kinetic parameters with $Cp_2HfCl_2$ .....	62
<b>Table 3-22.</b> Ethylene/1-hexene copolymerization kinetic parameters with $Cp_2HfCl_2$ .....	63
<b>Table 4-1.</b> Densities and mechanical properties of polyethylene samples.....	73
<b>Table 4-2.</b> Primary structure parameters, PSP2 and PSP2*, of polyethylene samples .....	76
<b>Table 4-3.</b> Virtual polymer blends. ....	79
<b>Table 4-4.</b> Range of properties for polymer blend components.....	80
<b>Table 4-5.</b> Binary blends with same PSP2* of Blend 3. ....	83
<b>Table 5-1.</b> Polymerization kinetics parameters for $Cp_2ZrCl_2$ and CGC-Ti .....	87
<b>Table 5-2.</b> Simulation conditions for mixing catalysts. ....	95
<b>Table 5-3.</b> Polymer properties of $Cp_2HfCl_2$ at Ethylene concentration of 0.6 mol/L and 1-hexene concentration of 0.1 mol/L.....	104
<b>Table 5-4.</b> Polymer properties of mixed $Cp_2HfCl_2$ / CGC-Ti at Ethylene concentration of 0.6 mol/L and 1-hexene concentration of 0.1 mol/L. ....	105
<b>Table 5-5.</b> Ethylene content at various mixing catalyst ratio for a 1-hexene fraction of 0.25. ..	106

## **Nomenclature**

### **Acronyms**

CGC	Constrained geometry catalyst
CFC	Cross Fractionation Technique
DSC	Differential scanning calorimetry
GPC	Gel permeation chromatography
HDPE	High-density polyethylene
LCB	Long chain branch
LDPE	Low-density polyethylene
LLDPE	Linear low-density polyethylene
MAO	Methylaluminoxane
MWD	Molecular weight distribution
PDI	Polydispersity index
PSP	Primary structure parameter
SCB	Short chain branch
SCBD	Short chain branch distribution
TIBA	Triisobutylaluminum

## Symbols

$\emptyset_i$	Molar fraction of living polymer chain terminated in monomer i
$D_r$	Deactivated active site
$C_{io}$	Initial catalyst concentration
$D_r$	Dead polymer chain
$Et$	Ethylene Concentration
$f_i$	Molar fraction of monomer i in liquid phase
$F_i$	Molar fraction of monomer i in copolymer
$F$	Ethylene flow rate
$k_p$	Propagation rate constant
$k_a$	Activation rate constant
$k_d$	Deactivation rate constant
$k_f$	Coordination rate constant
$k_{iH}$	Initiation rate constant
$k_{tH}$	Rate constant of transfer to hydrogen
$k_{t\beta}$	$\beta$ -hydride elimination rate constant
$k_{tAl}$	Rate constant of chain transfer to cocatalyst
$L_a$	Amorphous lamellae layer
$L_c$	Crystal lamellae layer
$M_n$	Number average molecular weight
$M_w$	Weight average molecular weight
PSP	Primary structure parameter
$P_{TM}$	Probability of tie-chain formation
$\rho$	Polymer density
$R_p$	Polymerization rate
$r_i$	Reactivity ratio of monomer i
$r_n$	Number average chain length
$T_m$	Melting temperature
$T_{peak}$	Melting peak from DSC analysis

$V_R$	Reaction medium volume
$X_c$	Weight percentage crystallinity
$Y_0$	Living polymer chains

# Chapter 1 : Introduction

## 1.1 Motivation and Objectives

Polyethylene is one polymer that is used in a wide range of applications such as automotive parts, pipes, processing equipment, films, medical equipment, household containers, and many others. Features like low processing cost, low feedstock cost and recyclability allow the polyethylene market to continue to grow for the foreseeable future. It is expected that its market value will increase from approximately 163 billion USD in 2017 to 215 billion USD by 2024, an annual growth rate of 4% approximately [1].

One reason for the economical increase of polyethylene in the market has been its flexibility to modify its molecular structure in accordance to its application. However, despite being in the market for more than 50 years, polyethylene still faces new challenges such as the reduction of its environmental impact. An example of reduction of its environmental impact was led by the company Poland. Development of a new polyethylene grade was studied to reduce the thickness of plastic water bottles while keeping similar mechanical properties. As a result, the company was able to reduce the amount of polymer required per bottle by 40%. [2].

The development of new polyethylene grades requires combining the knowledge of the catalyst package and the production process. In this thesis, the studies conducted will contribute a better understanding of the catalyst package in two different areas: 1) Estimation of kinetic parameters for a metallocene catalyst, and 2) Developing a model to correlate polymer structure with its mechanical properties.

The metallocene catalyst studied in this thesis is Bis(cyclopentadienyl) hafnium(IV) dichloride. The reactions were done in semi-batch reactors and the polymerization kinetic constants were studied modifying the following variables: Hydrogen/ethylene ratio, ethylene/1-hexene ratio, reaction temperature and ethylene concentration. Later, reaction mechanisms and mathematical models were proposed using the experimental data to explain the uptake ethylene curves and polymer characterization results. The mathematical models developed will help predict the polymer structure at different reaction conditions.

Additionally, a model was developed by Paul DesLauriers [3] to correlate polymer structure with its mechanical properties. In this thesis, the model was extended by using advance characterization

techniques such as Cross Fractionation Chromatography (CFC). The purpose of using this advance characterization technique is to include the comonomer composition distribution in the model. The model will predict a Primary Structure Parameter (PSP) that correlates with several mechanical properties of the polymer. Thus, if the polymer structure is known, the mechanical properties could be estimated or if a specific mechanical property is desired, the possible polymer structure needed can be estimated.

Finally, the kinetic and mechanical properties models were integrated to predict the mechanical properties of the polymer from reaction conditions. Thus, it can be simulated how the mechanical properties are affected when a variable in the reaction condition changes or when several catalysts are mixed in the reactor. Additionally, it can help identify the combination of variables with similar mechanical properties. This integration would help to obtain a starting point in the development of new polyethylene grades and therefore cut time and resources.

## **1.2 Thesis Outline**

This thesis is divided into six main chapters:

**Chapter 1** provides a brief overview of the research project.

**Chapter 2** describes the importance of the polyethylene, catalyst types, polymerization kinetic and mechanisms, and basic concepts of how mechanical properties are affected by polymer molecular structure.

**Chapter 3** describes the polymerization procedures and characterization techniques followed by a discussion of experimental results and development of mathematical models for the polymerization with bis(cyclopentadienyl) hafnium(IV) dichloride, and estimation of its kinetic parameters.

**Chapter 4** explains the model proposed by Paul Deslauriers [3] and how it was extended to include the short chain branching distribution. Additionally, the original model and its extension were compared, and virtual binary blends were simulated exploring the benefit of using the extended model.

**Chapter 5** shows the integration of the two modelling approaches in chapter 3 and chapter 4, allowing the mechanical properties of the resulting polymer being predicted directly from reaction conditions.

**Chapter 6** summarizes the key results, and recommendations for future work.

## Chapter 2 : Literature Review

### 2.1. Importance of Polyethylene

Polyethylene is a semi-crystalline polymer with the highest demand in the world due to its versatility, low cost, and low density [4]. Figure 2-1 shows the world plastics demand in 2015: 32% of the plastics market is composed of high-density polyethylene (**HDPE**), low-density polyethylene (**LDPE**), and linear low-density polyethylene (**LLDPE**).

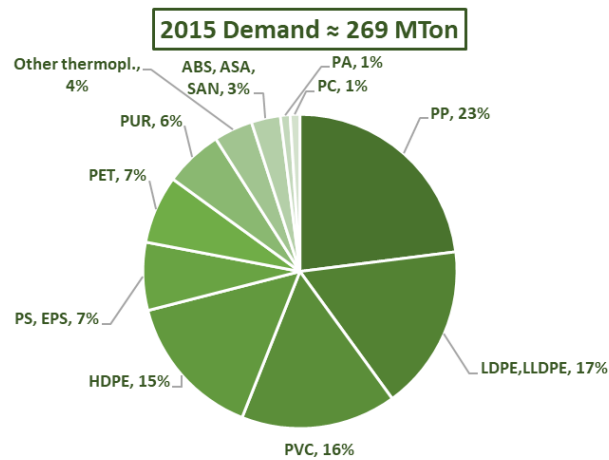


**Figure 2-1.** Plastics demand in the world in 2015 [4].

Polyethylene commodities account for 90% of the total production, and the other 10% corresponds to engineering polyethylene [4]. Engineering polyethylenes are plastics with outstanding properties for specialized applications, such as in the aerospace industry and, therefore, have higher market profitability.

The development and production of polyethylene, as commodities or engineering polymers, requires combining the knowledge of the catalyst package and of the production process. The main focus of this thesis is to quantify the performance of a metallocene catalyst for the production of high-density linear polyethylene, and to correlate how the structure of the polymer correlates with its mechanical properties. This information will help design commodity and engineering polyethylenes with properties tailored to specific applications.

## 2.2. Polyethylene Types

Polyethylenes are generally classified into three main categories: low-density polyethylene (**LDPE**), linear low-density polyethylene (**LLDPE**) and high-density polyethylene (**HDPE**) [5]. These categories are based on changes in polymer density as a function of the 1-olefin content, as illustrated in Figure 2-2.

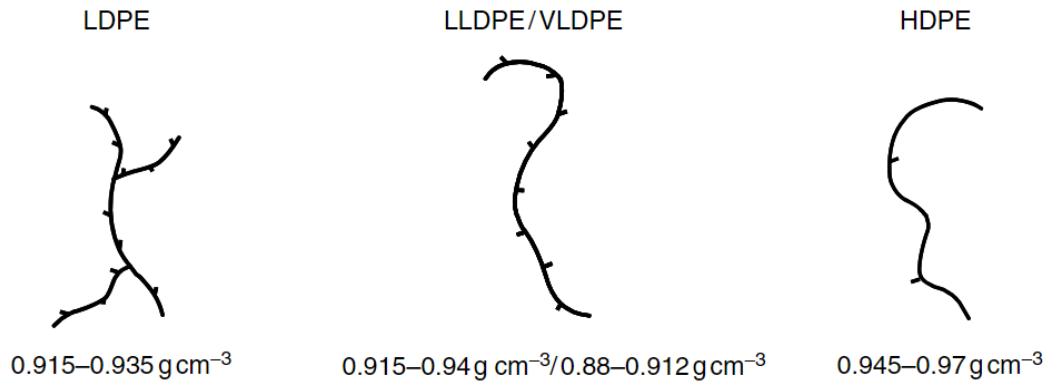


**Figure 2-2.** Types of polyethylene [6].

Low-density polyethylene has good optical properties, is easy to process, but is not very tough. It is produced by free-radical polymerization, using peroxides as initiators, under high pressures ( $> 500\text{ atm}$ ) and high temperatures ( $> 100\text{ }^{\circ}\text{C}$ ) in autoclave or tubular reactors [5]. This process leads to the formation of long and short chain branches, which can be controlled by polymerization conditions and reactor type. Long chain branches (LCB) are branches with 270 or more carbon atoms, while short chain branches (SCB) usually have between 2 to 6 carbon atoms [7].

Linear low-density polyethylene has good sealability and toughness, stiffness higher than LDPE, but relatively lower barrier properties, dart impact, tear and optical properties than LDPE. Linear low-density polyethylene is mainly produced in gas-phase and slurry reactors using coordination catalysts [5]. The typical polymerization conditions are in the range of  $80\text{ to }110\text{ }^{\circ}\text{C}$ , and  $10\text{ to }30\text{ atm}$  [8].

High-density polyethylene is stiffer than LDPE and LLDPE, has good barrier properties and chemical resistance, higher temperature resistance, but it is more brittle and hazier than LDPE and

LLDPE [5]. High-density polyethylene is produced in processes similar to those used to make LLDPE, also using a coordination catalyst.

### **2.3. Catalysts for Polyethylene Production**

The first type of polyethylene to be produced commercially was LDPE in the mid-1950s using a free radical polymerization process [9]. Due to its higher SCB content, LDPE chains in the solid phase have lower intermolecular forces that result in lower tensile and tear strength. However, despite its poorer mechanical properties and higher production costs compared to LLDPE, its superior optical properties and easy processability not only have kept LDPE in the market, but also have caused its demand to increase throughout the years [10].

In the mid-1950s, two independent research groups discovered almost simultaneously two types of catalysts for the production of HDPE: chromium oxide catalysts, discovered by John P. Hogan and Robert L. Banks from Phillips Petroleum, and aluminum alkyl activated titanium-based catalysts (Ziegler-Natta catalysts), discovered by Karl Ziegler and Giulio Natta [11]. These coordination catalysts led to the design and construction of many slurry and gas phase reactors for the commercial production of LLDPE and HDPE in the sixties and seventies.

Chromium based catalysts are mainly used for the production of HDPE, having mostly linear chains and broad molecular weight distribution (MWD). Chromium catalysts do not need a co-catalyst to activate the catalyst sites. Although the initiation mechanism is not well-known, it has been proposed that oxidation-reduction reactions between ethylene and chromium forms chromium (II) species that are the precursors for the active polymerization centers [12]. Figure 2-3 illustrates the structure of a first generation of chromium catalyst.

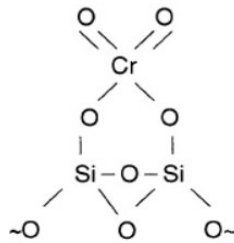


**Figure 2-3.** Monochromate chromium catalyst – First generation [12].

Ziegler-Natta catalysts are used to make LLDPE and HDPE. They consist of two components, a catalyst precursor, or precatalyst, based on titanium chlorides, and an alkyl aluminum co-catalyst, such as tri-ethylaluminum, which activates the precatalyst to form sites active for polymerization. Today, most Ziegler-Natta catalyst are supported on magnesia or silica to disperse the active sites throughout supports with high surface area and increase polymer yield. Ziegler-Natta catalysts also produce polyolefins with broad MWDs, but they are narrower than those made with chromium catalysts [13]. Figure 2-4 shows the activation and polymerization mechanism proposed by Cossee and Arlman for Ziegler-Natta catalysts.

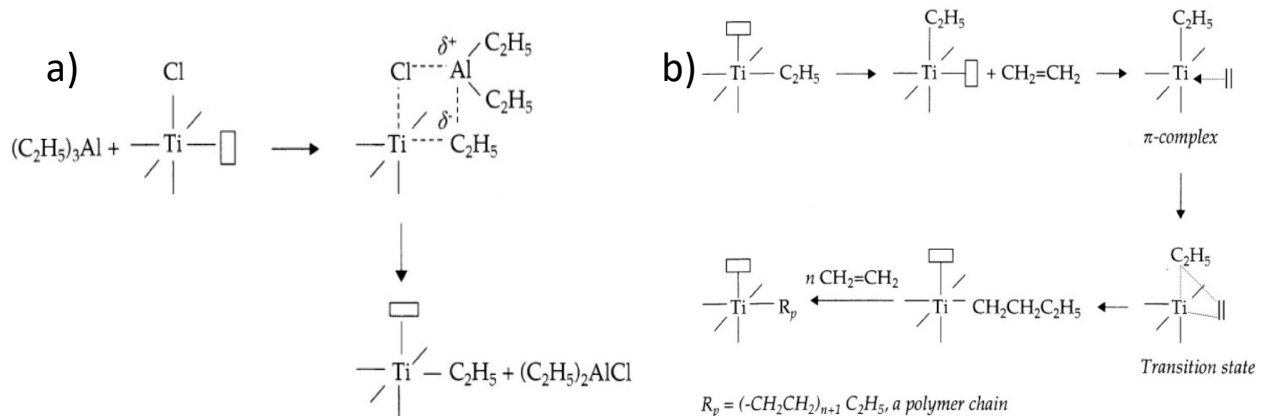


**Figure 2-4.** Cossee and Arlman mechanism: a) activation, and b) propagation [13].

In 1979, Kaminsky et al. discovered how to make stable metallocene catalysts, starting a new revolution in the polyolefin industry. Metallocene catalysts also consist of two components: a catalyst precursor and a cocatalyst. The catalyst precursor is an organometallic transition metal

complex in which the transition metal atom is generally “sandwiched” between two cyclopentadienyl rings (or its derivatives). The rings may be connected by different bridges to modify the angle between the rings (Figure 2-5) [14].

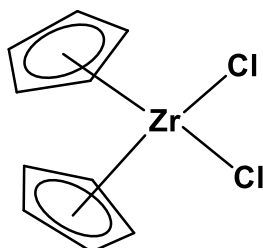


**Figure 2-5.** Typical metallocene catalyst structure [14].

An advantage of a metallocene catalyst is the capacity to control polymer molecular weight, comonomer incorporation and productivity by modifying its chemical structure. If the ligands of Figure 2-5 are modified and connected by a bridge, as shown in Figure 2-6, the polymer molecular weight and catalyst productivity is affected. For instance, the molecular weight of polyethylene made with  $\text{Cp}_2\text{ZrCl}_2$  (Figure 2-5) at 30 °C and 2.5 bar is 2.4 times higher than that made with  $[(\text{CH}_3)_2\text{Si}(\text{2-CH}_3\text{Ind})_2]\text{ZrCl}_2$  (Figure 2-6), and the productivity is almost twice as high. [15].

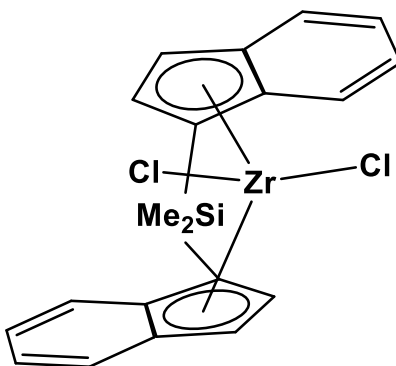


**Figure 2-6.** Metallocene catalyst structure for  $[(\text{CH}_3)_2\text{Si}(\text{2-CH}_3\text{Ind})_2]\text{ZrCl}_2$  [15].

In addition, if one of the cyclopentadienyl rings of  $\text{Cp}_2\text{ZrCl}_2$  is replaced with a nitrogen substituent that coordinates with the metal center, a “half sandwich” metallocene catalyst is obtained. These types of catalysts are also known as constrained geometry catalysts (CGC), as shown in Figure 2-7. A CGC can produce polyethylene with long chain branching and higher incorporation of comonomer due to its less sterically hindered active site and electronic environment around the active site [16].

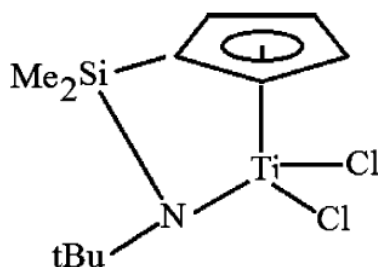


**Figure 2-7.** Structure of a constrained geometry catalyst [16] .

Another subtle modification in the structure of metallocenes consists in substituting the transition metal atom. The most studied transition metal in metallocenes is zirconium, but polymerization is also possible with hafnium and titanium. The nature of the transition metal strongly affects the type of polymer made. For instance, comparing  $\text{Cp}_2\text{ZrCl}_2$  and  $\text{Cp}_2\text{HfCl}_2$  analogues, Hf has slightly smaller atomic and ionic radii, forms stronger  $\sigma$ -bonds, and is more resistant to reduction than Zr. These properties result in stronger Hf-C bonds, which slows down both bond making and bond breaking reactions, causing  $\text{Cp}_2\text{HfCl}_2$  to have lower activity, but make polymers with higher molecular weights than  $\text{Cp}_2\text{ZrCl}_2$  [17]. In addition, the higher resistance to reduction also explains the lower catalyst deactivation rates of  $\text{Cp}_2\text{HfCl}_2$ .

Metallocenes, when activated with aluminum alkyl cocatalysts used with Ziegler Natta catalyst, can polymerize ethylene, but with very low productivity. However, once it was discovered that methylaluminoxane (MAO) could be used to activate metallocenes and generate stable active sites, the catalyst productivity enhanced to values between 10 to 100 times higher than Ziegler-Natta catalysts [18]. Methylaluminoxane is the product of the controlled reaction between water and

trimethylaluminum (TMA), which produce an oligomeric compound with degree of oligomerization between 6 to 20. In spite of its importance, the structure of MAO is still somewhat controversial [19]. Figure 2-8 shows one of the model structures proposed in the literature for MAO. More recently, borates and boranes have also been used to replace MAO, since they can be used in stoichiometric amounts, while MAO is needed in large excess to effectively activate metallocene catalysts.

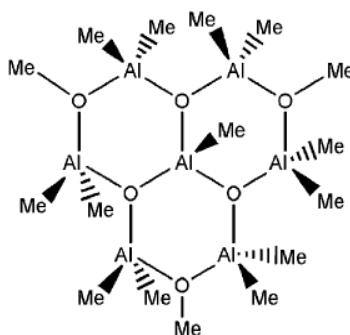


**Figure 2-8.** A possible MAO structure [20].

Catalyst activation and polymerization mechanism for a zirconium metallocene catalyst is shown in Figure 2-9.

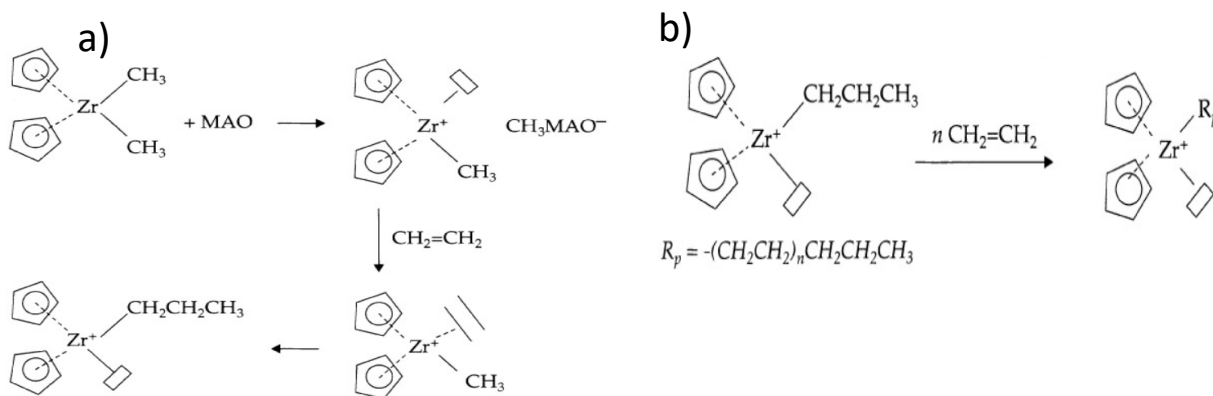


**Figure 2-9.** Reaction mechanism for metallocene catalysts: a) activation, and b) propagation [21].

Contrarily to Phillips and Ziegler-Natta catalysts, metallocenes are molecular single-site catalysts, producing polyolefins with narrow MWD and uniform comonomer content, as shown in Figure 2-10.

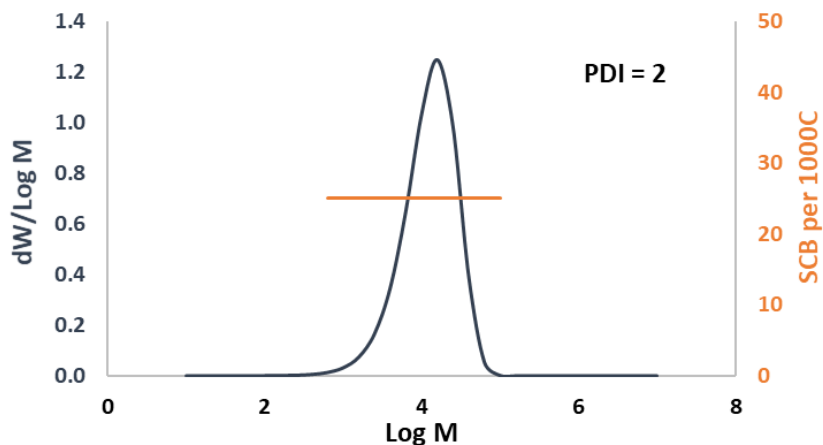


**Figure 2-10.** Molecular weight and comonomer content for an ethylene/1-olefin copolymer made with a metallocene catalyst. Comonomer content in polyolefins is often expressed as short chain branch frequency (SCB/1000 C).

Although the narrow MWD of polyolefins made with metallocene catalysts enhances their mechanical properties, it also makes them harder to process [19]. It is possible to broaden the MWD of polyolefins made with metallocene catalysts either by: 1) combining two metallocenes that make polyolefins with substantially different molecular weight averages in the same reactor [22], or 2) using a single metallocene in two (or more) reactors in series operated at different conditions to make polyolefins with different molecular weight averages [23]. In both strategies, it is essential to know the detailed polymerization kinetics of the metallocenes used in the process. Either of these two approaches can make polyolefins with broader (and even bimodal) MWD, with controlled comonomer content in the low and high molecular weight populations. This polymer is easier to process and could be tailored to fit customer needs. An example of bimodal polyethylene is shown in Figure 2-11.

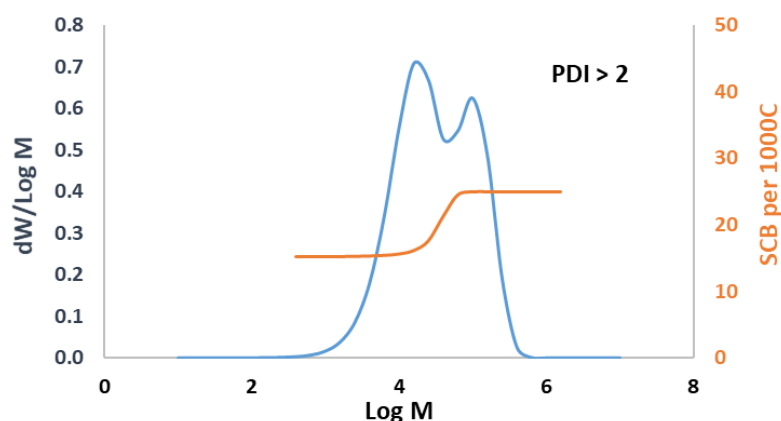
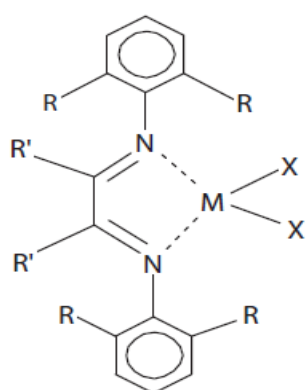


**Figure 2-11.** Molecular weight and comonomer content distribution for a hypothetical bimodal polyolefin.

Finally, in the early 1990s, Brookhart et al. discovered late transition metal catalysts for olefin polymerization. These catalysts are less oxyphilic than Ziegler-Natta, Phillips, and metallocene catalysts; as a result, they can polymerize olefins with polar comonomers, which act as poisons for the other coordination catalysts used to polymerize olefins. Despite the versatility of these catalysts, they still cannot compete commercially with existing free radical polymerization processes [19]. Figure 2-12 shows the molecular structure of a generic late transition metal catalyst.



M = Ni, Pd

X = Cl, Br, CH<sub>3</sub>, NCS

R' = H, CH<sub>3</sub>, C<sub>2</sub>H<sub>5</sub>

R'+R' =  $\alpha,\alpha$ -Dinaphthyl, cyclohexyl

R = CH<sub>3</sub>, *iso*-C<sub>3</sub>H<sub>7</sub>, CF<sub>3</sub>, C<sub>6</sub>H<sub>5</sub>, C<sub>6</sub>F<sub>5</sub>

**Figure 2-12.** Late transition metal catalyst [9].



The catalyst may deactivate through unimolecular thermal reactions or by reactions with traces of poisons present in the reactor. This is a general trend, as the activity of practically all coordination catalysts decrease as a function of polymerization time.

Finally, two important characteristics of the polymer can be deduced from Table 2-1: polymerization rate and polymer structure. When the reaction takes place in a semi-batch reactor operated at steady state, the polymerization rate can be expressed as

$$R_p = k_p[M][Y_o] \quad (2.1)$$

where  $[Y_o]$  is the total molar concentration of living chains in the reactor ( $\sum_{r=0}^{\infty}[P_r]$ ).

Since  $[Y_o]$  cannot be measured, it should be expressed as a function of known variables

$$\frac{d[Y_o]}{dt} = k_{iH}[M][P_H] - k_{tH}[H_2][Y_o] \quad (2.2)$$

Solving this differential equation, assuming  $[Y_o]$  at time zero (beginning of the polymerization) is equal to the initial catalyst concentration ( $C_{io}$ ), leads to

$$[Y_o] = \frac{k_{iH}}{k_{iH} + k_{tH}[H_2]} C_{io} e^{-k_d t} \quad (2.3)$$

Therefore, the final expression for the polymerization rate is

$$R_p = k_p[M] \frac{k_{iH}}{k_{iH} + k_{tH}[H_2]} C_{io} e^{-k_d t} \quad (2.4)$$

Thus, the polymerization rate, or molar ethylene consumption rate, at a specific time can be predicted with Equation (2.4). In addition, the total polymer yield as a function of time can be calculated by integrating Equation (2.4)

$$Polymer\ yield = k_p[M] \frac{k_{iH}}{k_d(k_{iH} + k_{tH}[H_2])} V_R C_{io} (1 - e^{-k_d t}) \quad (2.5)$$

$V_R$  is the reactor volume. Dividing the polymer yield by the initial amount of catalyst fed to the reactor, the catalyst productivity can be easily estimated.

$$Catalyst\ productivity = k_p[M] \frac{k_{iH}}{k_d(k_{iH} + k_{tH}[H_2])} (1 - e^{-k_d t}) \quad (2.6)$$

Catalyst productivity is an important variable because it is used to compare the cost/benefit among different catalyst types.

Regarding polymer structure, the number average chain length ( $r_n$ ), and weight average chain length ( $r_w$ ) of polymer made with a metallocene catalyst (that is behaving as a true single-site catalyst) can be estimated using the simple expressions [26]

$$r_n = \frac{R_p}{R_t} = \frac{1}{\tau} = \frac{k_p[M][Y_o]}{k_{tH}[H_2][Y_o]} = \frac{k_p[M]}{k_{tH}[H_2]} \quad (2.7)$$

$$r_w = \frac{2}{\tau} = \frac{2k_p[M][Y_o]}{k_{tH}[H_2][Y_o]} = 2 \frac{k_p[M]}{k_{tH}[H_2]} \quad (2.8)$$

The number average molecular weight ( $M_n$ ) and weight average molecular weight ( $M_w$ ) are estimated multiplying  $r_n$  and  $r_w$  by the molecular weight of the repeating unit ( $mw$ ).

Therefore, the theoretically polydispersity (PDI) of polymers made with single-site coordination catalyst is

$$PDI = \frac{r_w}{r_n} = 2 \quad (2.9)$$

Thus, if the propagation constant ( $k_p$ ) and the transfer to hydrogen constant ( $k_{tH}$ ) are known,  $\tau$  can be estimated. Paul Flory and Günter Schulz proposed the following expression for the weight chain length distribution of polymers made with single site catalyst [27]

$$w_{logr} = 2.306 \cdot r^2 \tau^2 e^{-r\tau} \quad (2.10)$$

Where  $r$  is a polymer chain length. The chain length distribution in Figure 2-9 was plotted using Equation (2.10) with  $\tau = 1.25 \cdot 10^{-4}$ , while that in Figure 2-10 was plotted using two catalysts that follow Equation (2.10) with  $\tau_1 = 1.25 \cdot 10^{-4}$  and  $\tau_2 = 2 \cdot 10^{-5}$ .

Polymers made experimentally with metallocene catalyst typically have PDI varying between 2 and 3 [28]. In these cases, even when PDI is slightly higher than the theoretically expected value of 2, it is usual to assume that the catalysts still behave as a single site catalyst. It is difficult to make polymer with PDI of 2 in laboratory-scale reactor because at the beginning of the polymerization, when the catalyst is injected in the reactor, reactor thermal instabilities due to the exothermic polymerization (even in a well-controlled reactor) may make the reactor deviate from

steady state operation for a short time, causing the MWD to broaden slightly. In addition, MWD are measured using gel permeation chromatography (GPC), that may also introduce some peak broadening during polymer analysis.

1-Olefins, typically 1-butene, 1-hexene, or 1-octene, are commonly copolymerized with ethylene to modify the mechanical properties of HDPE and LLDPE. In this case, the two monomers (A = ethylene, B = 1-olefin) compete to be incorporated into the living chains, as shown in Table 2-2. The rate of monomer propagation depends on the type of monomer being added to the chain, but also on the type of the last monomer incorporated into the chain (Terminal Model).

**Table 2-2.** Terminal model for copolymerization

Description	Chemical equations	Rate Constants
Propagation	$P_r^A + A \rightarrow P_{r+1}^A$	$k_{pAA}$
	$P_r^A + B \rightarrow P_{r+1}^B$	$k_{pAB}$
	$P_r^B + A \rightarrow P_{r+1}^A$	$k_{pBA}$
	$P_r^B + B \rightarrow P_{r+1}^B$	$k_{pBB}$

$P_r^A$  and  $P_r^B$  refer to living chains terminated in comonomers A or B, respectively.

The rate of copolymerization depends on the four individual propagation rate constants listed in Table 2-2. They can be used to define an apparent propagation rate constant ( $\widetilde{k}_p$ ), a value that depends on the fractions of monomer A and B ( $f_A$  and  $f_B$ , respectively) present in the reaction medium at a given polymerization time. It can be shown that,

$$\widetilde{k}_p = k_{pAA} + (k_{pBA} - k_{pAA}) \frac{\frac{k_{pAA}}{r_A} (1 - f_A)}{\frac{k_{pAA}}{r_A} (1 - f_A) + k_{pBA} f_A} \quad (2.11)$$

where,  $r_A$  and  $r_B$  are comonomer reactivity ratios defined as

$$r_A = \frac{k_{pAA}}{k_{pAB}} \quad (2.12)$$

$$r_B = \frac{k_{pBB}}{k_{pBA}} \quad (2.13)$$

Thus, if the comonomer (1-olefin) propagation constants ( $k_{pBB}$ ,  $k_{pAB}$ ) are lower than the monomer (ethylene) propagation constants ( $k_{pAA}$ ,  $k_{pBA}$ ), the apparent propagation constant will be lower than for pure ethylene polymerization, and the ethylene consumption and catalyst productivity will decrease.

For a single-site catalysts, the instantaneous average comonomer content in the copolymer,  $\overline{F}_A$ , can be calculated with the Mayo-Lewis equation [29]

$$\overline{F}_A = \frac{r_A \cdot f_A^2 + f_A \cdot (1 - f_A)}{r_A \cdot f_A^2 + 2 \cdot f_A \cdot (1 - f_A) + r_B \cdot (1 - f_A)^2} \quad (2.14)$$

Average comonomer content in Equation (2.14) is expressed as mole fraction. Usually, the 1-olefin comonomer content in polyolefins is measured by infrared (IR) detectors and reported as short chain branching (SCB) content. These two variable are related via the expression

$$F_B = \frac{2 \cdot SCB}{1000 + (2 - n_c) \cdot SCB} \quad (2.15)$$

where  $n_c$  is the number of carbon atoms in the 1-olefin comonomer molecule. The average comonomer content in ethylene/1-olefin copolymers made with single-site catalysts does not depend on chain length, as illustrated in Figure 2.9 [28].

Stockmayer developed an instantaneous bivariate distribution for the joint distribution of chain length and comonomer composition for binary linear copolymer given by the expression [30]

$$w_{\log r, F_A} = 2.30623 \cdot r^2 \cdot (\tau)^2 e^{-r\tau} \cdot \sqrt{\frac{r}{2\pi \cdot \beta}} \cdot e^{-\frac{r(\overline{F}_A - F_A)^2}{2\beta}} \quad (2.16)$$

Where  $\beta = \overline{F}_A(1 - \overline{F}_A)\sqrt{1 - 4\overline{F}_A(1 - \overline{F}_A)(1 - r_A r_B)}$ .

Stockmayer distribution allows us to calculate the weigh fraction of chains having a specific chain length and comonomer content in a given polymer population.

Stockmayer equation can be also expressed as a function of number average molecular weight, considering the following relations:

$$MW = r \cdot mw \quad (2.17)$$

$$M_n = \frac{1}{\tau} \quad (2.18)$$

Where  $MW$  is the molecular weight of a polymer chain,  $mw$  is the molecular weight of the repeating unit, and  $M_n$  is the number average molecular weight for the polymer. Thus, Stockmayer equation can be expressed as:

$$w_{\log r, F_A} = 2.30623 \cdot \left( \frac{MW}{M_n \cdot mw} \right)^2 \cdot e^{-\frac{MW}{M_n \cdot mw}} \cdot \sqrt{\frac{MW}{2\pi\beta \cdot mw}} \cdot e^{-\frac{MW(\overline{F_A} - F_A)^2}{2\beta \cdot mw}} \quad (2.19)$$

In the case of a catalyst containing more than one site type, such when two metallocenes are combined in a single reactor, the microstructure of whole polymer can be estimated based on the behavior of each site individually. In this case, the expression for molecular weight distribution of the whole polymer is considered a weight sum of the Flory distribution for each site type  $j$  as it is given by [31]

$$w_{\log r} = \sum_{j=1}^n m_j \cdot w_{\log r, j} \quad (2.20)$$

where  $m_j$  is the mass fraction of the polymer made on site type  $j$ .

The bivariate chain length distribution and comonomer composition distribution of a whole polymer is considered a weight sum of the Stockmayer distribution for each site type  $j$  as it is given by:

$$w_{\log r, F_A} = \sum_{j=1}^n m_j \cdot w_{\log r, F_A, j} \quad (2.21)$$

The following example explains in more details how to use Flory and Stockmayer distributions for a polymer made with two single-site catalysts that follow the polymerization mechanism explained in Table 2-1 and 2-2. The examples assume these catalysts were mixed in a semi-batch reactor, and Table 2-3 lists polymerization kinetic parameters and reactor conditions.

**Table 2-3.** Kinetic parameters and reaction conditions.

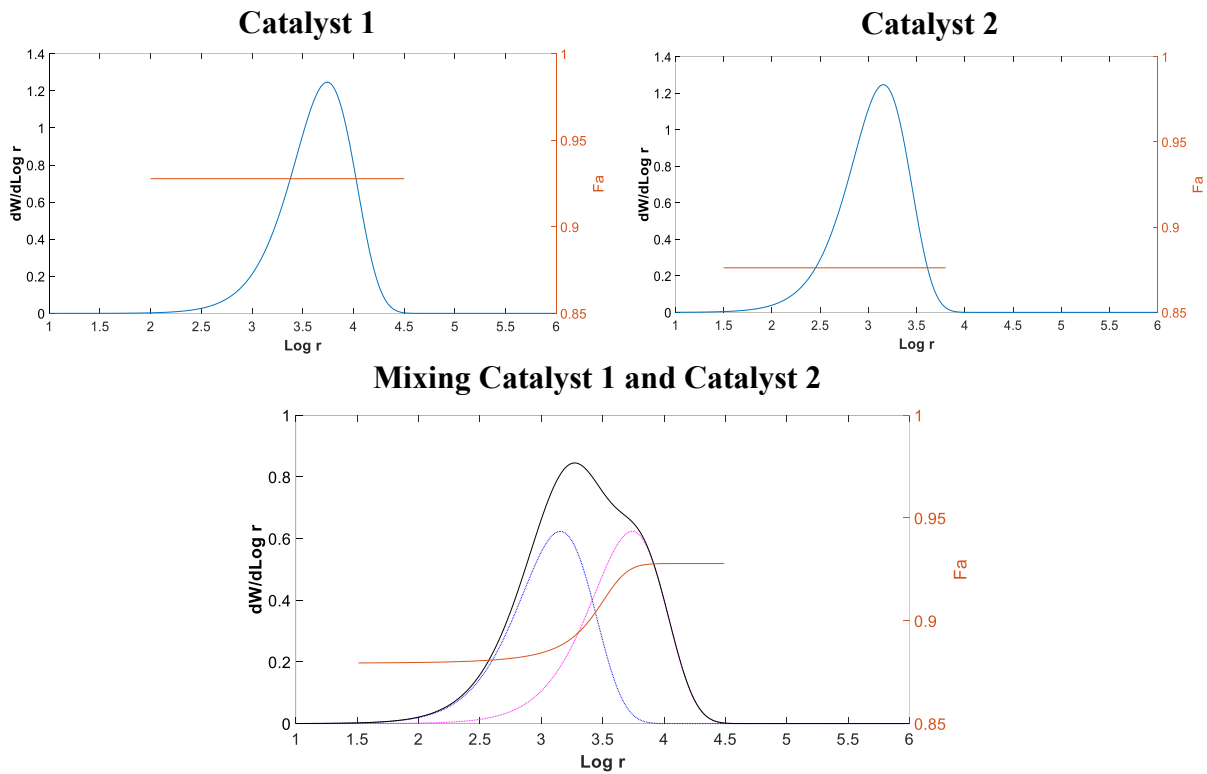
<b>Kinetic Parameters</b>	<b>Catalyst 1</b>	<b>Catalyst 2</b>
$k_{pAA}$ (L·mol <sup>-1</sup> s <sup>-1</sup> )	200,000	50,000
$k_{pBA}$ (L·mol <sup>-1</sup> s <sup>-1</sup> )	80,000	40,000
$k_{pAB}$ (L·mol <sup>-1</sup> s <sup>-1</sup> )	20,000	10,000
$k_{pBB}$ (L·mol <sup>-1</sup> s <sup>-1</sup> )	5,000	1,250
$k_{tH2}$ (L·mol <sup>-1</sup> s <sup>-1</sup> )	3,000	3,000
$r_A$	2.5	1.25
$r_B$	0.25	0.125
<b>Polymer mass fraction</b>	0.5	0.5
<b>Ethylene Concentration (L·mol<sup>-1</sup>)</b>		0.5
<b>Hydrogen Concentration (L·mol<sup>-1</sup>)</b>		0.01
<b>1-Hexene Concentration (L·mol<sup>-1</sup>)</b>		0.2

Table 2-4 shows some polymer properties estimated using Equations (2.7), (2.8) and (2.14).

**Table 2-4.** Polymer structure variables

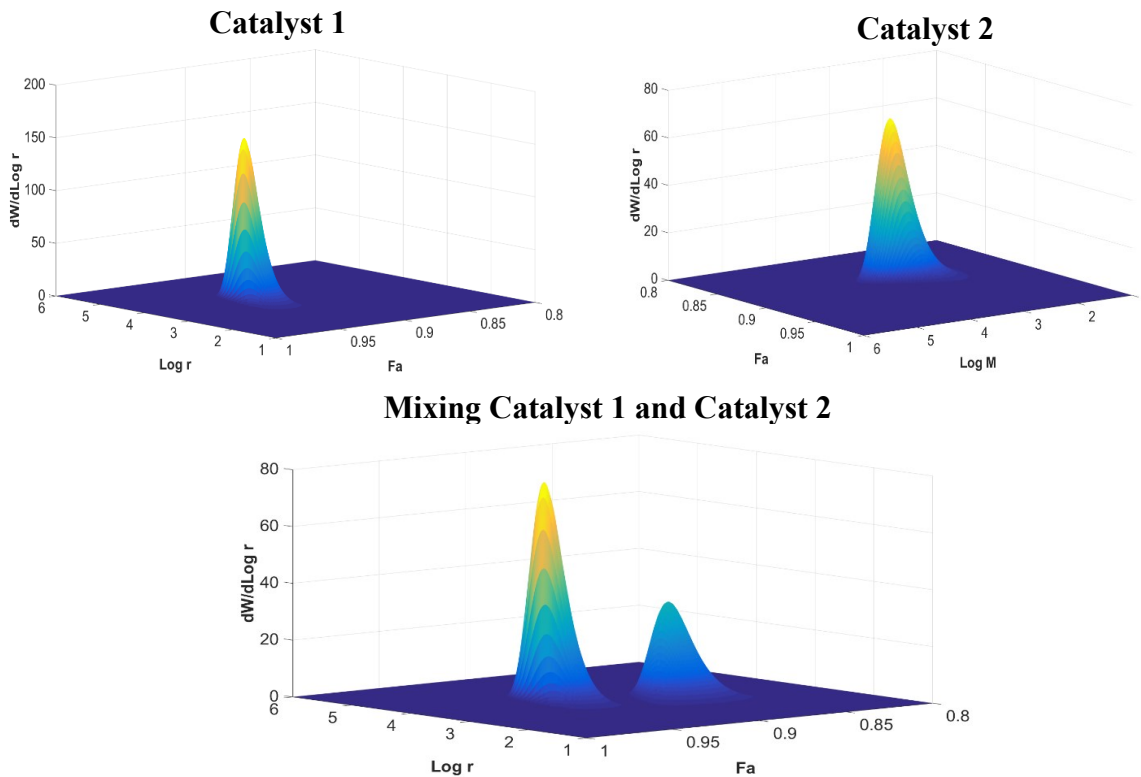
<b>Variables</b>	<b>Catalyst 1</b>	<b>Catalyst 2</b>
$r_n$	2,752	714
$r_w$	5,504	1,428
$\tau$	3.63E-04	1.40E-03
$\overline{F_A}$	0.928	0.876

Figure 2-14 shows the MWDs of the polymer produced by each catalyst and their 50/50 wt% blend.



**Figure 2-14.** Flory distribution for polymer made with Catalyst 1, Catalyst 2, and their 50/50 wt% blend.

Using Stockmayer distribution, more detailed information can be obtained about the polymer microstructure, since the chemical composition distribution (CCD) is superimposed on the MWD. (Figure 2-15).



**Figure 2-15.** Stockmayer distribution for catalyst 1, catalyst 2 and mix.

## 2.5. Mechanical Properties and Polyolefin Microstructure

Polyethylene owes its commercial success to its property/cost balance, which has led to the replacement of other materials such as wood and steel by cheaper polyethylene parts with similar properties. However, every day polyolefin converters face new challenges from their customers. For instance, there is a need for containers with thinner walls, but similar stiffness, to reduce plastic consumption and reduce environmental impact. But converters can only transform pellets they get from polyolefin manufacturers into final products, they cannot alter the intrinsic properties of the polyolefins they buy. It is producers to fulfill these market needs, which may be a challenging task because sometimes the properties that must be optimized simultaneously may be incompatible. Consider, for instance, stiffness and impact strength: if stiffness increases, impact strength generally decreases, and vice versa [32].

How has it been possible for polyethylene to continue making new breakthroughs? Because the polyolefin industry strives to understand how polymer microstructure affects its mechanical properties, and continuously tries to find new ways to produce polyolefins with new and well-controlled microstructures. Bimodal polyolefins with reverse comonomer incorporation is a good example of such product.

This, however, has not been an easy task. Consider HPDE, the polymer which is the main topic of this thesis. HDPE is a semi-crystalline polymer that combines a crystalline phase composed of chain-folded lamella, and an amorphous phase located between the crystalline lamellae. Some chains in traversing the amorphous phase may also link adjacent lamellae (tie molecules), further strengthening the polymer [33]. Figure 2-16 shows the solidification model propose by Fisher for a semi-crystalline polymer.

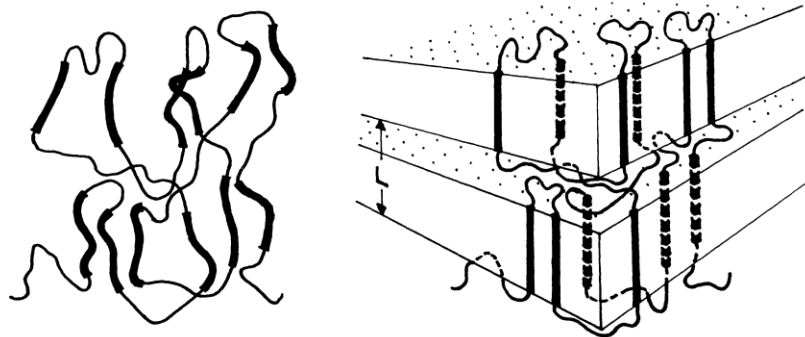


**Figure 2-16.** Solidification model for a semi-crystalline polymer [34].

Due to the complex distribution of amorphous and crystalline phases in semi-crystalline HDPE, it is difficult to develop a general model that can predict the mechanical properties of HPDE only from the knowledge of its microstructural properties. Nevertheless, most researchers agree that tie molecules and entanglements are correlated with the mechanical properties of HDPE.

Tie molecules and entanglements are molecular connections between crystalline segments. Figure 2-17 shows examples of both. These connections are held together by covalent bonds: without them, the crystallites between lamellae would be held by weak van der Waals forces; once under stress, the crystallites would slip over each other, resulting a brittle failure of the material [35].

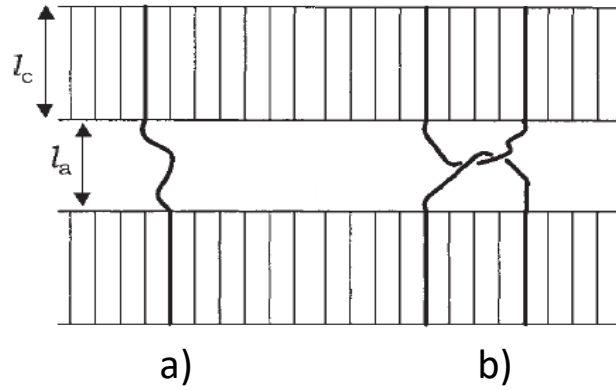


**Figure 2-17.** a) Tie molecules b) Entanglement loose loops [35].

Correlations between tie molecules and mechanical properties have been investigated by many researchers. Meinel and Peterlin [36] showed that for low density polyethylene, a higher concentration of entanglements and tie molecules increased interlamella cohesion, increasing tensile strength, draw ratio, and limiting the strain to break. Smith, Lemstra and Pijpers [37] demonstrated that when tie molecules increased in HDPE, a higher stress was required to break the polymer during draw tests. Similar conclusions were obtained by P.I Vincent [38], and G. Capaccio and I. M. Ward [39].

How can the concentration of entanglements and/or tie molecules be estimated for? The most accepted model was proposed by Huang and Brown [40]. The model assumes that the chain topology is kept during crystallization. The end-end distance of a polymer chains is estimated using Gaussian statistics for the chain segments. If this length is enough to connect two adjacent lamellae, it is probable that a tie molecule will be formed. According to this model, the probability of tie chain formation is given by

$$P_{TM} = \frac{1 \int_L^{\infty} r^2 \exp(-b^2 r^2) dr}{3 \int_0^{\infty} r^2 \exp(-b^2 r^2) dr} \quad (2.14)$$

where,

$P_{TM}$  = Probability of tie-chain formation

$L = 2L_c + L_a$  ( $L_c$  is the crystal lamellar thickness and  $L_a$  is the amorphous layer thickness).

$r$  = end-to-end distance of a random polymer coil.

$b = \frac{3}{2\bar{r}^2}$  ( $\bar{r}$  is the mean square value of the end-to-end distance for random coil conformation chain).

The factor  $1/3$  was introduced by Huang and Brown because two dimensions of the lamellar structure, in accordance with Fischer's solidification model, are much longer than  $L$ .

In this thesis, the Huang and Brown model was extended, and a new approach proposed by Paul DesLauriers was used to correlate the polymer structure with mechanical properties. These concepts will be discussed in more details in Chapter 4.

## Chapter 3 : Ethylene/1-Hexene Polymerization with Bis(cyclopentadienyl) Hafnium(IV) Dichloride

### 3.1. Introduction

This chapter studies the polymerization kinetics of ethylene and ethylene/1-hexene with bis(cyclopentadienyl) hafnium(IV) dichloride ( $\text{Cp}_2\text{HfCl}_2$ ) (Figure 3-1) to propose a polymerization mechanisms and estimate its main polymerization kinetic constants. This catalyst was selected due to its strong response to hydrogen to produce low average molecular and because there are no data with respect to the kinetic parameters of this catalyst in the open literature. This model is used in the following chapters of this thesis to relate polymerization conditions to polymer microstructure and properties.

### 3.2. Materials

Toluene (HPCL grade), used as a solvent during the polymerization was supplied by Sigma Aldrich. Ethylene (polymer Grade 3, Praxair) and 1-hexene (97% purity, Sigma Aldrich) were used as monomer and comonomer, respectively. The precatalyst, bis(cyclopentadienyl) hafnium(IV) dichloride ( $\text{Cp}_2\text{HfCl}_2$ , 97% purity, Sigma Aldrich) was activated with MAO (10% in toluene, Albemarle). Tri-isobutyl aluminum (TIBA) was used as impurity scavenger (25% in toluene solution, Sigma Aldrich). Hydrogen (ultra-high purity, Grade 5.0) as used as chain transfer agent, and nitrogen (ultra-high purity, Grade 5.0) was used to evacuate the reactor. Both were purchased from Praxair.

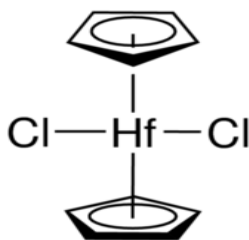


**Figure 3-1.** Bis(cyclopentadienyl) hafnium(IV) dichloride.

All polymerizations were conducted in solution, using toluene as a solvent. Toluene was purified by distillation over n-butyllithium/styrene/sodium for 24 hours, and then transferred to an amber 4-liter bottle. One-third of the bottle was filled with a mixture of molecular sieves (3, 4, and 5-Å) and Selexorb to remove any polar impurities. A manual valve connected to a tube extending to the bottom of the bottle was attached to the bottle cap, forcing the toluene to pass through the molecular sieves and Selexorb before it could be removed from the bottle. This process provided further toluene purification before it was used in the polymerizations (Figure 3-2). Metal rings were installed between the valve and plastic cap, and sealant was used to fill the gaps to keep the bottle under positive nitrogen pressure (approximately 0.17 MPa) and avoid inflow of oxygen and moisture into the bottle. The solvent storage bottle was checked daily to verify it was under positive pressure.



**Figure 3-2.** Toluene purification/storage bottle.

Ethylene was purified by passing it through columns packed with molecular sieves (3A/4A mixture) and copper(II) oxide to remove polar impurities, such as water and oxygen, that are catalyst poisons. MAO, TIBA and hydrogen were used without further purification. MAO was selected as co-catalyst because it is used in commercial facilities for polyethylene production.

Nitrogen was purified by passing it through a Big Universal Trap and a Big Oxygen Trap (supplied by Agilent), to remove polar impurities.

$\text{Cp}_2\text{HfCl}_2$  was purchased as a powder and was dissolved in toluene at concentration of 0.31 micromoles per gram of solution. This stock catalyst solution was used in all polymerizations.

An amber 1-liter bottle, filled up to one third of its volume with a mixture of molecular sieves (3, 4, and 5-Å) and Selexorb, was used to purify and store 1-hexene. The bottle was kept inside the glove box. Since  $\text{Cp}_2\text{HfCl}_2$ , MAO and TIBA are air sensitive, they were also stored and handled under nitrogen atmosphere inside the glove box. All reagents were prepared inside the glove box using 20 mL vials and corning Pasteur pipettes. The vials were sealed with rubber septa and open center metal seals to avoid contamination when the vials were withdrawn from the glove box.

### 3.3. Polymerization Procedure

Polymerizations were done using a 300 ml Parr autoclave reactor operated in semi-batch mode (Figure 3-3). Before every polymerization, the reactor was purged 10 times with high pressure nitrogen to remove impurities inside the reactor. Subsequently, the reactor was washed with 150 mL toluene and 0.3 g of TIBA (used as a scavenger), and heated to 130 °C. The reactor was kept at this temperature for approximately 5 min, before the mixture was blown out under nitrogen pressure. Finally, the reactor was cooled down to 30 °C.

Once the reactor reached a steady temperature of 30 °C, toluene, MAO and 1-hexene were injected by differential nitrogen pressure using transfer needles through the transfer nozzle V-6 (Figure 3-3). MAO was fed in ratio of 24000 moles of Al to one mole of  $\text{Cp}_2\text{HfCl}_2$  for all polymerizations. The molecular formula of MAO was assumed as  $\text{AlCH}_3\text{O}$  [20] and its molecular weight 58  $\text{g}\cdot\text{mol}^{-1}$  using this information the number of moles of MAO were estimated.

Once the reactants were in the reactor, the reactor was purged one more time with nitrogen to remove any oxygen or moisture traces that could have been introduced in the reactor during the transfer process.

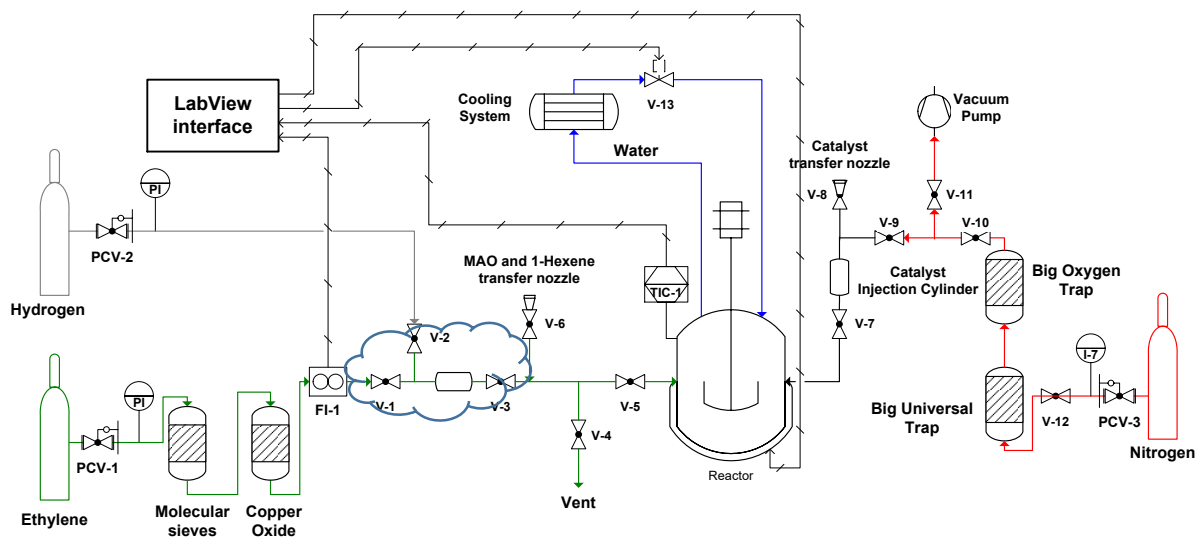


**Figure 3-3.** P&D reactor diagram.

Catalyst was added to the catalyst injection cylinder using a transfer needle under nitrogen pressure through nozzle V-8. Once the catalyst was in the injection cylinder, the pressure inside it was set to 0.24 MPa higher than in the reactor to flush all the catalyst into the reactor once valve V-7 was opened. When all reactants and catalyst system were in the reactor, the reactor temperature control, TIC-1, was raised to 120 °C, and the solution was stirred at a rate of 1300 rpm. All polymerizations were done at 120°C, unless otherwise indicated.

If H<sub>2</sub> had to be fed to the reactor, the desired amount was trapped in the space (30 ml) between valves, V-1, V-2 and V-3, as indicated by the blue cloud in Figure 3-3. As the H<sub>2</sub> pressure was controlled by the control valve PCV-2, the H<sub>2</sub> mass injected in the reactor could be easily estimated. Hydrogen, kept stagnant in this control volume, was carried into the reactor with ethylene at the beginning of the polymerization. The ethylene pressure was much higher than H<sub>2</sub> pressure in all polymerizations.

Once the reactor temperature reached the set point, ethylene was supplied on demand until the ethylene flow to the reactor was zero, indicating that toluene was saturated with ethylene. The ethylene flow was measured using mass flowmeter FI-1. One of the manipulated variables during the experiments was the concentration of ethylene in toluene. This variable was controlled by

regulating ethylene pressure inside the reactor using the pressure control valve PCV-1. The ethylene pressure is reported in absolute pressure.

After the toluene was saturated with ethylene, the reactor temperature was stable, and the ethylene mass flowmeter was zero, catalyst was fed to the reactor opening valve V-7 and closing it after few seconds. The reactor temperature and ethylene flow to the reactor were recorded using LabView as interface. Labview also controlled the reactor temperature by changing the open/close frequency of a solenoid valve that controlled the flow of cooling water to an internal coil in the reactor, and the power output to an external electrical heat mantle covering the reactor body. The temperature controller allowed for the fast regulation of the polymerization temperature, with a maximum deviation of  $\pm 0.1$  °C from the set point after a few minutes after the catalyst was injected in the reactor.

### **3.4. Polymer Characterization**

#### **3.4.1. Molecular Weight Distribution**

Polymer molecular weight distribution (MWD) was measured using a gel permeation chromatographer (GPC). This method of characterization relies on the time that a polymer chain in solution takes to exit a column (or a set of columns) filled with porous packing material (retention time); if the chain has a low molecular weight, its hydrodynamic volume is small and the its diffusion path inside the pores of the packing material is longer than that of chains with higher molecular weight [41]; therefore, its retention time will be higher. A calibration curve relating retention time to polymer molecular weight can then be used to calculate the MWD of the polymer being analyzed.

The GPC unit was calibrated using polystyrene standards of narrow MWD and the universal calibration curve procedure. The GPC (from Polymer Char) units was equipped with three linear columns (Agilent PLgel Olexis, 7.5×300 mm, 13 $\mu$ m particles, packed with crosslinked polydivinyl benzene particles) and three detectors: Fourier-transform infrared (IR), light scattering, and differential viscometer. Trichlorobenzene (TCB) was used as solvent and as continuous phase, at a flow rate of 1 ml/min at 145 °C.

### 3.4.2. Comonomer Content

The proportion of each comonomer in the copolymer depends on the concentration of the comonomers in the reaction medium and on their reactive ratios, which depend on comonomer type and on the catalyst used to make the copolymer [42]. In this study, the two comonomers were ethylene and 1-hexene. 1-Hexene decreases the crystallinity and melting temperature, and affects the mechanical properties of the copolymer; thus, it is important to quantify and identify the amount and distribution of the comonomer in the polymer.

The 1-hexene content in the copolymer can be estimated using the IR detector of the GPC unit. The IR detector measures the SCB frequency in the copolymer, which can be converted to comonomer molar fraction using the expression

$$F_B = \frac{2 \cdot SCB}{1000 + (2 - n_C) \cdot SCB} \quad (3.1)$$

where  $n_C$  is the number of carbon in the comonomer ( $n_C = 6$  for 1-hexene), and SCB is expressed as the number of SCB per 1000 C atoms in the chain.

The error of this measurement, however, is about  $\pm 1$  SCB/1000 C, which corresponds to a deviation of approximately 18% when the SCB in the copolymer is low. For instance, in the copolymers analyzed for 3 replicate polymerizations with  $Cp_2HfCl_2$ , the SCB of the 3 copolymers made at the same conditions were measured to be 4.9, 6.5 and 7.3 SCB/1000 C, corresponding to a 1-hexene molar fraction of 0.0099, 0.0133 and 0.015, respectively, which corresponds a deviation of 16% respect the average.

Another alternative to measure comonomer content is by correlating it with the melting temperature of the copolymer. In a previous publication from our research group [43], the following linear correlation was suggested to correlate 1-hexene molar fraction in ethylene/1-hexene copolymers to their melting temperature (onset) measured by differential scanning calorimetry (DSC)

$$F_{1-Hex} = -0.0011 \cdot T_m(^{\circ}C) + 0.1387 \quad (3.2)$$

where  $F_{1-Hex}$  is the mole fraction of 1-hexene in the copolymer and  $T_m$  its melting temperature.

The copolymer standards used to derive Equation (3.2) were produced with methyl(6-t-butoxyhexyl)silyl( $\eta$ 5-tetramethylcyclopentadienyl)(t-butylamido)titanium dichloride (CGC-Ti) and their 1-hexene molar fraction was determined with  $^{13}\text{C}$  NMR.  $^{13}\text{C}$  NMR is an absolute technique that does not require calibration. Unfortunately, it is also relatively expensive and require long analysis times to obtain accuracy measurements of copolymer composition, particularly if the molar fraction of comonomer is relatively low, as for HDPE samples.

A similar correlation between 1-hexene content and melting temperature was proposed by Adisson and et al. [44]. In this case, the 1-hexene content was measured by FTIR (also calibrated using standards characterized with  $^{13}\text{C}$  NMR), and the melting peak temperature (instead of onset of the melting peak) was selected for the correlation

$$T_{peak}(\text{°C}) = -1.6 \cdot SCB + 136 \quad (3.3)$$

Combining Equations (3.1) and (3.3) leads to

$$\frac{-800}{(T_{peak}(\text{°C}) - 136)} - 2 = \frac{1}{F_{1-Hex}} \quad (3.4)$$

Table 3-1 compares the 1-hexene molar fractions estimated with these three methods.

**Table 3-1.** Comparison of method to estimate 1-hexene content in the copolymer.

	IR detector		Onset (Soares group)		Peak (Adisson and et al.)	
	SCB per 1000C	F <sub>1-hex</sub>	Temp (°C)	F <sub>1-hex</sub>	Temp (°C)	F <sub>1-hex</sub>
<b>Sample 1</b>	7.3	0.0150	113.73	0.0136	126.46	0.01222
<b>Sample 2</b>	6.5	0.0133	114.39	0.0129	124.04	0.01541
<b>Sample 3</b>	4.9	0.0100	114.2	0.0131	127.67	0.01063
<b>Average</b>		<b>0.0128</b>		<b>0.0129</b>		<b>0.0128</b>
<b>Standard Error</b>		<b>0.00257</b>		<b>0.00075</b>		<b>0.00243</b>
<b>Percentage Error</b>		<b>20%</b>		<b>6%</b>		<b>19%</b>

Although the average 1-hexene content in the copolymer is similar using the three methodologies, the method proposed by the Soares group using the onset melting temperature value has the lowest standard error. In addition, it has been reported that  $T_{peak}$  changes with the heating rate, the thermal conductance of the sample and with the mass of the sample while the onset temperature is independent of test parameters [45]. Therefore, Equation (3.2) was used to analyze the 1-hexene content of the samples made in this investigation.

### 3.5. Polymerization Kinetics

#### 3.5.1. Estimation of Ethylene, 1-Hexene and Hydrogen Concentrations in Toluene

We need to know the concentrations of ethylene, 1-hexene and hydrogen in toluene (the polymerization medium) to estimate the polymerization kinetic constants with  $Cp_2HfCl_2$ . Several polymerizations were performed at different stir speed, the results suggested that for stirring speeds higher than 1000 rpm, the ethylene flow was more stable, suggesting that the mass transfer resistance is negligible, and therefore, the gas phase is in equilibrium with the liquid phase. Hysys was used to estimate concentration of gases in toluene, using as input toluene volume, 1-hexene mass, and number of moles of hydrogen fed to the reactor under a given temperature and pressure. The equation of state used to estimate these concentrations was the Peng-Robinson equation. The concentrations estimated by Peng-Robinson were consistent with values reported in the literature [24] [43] [46] [47]. The concentrations in equilibrium of each component are indicated in the reaction conditions tables of following sections.

#### 3.5.2. Polymerization Order with Respect to Ethylene Concentration

Information about the polymerization order with respect to ethylene concentration for unsupported  $Cp_2HfCl_2$  in toluene is not available in the literature. Therefore, the first step was to estimate this dependency. The equations for the productivity of a catalyst that decays according to a first order model and depends linearly on monomer concentration is given by [26]

$$Cat Prod = 28g \cdot mol^{-1} \cdot \frac{k_p [Et] V_R}{k_d} [1 - e^{-k_d t}] \quad (3.5)$$

Similarly, if the catalyst depends on the square of the monomer concentration

$$Cat\ Prod = 28\ g \cdot mol^{-1} \cdot \frac{k_p [Et]^2 V_R}{k_d} [1 - e^{-k_d t}] \quad (3.6)$$

Where  $k_p$  is propagation constant,  $k_d$  is decay constant,  $V_R$  is reactor volume,  $[Et]$  is ethylene concentration and  $t$  is time. In our case, the polymerizations were done in toluene and toluene occupies a volume fraction of the reactor. Thus,  $V_R$  is the volume of toluene fed in the reactor.

Fourteen ethylene polymerizations were conducted at 120 °C, varying ethylene pressure from 0.51 to 1.14 MPa to determine the order of polymerization of ethylene with  $Cp_2HfCl_2$ . These results are summarized in Table 3-2 and Figure 3-4. Figure 3-4 clearly show that the linear relation predicted between ethylene concentration and productivity by Equation (3.5) is not obeyed. On the other hand, when the productivity was plotted versus the square of the ethylene concentration (Figure 3.5), a much better fit of the experimental data was observed. Consequently, one could conclude that Equation (3.6) is adequate to describe the polymerization of ethylene with  $Cp_2HfCl_2$  under the investigated set of experimental conditions.

**Table 3-2.** Productivity for homopolymer reactions

Polymerization	$P_E$ (MPa)*	Productivity ( $g \cdot \mu mol^{-1} \cdot h^{-1}$ )**	$[Et]$ ( $mol \cdot L^{-1}$ )*
Homo_60_1	0.51	63.60	0.23
Homo_60_2	0.51	67.22	0.23
Homo_70_1	0.58	87.98	0.27
Homo_80_1	0.65	112.82	0.31
Homo_100_1	0.79	191.34	0.39
Homo_100_2	0.79	204.26	0.39
Homo_100_3	0.79	202.53	0.39
Homo_100_4	0.79	196.91	0.39
Homo_120_1	0.93	281.23	0.47
Homo_120_2	0.93	267.59	0.47
Homo_140_1	1.07	388.96	0.56
Homo_150_1	1.14	429.41	0.60
Homo_150_2	1.14	424.13	0.60
Homo_150_3	1.14	459.96	0.60

\*  $P_E$  is the ethylene pressure in the reactor and  $[Et]$  is the ethylene concentration in toluene.

\*\*Refers to the gram of polymer produce by micromole of catalyst fed to the reactor

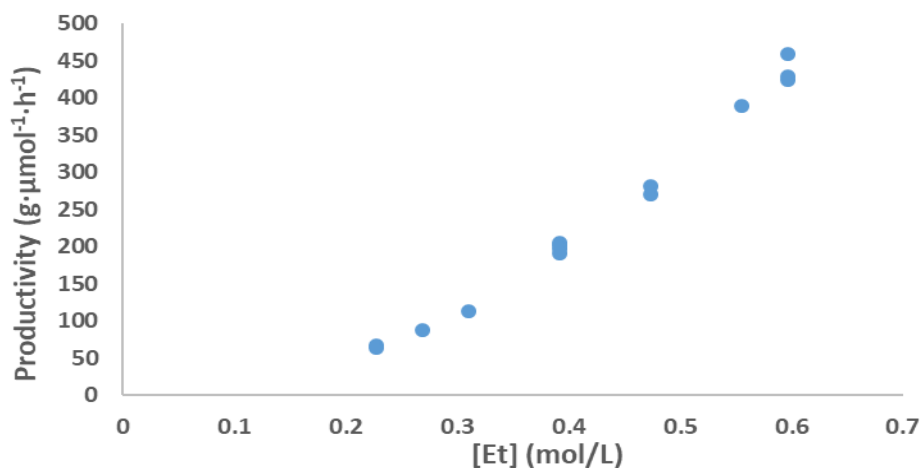


**Figure 3-4.** Catalyst productivity for the polymerization of ethylene with  $\text{Cp}_2\text{HfCl}_2$  for varying ethylene concentrations.

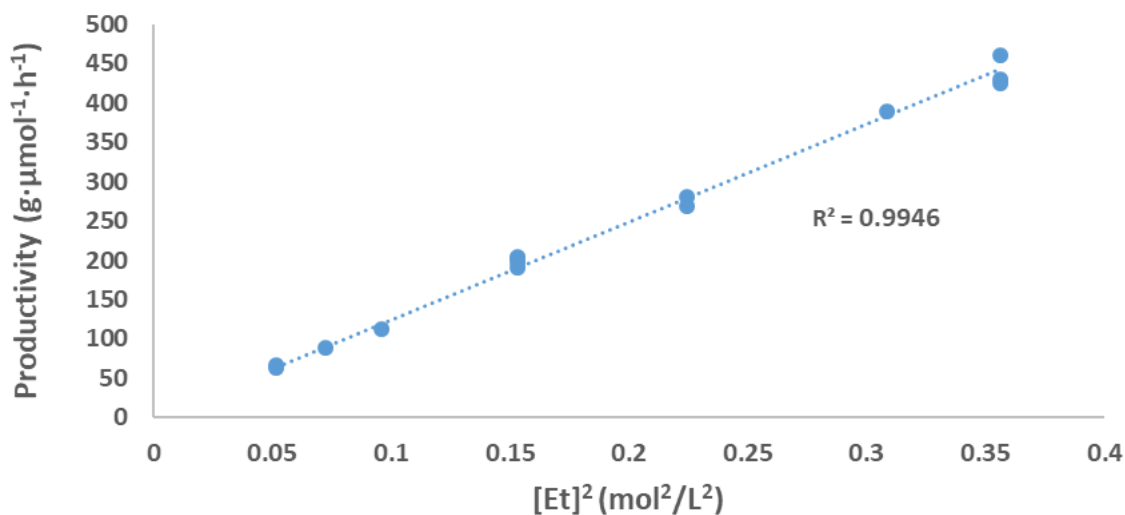


**Figure 3-5.**  $\text{Cp}_2\text{HfCl}_2$  productivity as a function of the square of ethylene concentration

Table 3-3 lists a mechanism for the polymerization of ethylene with  $\text{Cp}_2\text{HfCl}_2$ , following the trigger mechanism first proposed by Ystenes [29]. In the trigger mechanism, monomer is inserted into the polymer chain growing at the catalyst site following two steps: the monomer firstly complexes with the metal center, but can only be inserted into the polymer chain after a second

monomer complexes with the center and “triggers” the insertion. This mean that the coordination site is never monomer free; it is always occupied by a monomer ( $P_r \cdot M$ ).

**Table 3-3.** Proposed mechanism for the polymerization of ethylene with  $Cp_2HfCl_2$ .

Description	Chemical equations	Rate Constants
Activation	$C + Al-Et_3 \rightarrow P_0$	$k_a \rightarrow \infty$
Coordination	$P_r + M \rightarrow P_0 \cdot M$	$k_f$
Propagation	$P_r \cdot M + M \rightarrow P_{r+1} + M$	$k_p$
First order deactivation	$P_r \rightarrow C_d + D_r$	$k_d$

C is catalyst,  $Al-Et_3$  is MAO, M is ethylene,  $C_d$  is dead catalyst and  $D_r$  is dead chain.

According to the mechanism in Table 3-3, the rate of polymerization is given as

$$R_p = -\frac{d[M]}{dt} = k_p [M] \sum_{r=0}^{\infty} [P_r \cdot M] \quad (3.7)$$

The total concentration of living chains of all lengths is defined as

$$\sum_{r=0}^{\infty} [P_r \cdot M] = [Y_0 \cdot M] \quad (3.8)$$

Assuming that catalyst activation is instantaneous,  $[Y_0] = C_{i0}$ . The molar balances for  $[Y_0 \cdot M]$  and  $[Y_0]$  become

$$\frac{d[Y_0]}{dt} = k_p [Y_0 \cdot M] [M] - k_f [Y_0] [M] - k_d [Y_0] \quad (3.9)$$

$$\frac{d[Y_0 \cdot M]}{dt} = k_f [Y_0] [M] - k_p [Y_0 \cdot M] [M] \quad (3.10)$$

Making the pseudo steady-state hypothesis for the intermediate species  $[Y_0 \cdot M]$

$$k_f [Y_0] [M] = k_p [Y_0 \cdot M] [M] \quad (3.11)$$

Substituting Equation (3.11) in Equation (3.9)

$$\frac{d[Y_0]}{dt} = k_p [Y_0 \cdot M] [M] - k_f [Y_0] [M] - k_d [Y_0] = -k_d [Y_0] \quad (3.12)$$

Solving the resulting differential equation

$$[Y_0] = C_{io} e^{-k_d t} \quad (3.13)$$

Combining Equations (3.7), (3.8) and (3.13), the rate of polymerization can be finally written as

$$R_p = -\frac{d[M]}{dt} = k_p [M] [Y_0 \cdot M] = k_p [M] k_f [M] [Y_0] = k_p k_f [M]^2 C_{io} e^{-k_d t} \quad (3.14)$$

Equation (3.14) can be expressed as the rate of ethylene molar flow ( $Fl_E$ ):

$$-\frac{d(Fl_E)}{dt} = k_p k_f [M]^2 C_{io} V_R e^{-k_d t} \quad (3.15)$$

Because of the format of function defined in Equation (3.15), it is impossible to isolate  $k_p$  from  $k_f$  so these two constants cannot be estimated independently. Consequently, only the product of these two constants,  $k_p \cdot k_f$ , will be estimated.

Table 3-4 lists the conditions for the polymerization runs used to estimate the parameters of Equation (3.15). All polymerizations were conducted at 120 °C. One characteristic of these polymerizations is that the amount of catalyst had to be varied as a function of ethylene pressure, to assure that the amount of polymer made was enough for the proper measured of polymerization rates, but did not exceed the ability to the cooling system to keep the reactor temperature stable during the polymerization.

Normalized ethylene uptake curves are compared in Figure 3-6. These curves were normalized for an initial ethylene concentration of 2.4  $\mu\text{mol/L}$  so they could be meaningfully compared, but for the parameter estimation procedure described below, the original uptake curves were used.

Table 3-4. Ethylene polymerization conditions.

Polymerization	$P_E$ (MPa)	$[C_{i0}]$ ( $\mu\text{mol} \cdot \text{L}^{-1}$ ) *	$V_R$ (ml)	$[Et]$ ( $\text{mol} \cdot \text{L}^{-1}$ )
Homo_60_1	0.51	2.39	149.8	0.23
Homo_60_2	0.51	1.79	153.4	0.23
Homo_70_1	0.58	1.85	149.4	0.27
Homo_80_1	0.65	1.24	149.6	0.31
Homo_100_1	0.79	0.88	150.0	0.39
Homo_100_2	0.79	0.76	150.2	0.39
Homo_100_3	0.79	0.73	149.8	0.39
Homo_100_4	0.79	0.66	144.8	0.39
Homo_120_1	0.93	0.52	149.9	0.47
Homo_120_2	0.93	0.49	150.5	0.47
Homo_140_1	1.07	0.27	150.7	0.56
Homo_150_1	1.14	0.38	150.1	0.60
Homo_150_2	1.14	0.20	149.7	0.60
Homo_150_3	1.14	0.38	150.1	0.60

\*  $[C_{i0}]$  is the initial catalyst concentration.

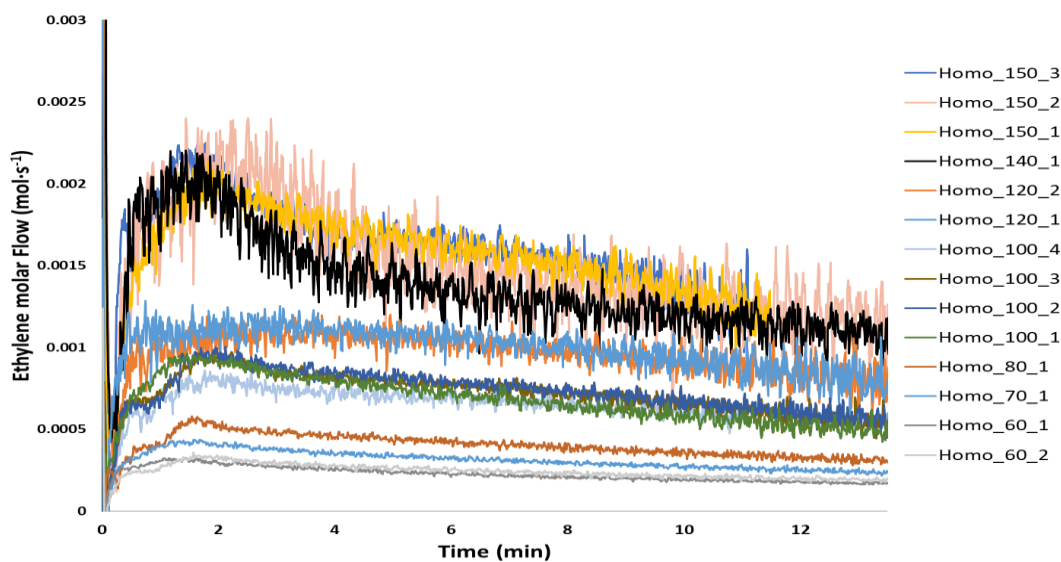
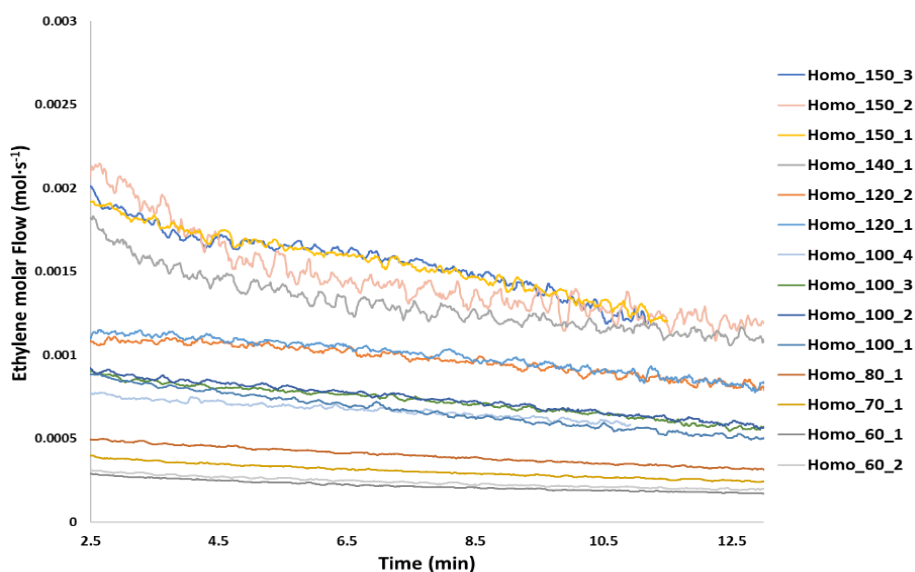


Figure 3-6. Normalized ethylene uptake curves polymerizations with  $\text{Cp}_2\text{HfCl}_2$ .

The flow rates of ethylene flow are noisier when ethylene pressures exceed 0.79 MPa, likely caused by the specifications of the pressure regulator (see Chapter 6 for more details). To reduce

the noise in the data, a 20-second moving average smoothing method was applied to all curves. Moreover, because reactor conditions are more unstable at the very beginning of the polymerization, just after catalyst injection, all points collected within the first 200 s were ignored during data analysis. The curves resulting from this data treatment are shown in Figure 3-7.



**Figure 3-7.** Smoothed ethylene uptake curves for polymerizations with  $\text{Cp}_2\text{HfCl}_2$ .

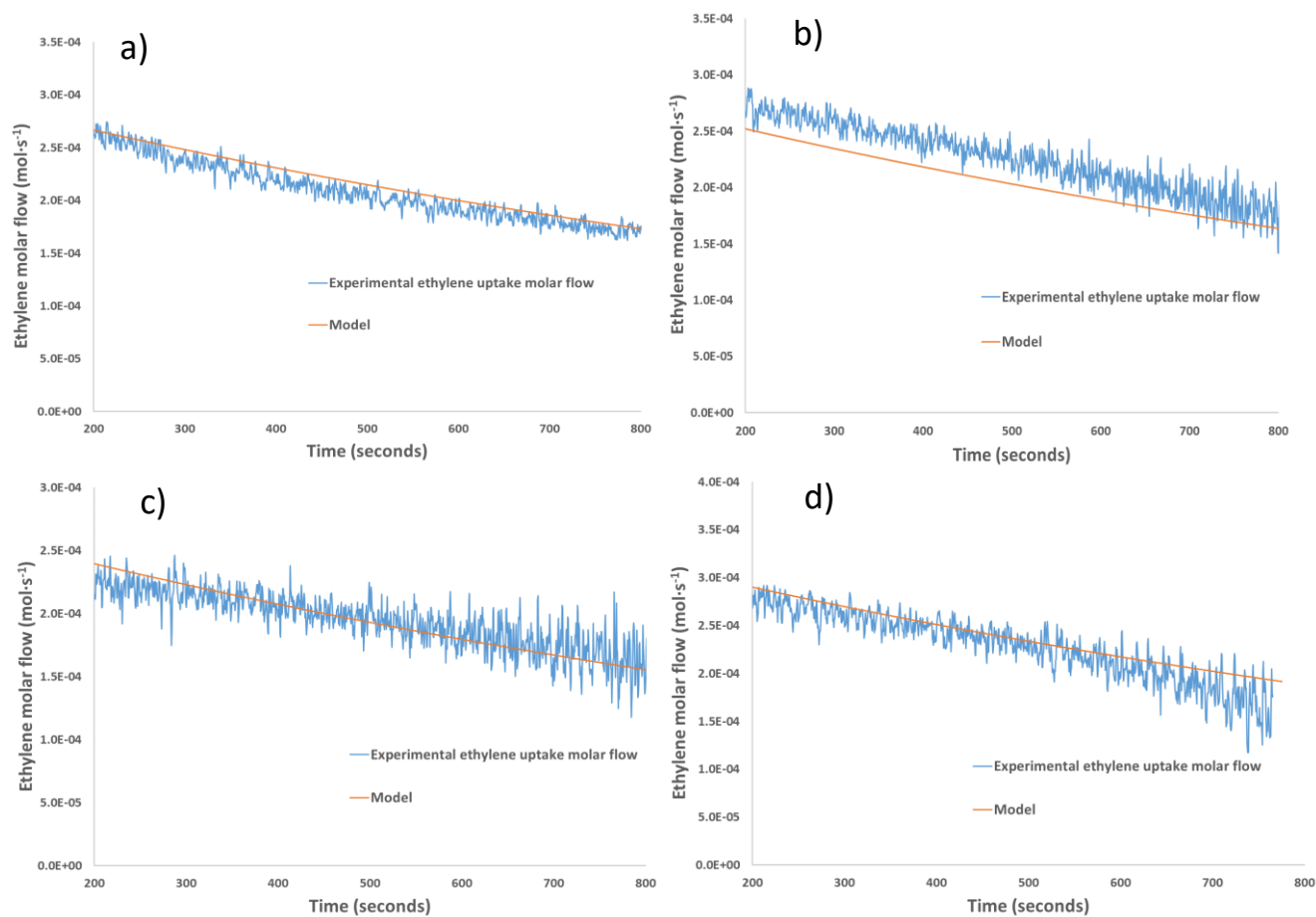
Equation (3.13) was fitted to the data shown in Figure 3-7 to estimate the values of  $k_p \cdot k_f$  and  $k_d$  using the function **fitnlm** (Fit nonlinear regression model) in Matlab. The function fitnlm minimizes least square difference between the experimental ethylene flow respect the model using Levenberg-Marquardt nonlinear least squares algorithm [48]. For model estimation, 10 polymerization runs were used to estimate the model parameters, and the 4 remaining polymerizations were used to validate the model. Table 3-5 lists the parameters estimated by Matlab.

Figure 3-8 compares model predictions with the ethylene uptake curves of the validating polymerizations (not used for model fitting). The data fit shows that the model can describe these polymerizations adequately.

**Table 3-5.** Ethylene polymerization kinetic parameters with  $\text{Cp}_2\text{HfCl}_2$ .

Parameter	Value	SE*	t statistics
$k_p k_f (\text{L}^2\text{mol}^{-2}\text{s}^{-1})$	17,000	28.8	580.33
$k_d (\text{s}^{-1})$	0.00072	$3.66 \times 10^{-6}$	196.84
<b>Number of observations</b>		10,923	
<b>R<sup>2</sup></b>		0.929	

\*SE is standard Error and T is t statistics.



**Figure 3-8.** Validating experimental ethylene uptake curves versus model predictions: a) Homo\_60\_1, b) Homo\_100\_2, c) Homo\_120\_2, and d) Homo\_150\_1.

Finally, Equation (3.15) was integrated over the polymerization time using the following expression

$$- \int d(Fl_E) = \int_0^t k_p k_f [Et]^2 C_{io} V_R e^{-kat} dt \quad (3.16)$$

$$m_p = 28 g \cdot mol^{-1} \cdot \frac{k_p k_f [Et]^2}{k_d} C_{io} V_R [1 - e^{-kat}] \quad (3.17)$$

Where  $m_p$  is polymer yield in grams and  $28 g \cdot mol^{-1}$  is the molar mass of ethylene. Catalyst productivity (*Cat Prod*) was estimated dividing Equation (3.17) over the initial moles of catalyst and the productivity was normalized at 1 hour, leading to the equation

$$\begin{aligned} Cat Prod \left( \frac{g}{\mu mol \cdot h} \right) &= \frac{28 g \cdot mol^{-1}}{1 \cdot 10^6 \mu mol \cdot mol^{-1}} \cdot \frac{k_p k_f [Et]^2}{k_d} [1 - e^{-kat}] \cdot \frac{3600}{t} \\ &= \frac{2,337,160 [Et]^2 [1 - e^{-0.00072 \cdot t(s)}]}{t(s)} \end{aligned} \quad (3.18)$$

Figure 3-9.a compares experimental and estimated productivities. Predicted productivities are slightly higher because the model does not account for the first few seconds of polymerization, as explained above, and is indicated in Figure 3-9.b, but rather sets the flow rate of ethylene flow to zero for the first 150 s of polymerization (region within the red circle).

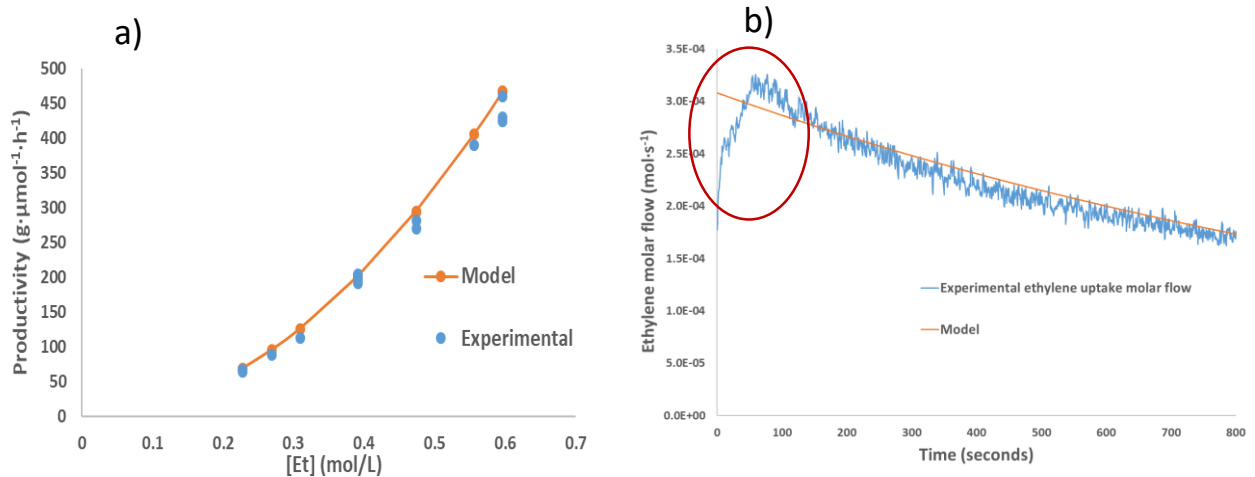


**Figure 3-9:** a) experimental vs predicted productivities and b) model limitations for the first 150 s of polymerization.

### 3.5.3. Arrhenius Constant Estimation

The kinetics constants estimated in Section 3.5.2 were estimated at 120 °C, but they are not valid for other polymerization temperatures. Since polymerization temperatures may vary from process to process, as well as from polymer grade to grade, it is important to estimate the temperature dependence of these constants to simulate commercial reactors.

Ethylene polymerizations were repeated at 100 °C and 140 °C, keeping the ethylene pressure at 0.79 MPa to estimate the Arrhenius law constants for the kinetic parameters, using the same polymerization mechanism proposed in Section 3.5.2.

Polymerizations at 100 °C were challenging to perform. At this lower temperature, the solubility of polyethylene in toluene decreases, causing the polymer to precipitate, likely carrying with it a fraction of the catalyst, affecting the shape of the ethylene uptake curve. The precipitated polymer also got deposited on the cooling coils, making it hard to control the reactor temperature. The decrease in solubility of polyethylene in toluene was estimated using Hildebrand parameters for toluene and polyethylene [49], and the Flory-Huggins model [50]. According to these calculations, polyethylene solubility decreased by almost 50% when the temperature was reduced from 120° C to 100 °C. To minimize this problem, the polymerization time was reduced from 13 to 9 min, since at shorter polymerization times less polymer was produced, which caused less fouling on the reactor cooling coils.

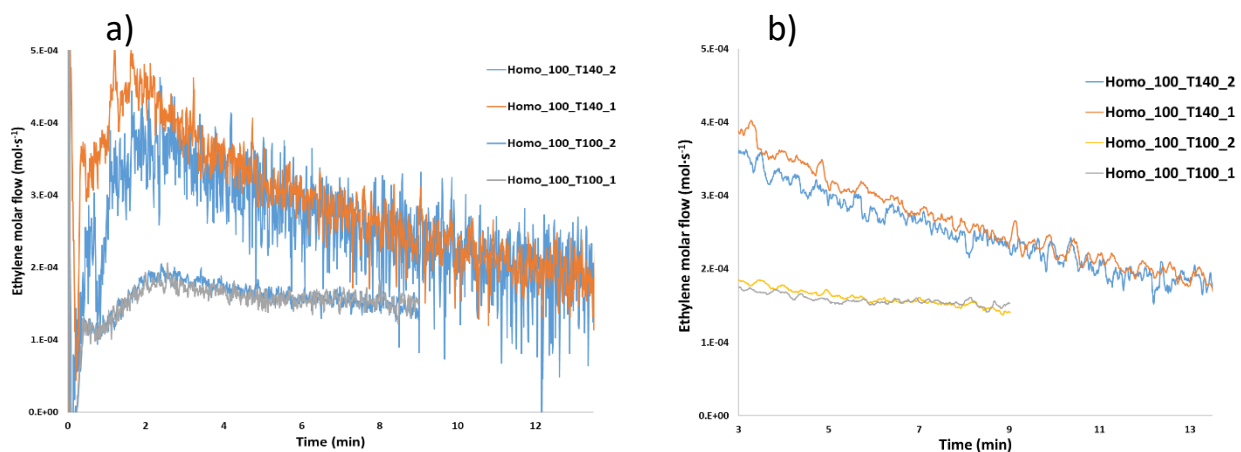
Table 3-6 lists the polymerization conditions for these experiments. All polymerizations were done at 0.79 MPa ethylene pressure. Ethylene uptake curves for each polymerization are shown in Figure 3-10.a. Those curves were normalized to an initial catalyst concentration of 3.91 $\mu$ mol/L, similarly to what was done for Figure 3-6.

**Table 3-6.** Ethylene polymerization conditions at 100 and 140 °C

Polymerization	Temp (°C)*	[C <sub>io</sub> ] ( $\mu$ mol·L <sup>-1</sup> )	V <sub>R</sub> (ml)	[Et] (mol·L <sup>-1</sup> )
Homo_100_T100_1	100	0.39	150.2	0.49
Homo_100_T100_2	100	0.40	150.2	0.49
Homo_100_T140_1	140	0.88	150.4	0.31
Homo_100_T140_2	140	0.57	150.6	0.31

\*Temp is the polymerization temperature.

Similarly to the procedure described in Section 3.5.2, a moving average of 20 seconds was applied to all curves, and the analysis of the data was done after the initial 200 seconds of polymerization, as shown in Figure 3-10.b.



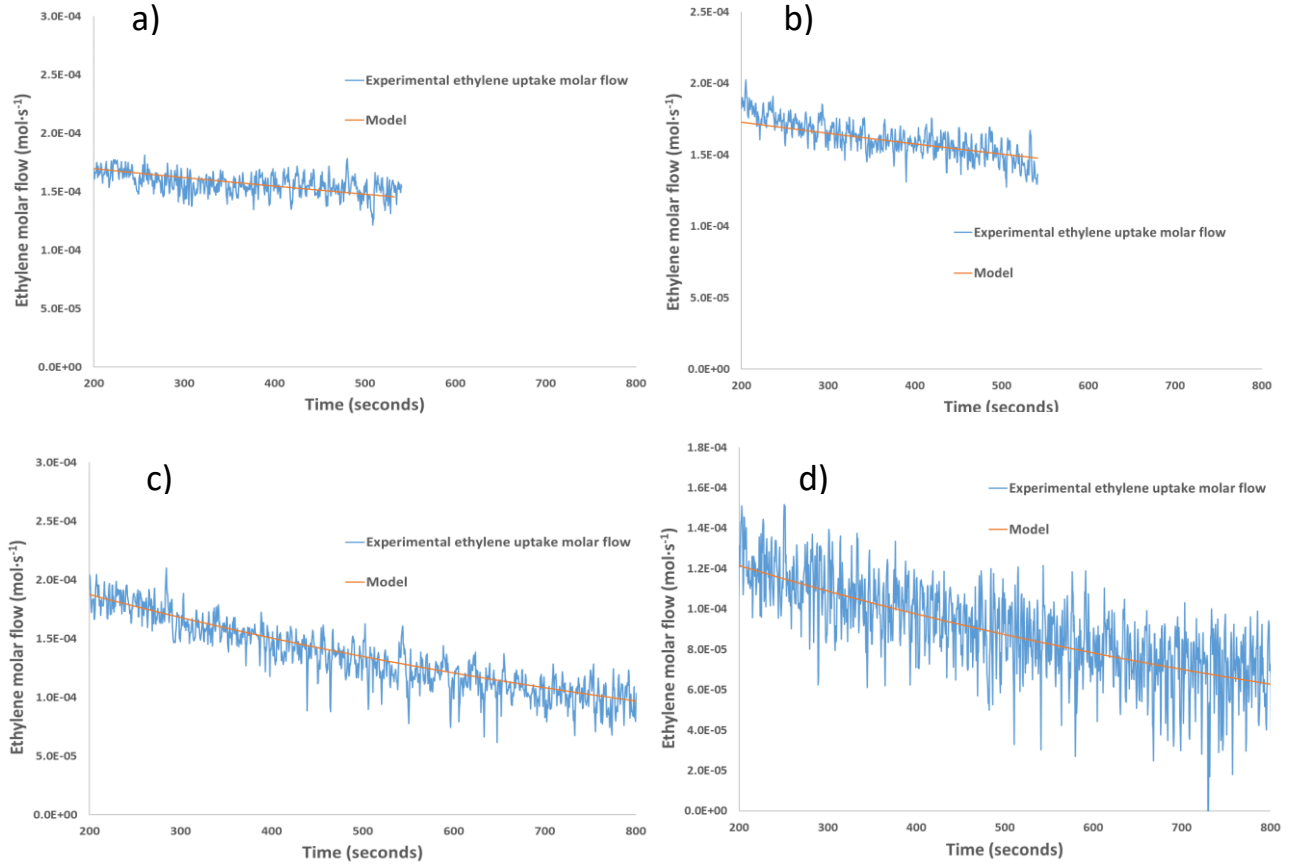
**Figure 3-10.** a) Normalized and, b) moving average uptake ethylene curves polymerizations at 100 °C and 140 °C.

Table 3-7 summarizes the values for the kinetic parameters at these two new temperatures.

**Table 3-7.** Ethylene kinetic parameters for polymerization with  $\text{Cp}_2\text{HfCl}_2$  at 100 and 140 °C

Temp. (°C)	Parameters	Values	SE	T
100	$k_p k_f$ ( $\text{L}^2\text{mol}^{-2}\text{s}^{-1}$ )	13,250	38.1	347.7
	$k_d$ ( $\text{s}^{-1}$ )	0.00046	$7.7 \times 10^{-6}$	60.2
<b>Number of observation: 1,331</b>			<b>R-Squared: 0.746</b>	
140	$k_p k_f$ ( $\text{L}^2\text{mol}^{-2}\text{s}^{-1}$ )	18,540	40.5	457.7
	$k_d$ ( $\text{s}^{-1}$ )	0.0011	$4.7 \times 10^{-6}$	243.2
<b>Number of observation: 2,339</b>			<b>R-Squared: 0.981</b>	

Figure 3-11 shows that the model describes the ethylene uptake curves for these polymerizations adequately.



**Figure 3-11.** Experimental values versus model predictions for polymerizations with  $\text{Cp}_2\text{HfCl}_2$  at 100 °C and 140 °C: a) Homo\_100\_T100\_1, b) Homo\_100\_T100\_2, c) Homo\_100\_T140\_1, and d) Homo\_100\_T140\_2.

Arrhenius law is express as

$$k = A \cdot e^{\frac{-E_a}{RT}} \quad (3.19)$$

which can be linearized as

$$\ln(k) = \ln(A) - \frac{E_a}{RT} \quad (3.20)$$

The polymerization kinetic parameters from Table 3.5 and Table 3.7 were plotted versus the reciprocal of the polymerization temperature (Figure 3-12) to estimate pre-exponential factors and activation energies for each kinetic constant. Table 3-8 summarizes these values.

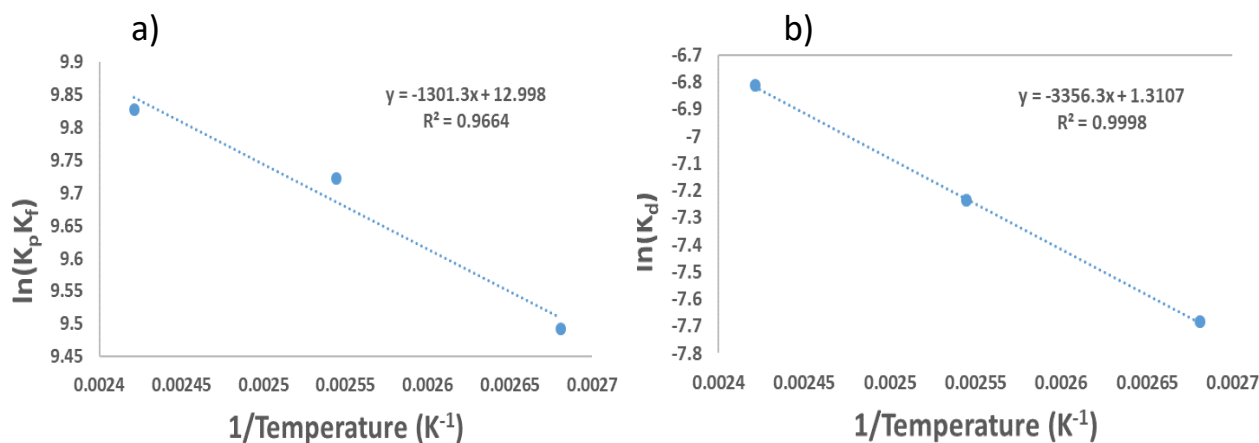


**Figure 3-12.** Arrhenius plot for: a)  $k_p \cdot k_f$  and b)  $k_d$ .

**Table 3-8.** Pre-exponential factors and activation energies for propagation and decay constants for the polymerization of ethylene with  $\text{Cp}_2\text{ZrCl}_2$ .

Kinetic Constants	$A$	$E_a$ (J/mol)
$k_p k_f$	441,530 $\text{L}^2\text{mol}^{-2}\text{s}^{-1}$	10,820
$k_d$	3.70 $\text{s}^{-1}$	27,900

The number and weight average molecular weights of the polyethylene made at 100° C, 120 °C and 140 °C, and 0.79 MPa ethylene pressure are listed in Table 3-9 and illustrated in Figure 3-13.

**Table 3-9.** Number and weight average molecular weight at 100 °C, 120 °C and 140 °C.

Temp. (°C)	$M_w$ (g·mol <sup>-1</sup> )	$M_n$ (g·mol <sup>-1</sup> )	<i>PDI</i>
120	132,100	45,100	2.9
140	54,900	23,000	2.4
100	233,100	81,000	2.9

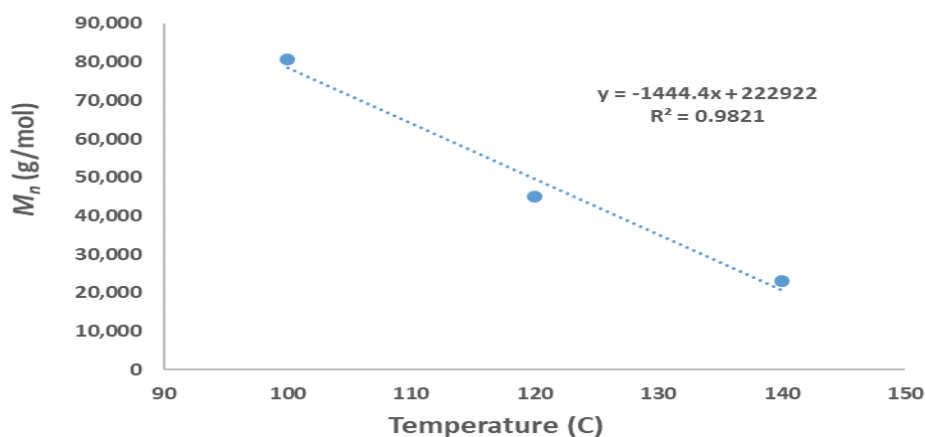


**Figure 3-13.** Number average molecular weights ( $M_n$ ) of polyethylene made at 100 °C, 120 °C and 140 °C with  $Cp_2HfCl_2$ .

The results from Table 3-9 show that in spite of having a higher polymerization constant at higher temperature, the average molecular weight is lower. This can be explained by a higher transfer kinetic constants a higher temperature. That means that the transfer constants increase more rapidly than the propagation constant when the reaction temperature increase.

### 3.5.4. Effect of Hydrogen on the Polymerization Rate of Ethylene

Hydrogen is the chain transfer agent most frequently used to control the molecular weight of polyethylene, but it usually also reduces catalyst activity [26].

Besides transfer to hydrogen, other transfer reactions such as transfer to monomer, transfer to cocatalyst, and  $\beta$ -hydride elimination affect polymer molecular weight [26]. Although, these

transfer reactions in general are not as significant as transfer to hydrogen, they should be estimated to have a better prediction of the polymer molecular weight when hydrogen is not present.

Table 3-10 shows number and weight average molecular weights for polymerization of ethylene reactions with and without hydrogen. The reactions were done at 120 °C.

**Table 3-10.** Number and weight average molecular weight for polymerization of ethylene reactions with/without hydrogen.

Polymerization	$P_E$ (MPa)	$[H_2]$ (mmol·L <sup>-1</sup> )*	$[Et]$ (mol·L <sup>-1</sup> )	$M_n$ (g·mol <sup>-1</sup> )	$M_w$ (g·mol <sup>-1</sup> )	PDI
Homo_60_1	0.51	0	0.23	21,400	55,200	2.6
Homo_60_2	0.51	0	0.23	17,900	49,800	2.8
Homo_100_4	0.79	0	0.39	39,400	98,500	2.5
Homo_100_5	0.79	0	0.39	43,000	115,300	2.7
Homo_120_1	0.93	0	0.47	45,300	134,100	3.0
Homo_150_2	1.14	0	0.60	63,800	181,100	2.8
Homo_150_3	1.14	0	0.60	65,100	190,900	2.9
Homo_100_H_1	0.79	3.89	0.36	3,400	7,200	2.1
Homo_100_H_2	0.79	2.99	0.37	5,300	13,100	2.5
Homo_100_H_3	0.79	2.14	0.37	9,100	20,400	2.2
Homo_150_H_1	1.14	5.27	0.55	3,600	8,200	2.2
Homo_150_H_2	1.14	3.95	0.56	4,900	11,400	2.3
Homo_150_H_3	1.14	2.63	0.58	8,900	20,900	2.3

\* $[H_2]$  is hydrogen concentration in toluene.

Based on the polymerization mechanism proposed in Table 3-3, Table 3-11 shows the extended mechanism including transfer reactions.

**Table 3-11.** Proposed mechanism for the polymerization of ethylene including transfer reactions with  $\text{Cp}_2\text{HfCl}_2$ .

Description	Chemical equations	Rate Constants
Activation	$C + Al-Et_3 \rightarrow P_0$	$k_a \rightarrow \infty$
Coordination	$P_0 + M \rightarrow P_0 \cdot M$	$k_f$
Propagation	$P_r \cdot M + M \rightarrow P_{r+1} + M$	$k_p$
Monomer	$P_r \cdot M + M \rightarrow P_0 + D_r$	$k_{tM}$
$\beta$ -Hydride elimination	$P_r \cdot M \rightarrow P_0 + D_r$	$k_{t\beta}$
Transfer to cocatalyst	$P_r \cdot M + Al-A_3 \rightarrow P_0 + D_r$	$k_{tAl}$
Transfer to hydrogen	$P_r \cdot M + H_2 \rightarrow P_H \cdot M + D_r$	$k_{tH}$

The polymer number average chain length,  $r_n$ , is the ratio of propagation rate to chain transfer rate [26]

$$r_n = \frac{R_p}{R_t} \quad (3.21)$$

$R_p$  was defined in Equations (3.7) and (3.8) and  $R_t$  refers to all chain transfer reactions in the mechanism. In our case, the chain transfer reactions are:

*Transfer to Monomer*

$$R_{tM} = k_{tM}[M][Y_0 \cdot M] \quad (3.22)$$

*$\beta$ -Hydride elimination*

$$R_{t\beta} = k_{t\beta}[Y_0 \cdot M] \quad (3.23)$$

*Transfer to cocatalyst*

$$R_{tAl} = k_{tAl}[Y_0 \cdot M][Al] \quad (3.24)$$

*Transfer to hydrogen*

$$R_{tH} = k_{tH} [Y_0 \cdot M][H_2] \quad (3.25)$$

$r_n$  can also be defined as [26]

$$r_n = \frac{M_n}{mw} \quad (3.26)$$

where  $mw$  is the molecular weight of the monomer; 28.05 g/mol for ethylene.

Combining Equations (3.7), (3.8) and (3.21) to (3.26), and rearranging the terms,  $r_n$  or  $M_n$  can be expressed in term of propagation and transfer rate constants as

$$\begin{aligned} \frac{1}{r_n} = \frac{mw}{M_n} = \frac{R_t}{R_p} &= \frac{k_{tM} [Y_0 \cdot M][M] + k_{t\beta} [Y_0 \cdot M] + k_{tAl} [Y_0 \cdot M][Al] + k_{tH} [Y_0 \cdot M][H_2]}{k_p [M][Y_0 \cdot M]} \\ &= \frac{k_{tM}}{k_p} + \frac{(k_{t\beta} + k_{tAl} [Al])}{k_p [M]} + \frac{k_{tH} [H_2]}{k_p [M]} \end{aligned} \quad (3.27)$$

From Equation (3.27),  $M_n$  is function of hydrogen, aluminum and ethylene concentrations, and transfer and propagation constants. In a first step  $\frac{k_{tM}}{k_p}$  and  $\frac{(k_{t\beta} + k_{tAl} [Al])}{k_p}$  were estimated when the hydrogen concentration was zero. Figure 3-14 shows a plot of  $\frac{mw}{M_n}$  versus  $\frac{1}{[M]}$  for the polymerizations done without hydrogen.

Figure 3-14.a shows that the estimate for  $\frac{(k_{t\beta} + k_{tAl} [Al])}{k_p}$  was 0.0004, and for  $\frac{k_{tM}}{k_p}$  was -0.0002. The negative value has no physical meaning, but indicates that this is a small value. Thus, the correlation was modified by setting the intercept to zero (Figure 3-14.b). The resulting equation still has a good correlation between the variables with a  $R^2 = 0.93$ . As a result, that  $\frac{(k_{t\beta} + k_{tAl} [Al])}{k_p}$  was estimated to be 0.0003 and  $\frac{k_{tM}}{k_p}$  near to zero.

To estimate  $\frac{k_{tH}}{k_p}$ , Equation (3.27) was re-arranged to

$$\left( \frac{mw}{M_n} - \frac{k_{tM}}{k_p} \right) \cdot [M] = \frac{(k_{t\beta} + k_{tAl} [Al])}{k_p} + \frac{k_{tH} [H_2]}{k_p} \quad (3.28)$$

Assuming the value estimated for  $\frac{k_{tM}}{k_p}$  was zero, Equation (3.28) could be simplified to

$$\left( \frac{mw}{M_n} \right) \cdot [M] = \frac{(k_{t\beta} + k_{tAl} [Al])}{k_p} + \frac{k_{tH} [H_2]}{k_p} \quad (3.29)$$

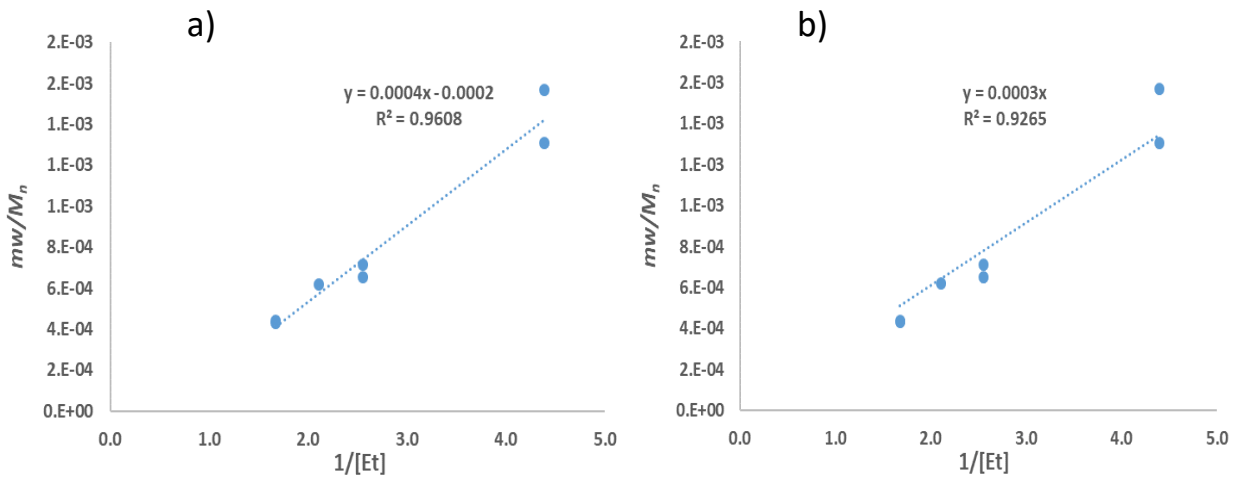


**Figure 3-14.** Relations between  $M_n$  and ethylene concentration: a) Non adjusted intercept, and b) intercept set to zero.

To estimate  $\frac{k_{tH}}{k_p}$ , the term  $\left(\frac{mw}{M_n}\right) \cdot [M]$  was estimated for polymerizations with hydrogen (Figure 3.15).

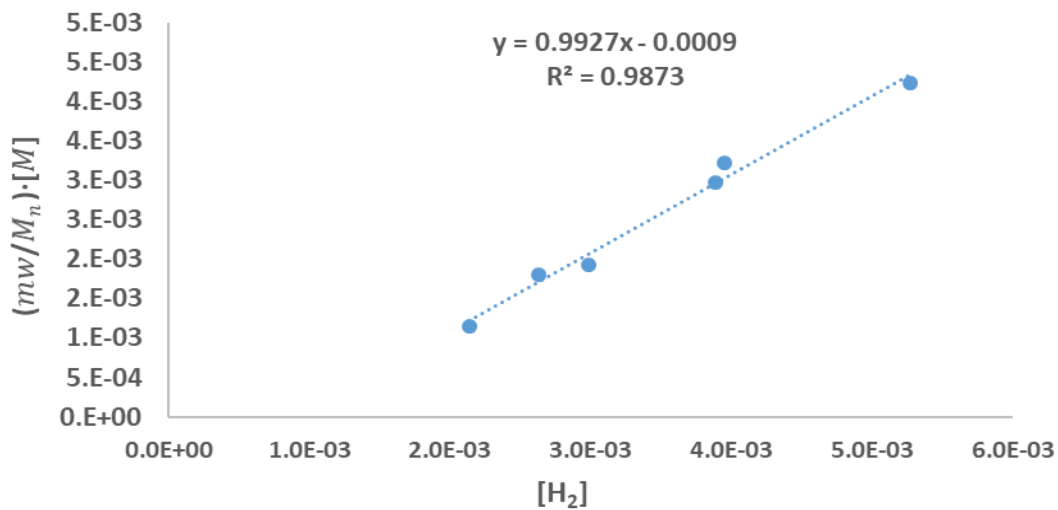


**Figure 3-15.** Correlation of  $\left(\frac{mw}{M_n}\right) \cdot [M]$  versus hydrogen concentration.

The data in Figure 3-16 show that  $\frac{k_{tH}}{k_p} = 0.9927$  and  $\frac{(k_{t\beta} + k_{tAl} [Al])}{k_p} = -0.0009$ . The negative value for the last term has no physical meaning, but it indicates that it is a much smaller value than  $\frac{k_{tH}}{k_p}$ ,

as expected. Besides, the estimate for  $\frac{(k_{t\beta} + k_{tAl} [Al])}{k_p}$  in Figure 3-15 was 0.0003. Thus, the value for this parameter is likely between 0 and 0.0003. Table 3-12 summarizes the values proposed for these constants.

**Table 3-12.** Ratio of transfer constants to propagation constant

Parameters	Values
$\frac{k_{tM}}{k_p}$	$1 \times 10^{-5}$
$\frac{(k_{t\beta} + k_{tAl} [Al])}{k_p}$	$2.8 \times 10^{-5}$
$\frac{k_{tH}}{k_p}$	0.9927

The values for  $M_n$  predicted with Equation (3.27) were validated using the parameters estimated in Table 3-12, and was compared with the experimental values from Table 3-10 (Figure 3-16).

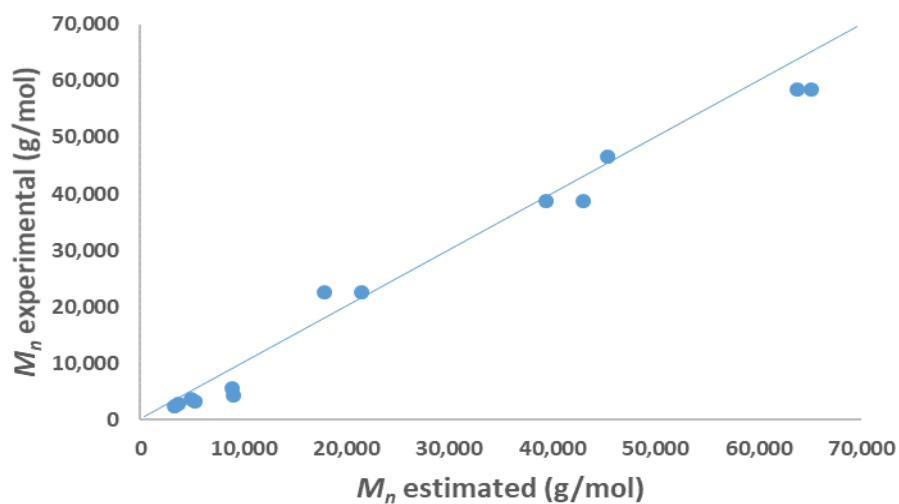


**Figure 3-16.** Number average molecular weight estimated versus experimental.

Although the estimates do not exactly fall on the 45° line, they provide reasonable predictions for  $M_n$ .

Table 3-11 also proposes that when a living polymer chain reacts with hydrogen, one hydrogen atom is added to the end of a dead polymer chain, while the other hydrogen atom bonds to the metal center, forming a metal hydride represented as  $P_H \cdot M$ . This species may have lower reactivity toward monomer addition [26], which explains why catalyst productivity decreases when hydrogen is added to the reactor (Table 3-13).

**Table 3-13.** Proposed mechanism for the polymerization of ethylene with transfer and re-activation reactions with  $Cp_2HfCl_2$ .

Description	Chemical equations	Rate Constants
Activation	$C + Al-Et_3 \rightarrow P_0$	$k_a \rightarrow \infty$
Coordination	$P_0 + M \rightarrow P_0 \cdot M$	$k_f$
Propagation	$P_r \cdot M + M \rightarrow P_{r+1} + M$	$k_p$
Transfer to monomer	$P_r \cdot M + M \rightarrow P_0 + D_r$	$k_{tM}$
$\beta$ -Hydride elimination	$P_r \cdot M \rightarrow P_0 + D_r$	$k_{t\beta}$
Transfer to cocatalyst	$P_r \cdot M + Al-A_3 \rightarrow P_0 + D_r$	$k_{tAl}$
Transfer to hydrogen	$P_r \cdot M + H_2 \rightarrow P_H \cdot M + D_r$	$k_{tH}$
Initiation	$P_H \cdot M + M \rightarrow P_1 + M$	$k_{iH}$
First order deactivation	$P_r \rightarrow C_d + D_r$	$k_d$

Similarly to Equation (3.14) in Section 3.5.2, an expression based on the ethylene consumption in the reactor was derived as a function of the mechanism proposed in Table 3-13. The rate of polymerization is given as

$$R_p = -\frac{d[M]}{dt} = k_p k_f [M]^2 [Y_0] \quad (3.30)$$

The total concentration of living species in the reactor can be expressed as

$$[P^*] = [Y_0] + [P_H \cdot M] \quad (3.31)$$

Combining Equations (3.30) and (3.31), and rearranging as a function of living species

$$R_p = k_p k_f [M]^2 \frac{[P^*]}{[Y_0] + [P_H \cdot M]} [Y_0] = k_p k_f [M]^2 \frac{[Y_0]}{[Y_0] + [P_H \cdot M]} [P^*] \quad (3.31)$$

$$R_p = k_p k_f [M]^2 \frac{1}{1 + \frac{[P_H \cdot M]}{[Y_0]}} [P^*] \quad (3.32)$$

The molar balance for metal hydride species is

$$\frac{d[P_H \cdot M]}{dt} = k_{tH} [Y_0 \cdot M][H_2] - k_{iH} [P_H \cdot M][M] \quad (3.33)$$

Assuming steady state for the intermediate species simplifies Equation (3.33), leads to

$$\frac{d[P_H \cdot M]}{dt} = 0 = k_{tH} [Y_0 \cdot M][H_2] - k_{iH} [P_H \cdot M][M] \quad (3.34)$$

$$k_{iH} [P_H \cdot M][M] = k_{tH} [Y_0 \cdot M][H_2] \rightarrow \frac{[P_H \cdot M]}{[Y_0 \cdot M]} = \frac{k_{tH} [H_2]}{k_{iH} [M]} \quad (3.34)$$

$$\frac{[P_H \cdot M]}{[Y_0]} = \frac{k_f k_{tH} [H_2][M]}{k_{iH} [M]} = \frac{k_f k_{tH} [H_2]}{k_{iH}} \quad (3.34)$$

Substitution Equation (3.34) in Equation (3.32) results in

$$R_p = k_p k_f [M]^2 \frac{1}{1 + \frac{k_f k_{tH} [H_2]}{k_{iH}}} [P^*] = k_p k_f [M]^2 \frac{k_{iH}}{k_{iH} + k_f k_{tH} [H_2]} [P^*] \quad (3.35)$$

Although there are different types of living species in the reactor ( $P_r \cdot M$ ,  $P_o$  and  $P_H \cdot M$ ), the total concentration of living species is affected by the initial catalyst concentration (Generation) and by the catalyst decay rate (Consumption). As a result, the generation and decay of living species can be described by:

$$\textbf{Generation: } [P^*] = C_{i0} \quad (3.36)$$

$$\textbf{Decay: } [P^*] = k_d [Y_0] \quad (3.37)$$

The molar balance of the living species is giving by

$$\frac{d[P^*]}{dt} = \frac{d[[Y_0] + [P_H \cdot M]]}{dt} = C_{i0} - k_d [Y_0] \quad (3.38)$$

$$\frac{d[Y_0]}{dt} + \frac{d[P_H \cdot M]}{dt} = C_{i0} - k_d [Y_0] \quad (3.39)$$

Assuming steady state for the intermediate species, Equation (3.39) can be simplified to

$$\frac{d[Y_0]}{dt} = C_{io} - k_d [Y_0] \quad (3.40)$$

Solving differential Equation (3.40), where at  $t = 0$ ,  $[Y_0] = 0$

$$[P^*] = [Y_0] = C_{io} e^{-k_d t} \quad (3.41)$$

Replacing Equation (3.41) in Equation (3.35), a final expression for the polymerization rate is given by

$$R_p = k_p k_f [M]^2 \frac{k_{iH}}{k_{iH} + k_f k_{tH} [H_2]} C_{io} e^{-k_d t} = k_p k_f [M]^2 \frac{k_{iH}}{k_{iH} + k_p k_f \left(\frac{k_{tH}}{k_p}\right) [H_2]} C_{io} e^{-k_d t} \quad (3.42)$$

Equation (3.42) can be expressed as the rate of ethylene molar flow ( $Fl_E$ ):

$$-\frac{d(Fl_E)}{dt} = k_p k_f [M]^2 \frac{k_{iH}}{k_{iH} + k_p k_f \left(\frac{k_{tH}}{k_p}\right) [H_2]} C_{io} V_R e^{-k_d t} \quad (3.43)$$

Equation (3.43) was fitted to the data shown in Figure 3.17.b. In this case,  $\frac{k_{tH}}{k_p}$  was estimated previously Table 3-12. Thus, there is one constant less to estimated.

Table 3-14 lists the conditions for the polymerizations used to study the influence of hydrogen concentration on ethylene polymerization rate. All polymerizations were performed at 120 C.

**Table 3-14.** Ethylene polymerization conditions varying hydrogen concentration.

Polymerization	P <sub>E</sub> (MPa)	[Et] (mol·L <sup>-1</sup> )	[H <sub>2</sub> ] (mmol·L <sup>-1</sup> )	[C <sub>io</sub> ] (μmol·L <sup>-1</sup> )	V <sub>R</sub> (ml)
Homo_100_H_1	0.79	0.36	3.89	2.04	150.0
Homo_100_H_2	0.79	0.37	2.99	2.04	150.0
Homo_100_H_3	0.79	0.37	2.14	2.68	150.0
Homo_150_H_1	1.14	0.55	5.27	1.22	149.6
Homo_150_H_2	1.14	0.56	3.95	1.19	149.6
Homo_150_H_3	1.14	0.58	2.63	1.25	149.6

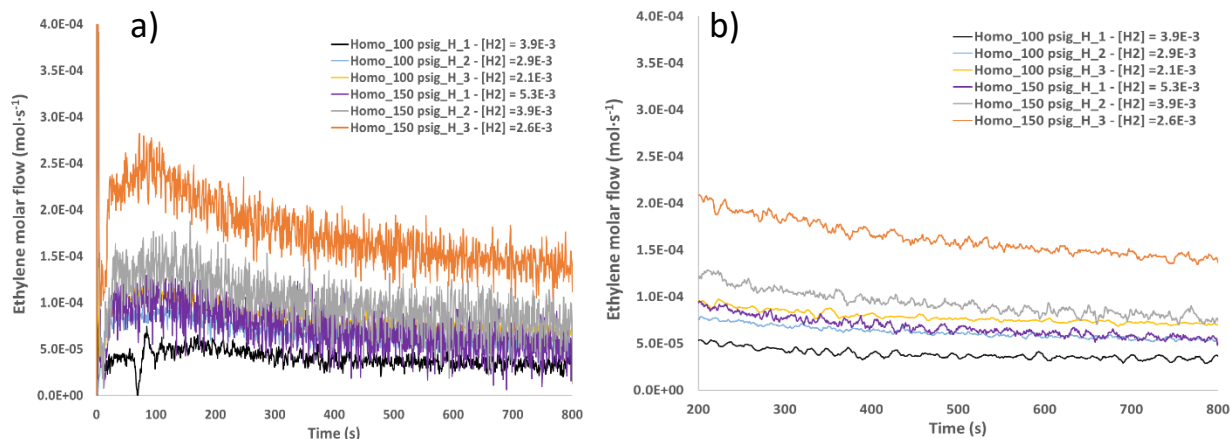


**Figure 3-17.** a) Normalized and b) moving average uptake ethylene curves polymerizations varying hydrogen concentration.

Matlab was used to estimate the kinetic constants of Equation (3.43) using the function fitnlm. Besides the previous information, the ethylene polymerization without hydrogen from section 3.5.2 was also included in order to have a model to predict the consumption of ethylene with and without hydrogen. The results are presented in Table 3-15.

**Table 3-15.** Kinetic Parameters of ethylene polymerizations with/without hydrogen

Parameter	Value	SE	T
$k_p k_f$ ( $L^2 mol^{-2} s^{-1}$ )	16,510	24.5	674.3
$k_{iH}$ ( $L^2 mol^{-2} s^{-1}$ )	11.6	0.024	483.2
$k_d$ ( $s^{-1}$ )	0.00069	$3.1 \times 10^{-6}$	224.4
<b>Number of observation:</b>		18,036	
<b>R-Squared:</b>		0.964	

The values estimated for  $k_p k_f$  and  $k_d$  are similar to those reported in Table 3-5.  $k_{tH}$  can be estimated using the value of its ratio to propagation constant from Table 3-12.

$$\frac{k_{tH}}{k_p} = \frac{k_{tH} k_f}{k_p k_f} = 0.9927 \rightarrow k_{tH} k_f = 0.9927 \cdot k_p k_f = 16,392 \quad (3.43)$$

These constants were tested in the polymerization reaction with hydrogen of Table 3-14 and ethylene polymerization of section 3.5.2 (Homo\_60\_1, Homo\_100\_2, Homo\_120\_2 and Homo\_150\_1). Figures 3-18 and 3-19 compare the model and experimental ethylene uptake curves.

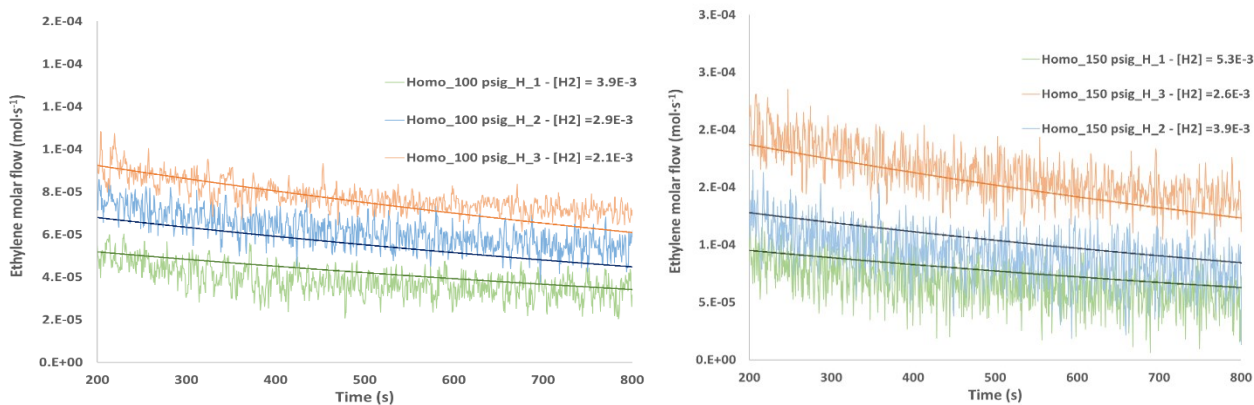


**Figure 3-18.** Ethylene polymerizations with hydrogen versus model

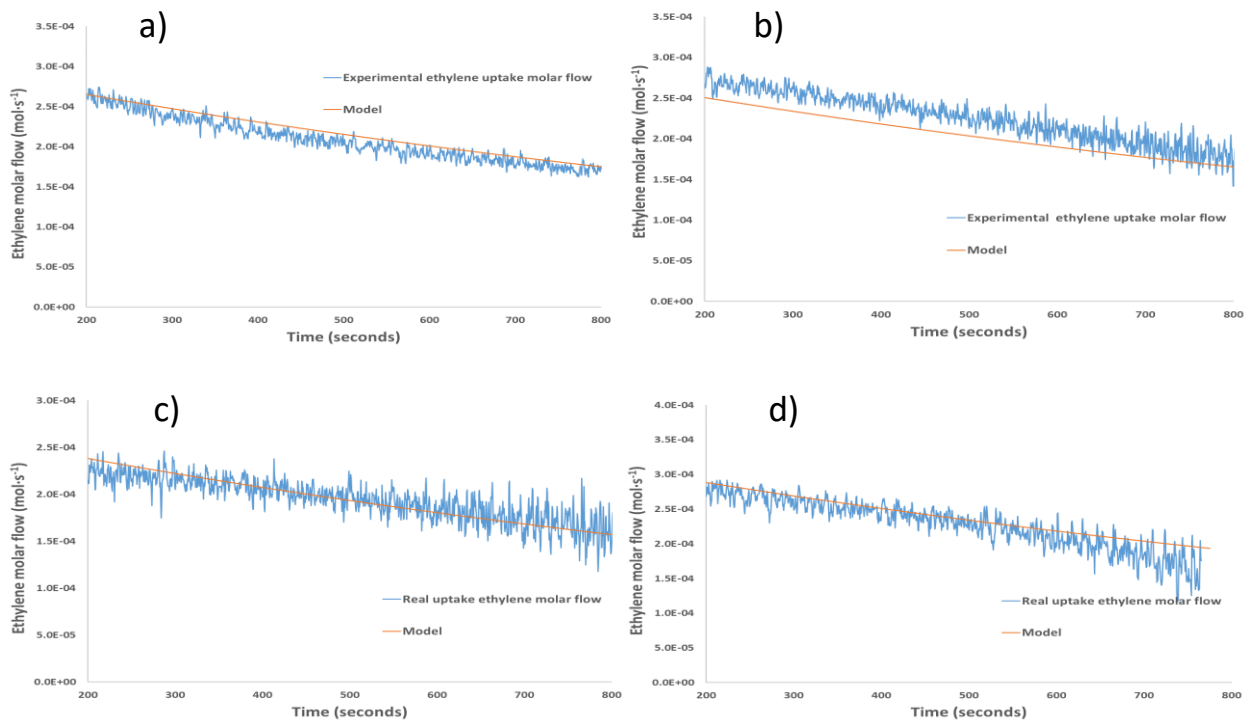


**Figure 3-19.** Experimental values versus model predictions for polymerizations with  $Cp_2HfCl_2$  without hydrogen: a) Homo\_60\_1, b) Homo\_100\_2, c) Homo\_120\_2, and d) Homo\_150\_1.

Thus, the model proposed in Table 3-13 explains the ethylene uptake curves and the number average molecular weight of the catalyst  $\text{Cp}_2\text{HfCl}_2$

### 3.5.5. Ethylene/1-Hexene Copolymerization with $\text{Cp}_2\text{HfCl}_2$

Finally, the kinetic constants of the catalyst toward a comonomer, in this case 1-Hexene, was estimated. First, the reactivity ratios ( $r_A$  and  $r_B$ ) of the catalyst toward ethylene and 1-hexene was estimated. The Mayo-Lewis equation, relates the average mole fraction of monomer A in the copolymer,  $\overline{F}_A$ , to mole fraction of monomer A in the reactor,  $f_A$ , through the reactivity ratios as it is expressed in the Equation (3.44) [29].

$$\overline{F}_A = \frac{r_A \cdot f_A^2 + f_A \cdot (1 - f_A)}{r_A \cdot f_A^2 + 2 \cdot f_A \cdot (1 - f_A) + r_B \cdot (1 - f_A)^2} \quad (3.44)$$

Where  $r_A = \frac{k_{pAA}}{k_{pAB}}$  and  $r_B = \frac{k_{pBB}}{k_{pBA}}$ . In our case, A is ethylene and B is 1-hexene.

Twelve ethylene/1-hexene copolymerizations were conducted to estimate the reactivity ratios. Table 3-16 lists the ethylene and 1-hexene concentrations in toluene for each copolymerization, and the average 1-hexene content in the copolymers ( $F_{1\text{-hexene}}$ ) expressed as mole fraction.

The mole fraction of ethylene concentration in toluene is defined by the following expression:

$$f_{ethylene} = \frac{[Ethylene]}{[Ethylene] + [1 - hexene]} \quad (3.45)$$

And the average ethylene content in the copolymer by:

$$F_{ethylene} = 1 - F_{1\text{-hexene}} \quad (3.46)$$

$f_{ethylene}$  and  $F_{ethylene}$  are estimated in Table 3-17.

**Table 3-16.** Ethylene and 1-hexene concentrations for copolymerizations with Cp<sub>2</sub>HfCl<sub>2</sub> and the average 1-Hexene content in the copolymer.

Reaction	P <sub>E</sub> (MPa)	[Et] (mol·L <sup>-1</sup> )	[1-Hexene] (mol·L <sup>-1</sup> )*	Melting Temp. (°C)	F <sub>1-Hexene</sub>
Copo_60_1	0.51	0.223	0.34	86.8	0.043
Copo_100_1	0.79	0.393	0.17	113.7	0.014
Copo_100_2	0.79	0.390	0.39	106.7	0.021
Copo_100_3	0.79	0.387	0.51	99.7	0.029
Copo_100_4	0.79	0.384	0.68	87.0	0.043
Copo_100_5	0.79	0.378	1.01	77.6	0.053
Copo_100_6	0.79	0.378	1.01	78.6	0.052
Copo_125_1	0.96	0.490	0.63	106.4	0.022
Copo_150_1	1.14	0.601	0.24	114.4	0.013
Copo_150_2	1.14	0.597	0.50	109.6	0.018
Copo_150_3	1.14	0.597	0.50	108.4	0.019
Copo_150_4	1.14	0.594	0.76	104.0	0.024

\* [1-Hexene] is 1-hexene concentration in toluene.

**Table 3-17.** Estimated mole fraction of ethylene concentration in toluene for copolymerizations and the average ethylene content in the copolymer.

Copolymerization	<i>f</i> <sub>Ethylene</sub>	<i>F</i> <sub>Ethylene</sub>
Copo_60_1	0.393	0.957
Copo_100_1	0.696	0.986
Copo_100_2	0.500	0.979
Copo_100_3	0.431	0.971
Copo_100_4	0.361	0.957
Copo_100_5	0.272	0.947
Copo_100_6	0.272	0.948
Copo_125_1	0.437	0.978
Copo_150_1	0.714	0.987
Copo_150_2	0.544	0.982
Copo_150_3	0.543	0.981
Copo_150_4	0.440	0.976
Homopolymers	1	1

Using the results from Table 3-17 and the function fitlm in Matlab, the reactivity ratios of Equation (3.44) were estimated. Table 3-18 shows the final results and Figure 3-20 compares the results of the Mayo-Lewis equation versus experimental values.

**Table 3-18.** Estimated reactivity ratios for ethylene/1-hexene copolymerizations with  $\text{Cp}_2\text{HfCl}_2$

Parameters	Values	SE	T
$r_A$	42.1	5.3	7.9
$r_B$	0	0.06	0
<b>Number of observation:</b>	13		
<b>R-Squared:</b>	0.91		

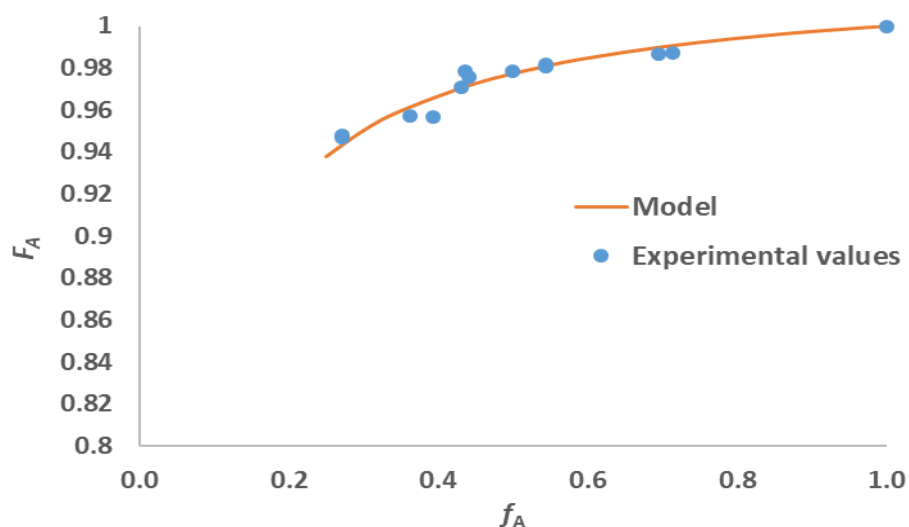


**Figure 3-20.** Experimental average ethylene content in copolymers vs the Mayo-Lewis equation for  $\text{Cp}_2\text{HfCl}_2$

Table 3-19 shows the proposed mechanism for ethylene/1-hexene copolymerization with  $\text{Cp}_2\text{HfCl}_2$ . The trigger mechanism was used in previous sections to explain the second order behavior of the catalyst and it was used Table 3-19. However, in this case, the coordination nature

between the type of monomer and the catalyst could affect the “trigger” mechanism to the polymer chain, as a result, two coordination reactions were proposed. The Bernoullian model [26] was used to explain the propagation reactions for the copolymerization. However, as each monomer could propagate different with the species  $[P_r \cdot A]$  and  $[P_r \cdot B]$ , the resulting model looks like a terminal model [26]. This explains why four propagation constants are used for the copolymerization mechanisms.

**Table 3-19.** Proposed ethylene/1-hexene copolymerization mechanism with  $Cp_2HfCl_2$

Description	Chemical equations	Rate Constants
<b>Activation</b>	$C + Al-Et_3 \rightarrow P_0$	$k_a \rightarrow \infty$
<b>Coordination</b>	$P_0 + A \rightarrow P_0 \cdot A$	$k_f$
	$P_0 + B \rightarrow P_0 \cdot B$	$k_f$
<b>Propagation</b>	$P_r \cdot A + A \rightarrow P_{r+1} + A$	$k_{pAA}$
	$P_r \cdot A + B \rightarrow P_{r+1} + B$	$k_{pAB}$
	$P_r \cdot B + A \rightarrow P_{r+1} + A$	$k_{pBA}$
	$P_r \cdot B + B \rightarrow P_{r+1} + B$	$k_{pBB}$
<b>First order deactivation</b>	$P_r \rightarrow C_d + D_r$	$k_d$

$A$  is ethylene,  $B$  is 1-hexene, and  $M$  to ethylene plus 1-hexene.

The polymerization rate of ethylene ( $A$ ) could be expressed as:

$$R_A = -\frac{d[A]}{dt} = k_{pAA}[A][Y_0 \cdot A] + k_{pBA}[A][Y_0 \cdot B] = (k_{pAA}[Y_0 \cdot A] + k_{pBA}[Y_0 \cdot B])[A] \quad (3.47)$$

The total living polymer chains coordinates with ethylene ( $\phi_A$ ) and 1-hexene ( $\phi_B$ ) could be expressed as:

$$[Y_0 \cdot M] = [Y_0 \cdot A] + [Y_0 \cdot B] \rightarrow 1 = \frac{[Y_0 \cdot A]}{[Y_0 \cdot M]} + \frac{[Y_0 \cdot B]}{[Y_0 \cdot M]} = \phi_A + \phi_B \quad (3.48)$$

$$\phi_A + \phi_B = 1 \quad (3.49)$$

The total living polymer chains  $\phi_A$  and  $\phi_B$  can be estimated using the hypothesis Long Chain Approximation [26]. This considers that the number of AB insertions should be equal to BA insertions. This can be expressed by the following expression:

$$k_{pAB}[Y_0 \cdot A][B] = k_{pBA}[Y_0 \cdot B][A] \rightarrow k_{pAB}\phi_A f_B = k_{pBA}\phi_B f_A \quad (3.50)$$

$$k_{pAB}\phi_A f_B = k_{pBA}(1 - \phi_A)f_A \rightarrow \phi_A = \frac{k_{pBA}f_A}{k_{pAB}f_B + k_{pBA}f_A} \quad (3.51)$$

$f_A$  was defined in Equation (3.45).

Combining Equations (3.51) and (3.47), the polymerization rate of ethylene can be expressed in terms more feasible to estimate:

$$R_A = (k_{pAA}\phi_A + k_{pBA}\phi_B)[Y_0 \cdot M][A] \rightarrow R_A = (k_{pAA}(1 - \phi_B) + k_{pBA}\phi_B)[Y_0 \cdot M][A] \quad (3.52)$$

$$R_A = \left( k_{pAA} + (k_{pBA} - k_{pAA}) \frac{k_{pAB}f_B}{k_{pAB}f_B + k_{pBA}f_A} \right) [Y_0 \cdot M][A] \quad (3.53)$$

$$R_A = \left( k_{pAA} + (k_{pBA} - k_{pAA}) \frac{\frac{k_{pAA}}{r_A} f_B}{\frac{k_{pAA}}{r_A} f_B + k_{pBA}f_A} \right) [Y_0 \cdot M][A] \quad (3.54)$$

The term  $\left( k_{pAA} + (k_{pBA} - k_{pAA}) \frac{\frac{k_{pAA}}{r_A} f_b}{\frac{k_{pAA}}{r_A} f_B + k_{pBA}f_A} \right)$  could be replaced by the pseudo constant  $\widetilde{k}_p$ .

$$R_A = -\frac{d[A]}{dt} = \widetilde{k}_p [Y_0 \cdot M][A] \quad (3.55)$$

If the copolymer reactions are done at constant  $f_A$  and  $f_B$ , Equation (3.55) could be solve similarly to Equation (3.7), thus, the polymerization rate of ethylene could be expressed as:

$$R_A = -\frac{d[A]}{dt} = \widetilde{k}_p k_f [M][A] C_{io} e^{-k_d t} \quad (3.56)$$

$$R_A = \left( k_{pAA}k_f + (k_{pBA}k_f - k_{pAA}k_f) \frac{\frac{k_{pAA}k_f}{r_A} f_b}{\frac{k_{pAA}k_f}{r_A} f_B + k_{pBA}k_f f_A} \right) [M][A] C_{io} e^{-k_d t} \quad (3.57)$$

Table 3-20 lists the conditions for the copolymerization runs used to estimate the parameters of Equation (3.57).  $r_A$  was estimated in Table 3-18, thus, there is one parameter less to estimated.

**Table 3-20.** Ethylene/1-hexene copolymerization conditions

<b>Reactions</b>	<b>[Et] (mol·L<sup>-1</sup>)</b>	<b>[1-Hexene] (mol·L<sup>-1</sup>)</b>	<b>[C<sub>io</sub>] (μmol·L<sup>-1</sup>)</b>	<b>V<sub>R</sub> (ml)</b>
Copo_60_1	0.223	0.34	1.30	149.9
Copo_100_1	0.393	0.17	0.80	149.8
Copo_100_2	0.390	0.39	0.78	150.4
Copo_100_3	0.387	0.51	0.63	150.0
Copo_100_4	0.384	0.68	0.81	149.5
Copo_100_5	0.378	1.01	0.75	150.6
Copo_100_6	0.378	1.01	1.10	150.3
Copo_125_1	0.490	0.63	0.56	150.0
Copo_150_1	0.601	0.24	0.36	156.7
Copo_150_2	0.597	0.50	0.39	150.3
Copo_150_3	0.597	0.50	0.38	150.3
Copo_150_4	0.594	0.76	0.34	149.9

Ethylene uptake curves for each polymerization are shown in Figure 3-21. Those curves were normalized to an initial catalyst concentration of 6.3 μmol/L, similarly to what was done for Figure 3-6.

Similarly to the procedure described in Section 3.5.2, a moving average of 20 seconds was applied to all curves, and the analysis of the data was done after the initial 200 seconds of polymerization, as shown in Figure 3-22.

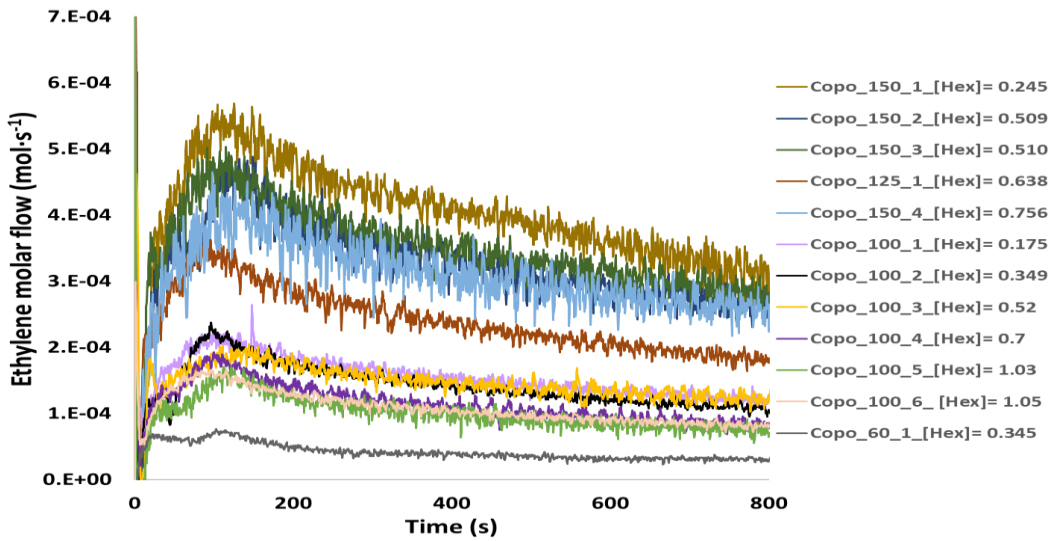


Figure 3-21. Normalize ethylene uptake curve for ethylene/1-hexene copolymerization.

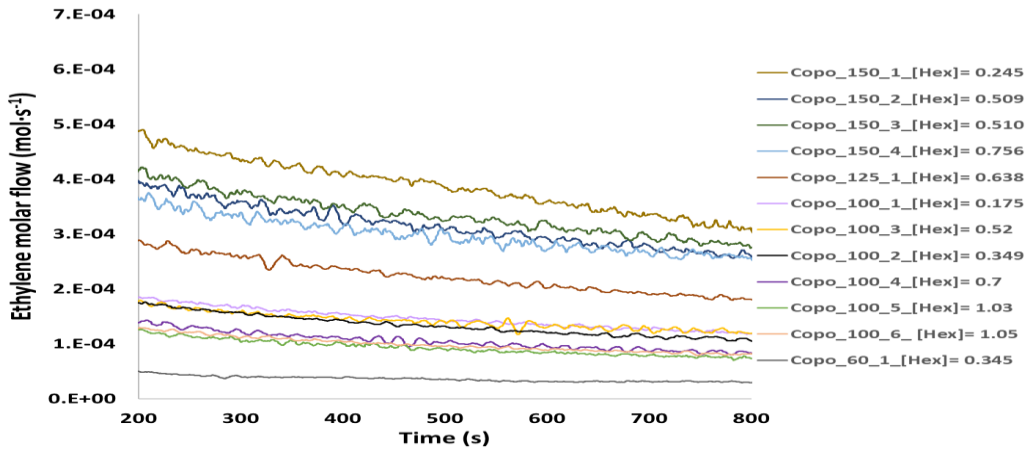


Figure 3-22. Moving average ethylene uptake curve for ethylene/1-hexene copolymerization.

Equation (3.57) was fitted to the data shown in Figure 3-22 to estimate the values of  $k_{pAA}k_f$ ,  $k_{pBA}k_f$  and  $k_d$  using the function `fitnlm` (Fit nonlinear regression model) in Matlab. For model estimation, 9 copolymerization runs and 2 ethylene polymerization from section 3.5.2 were used to estimate the model parameters, and the 3 remaining copolymerizations were used to validate the model. Table 3-21 lists the parameters estimated by Matlab.

**Table 3-21.** Ethylene/1-hexene copolymerization kinetic parameters with  $\text{Cp}_2\text{HfCl}_2$

Parameters	Values	SE	T
$k_{pAA} k_f (\text{L}^2\text{mol}^{-2}\text{s}^{-1})$	17,350	34.9	496.6
$k_{pBA} k_f (\text{L}^2\text{mol}^{-2}\text{s}^{-1})$	230.3	0.54	428.1
$k_d (\text{s}^{-1})$	0.000723	$4.0 \times 10^{-6}$	179.7
<b>Number of observation:</b>		19,163	
<b>R-Squared:</b>		0.893	

Figure 3-23 compares model predictions with the copolymerization uptake curves of the validating polymerizations (not used for model fitting). The data fit shows that the model can describe these polymerizations adequately.

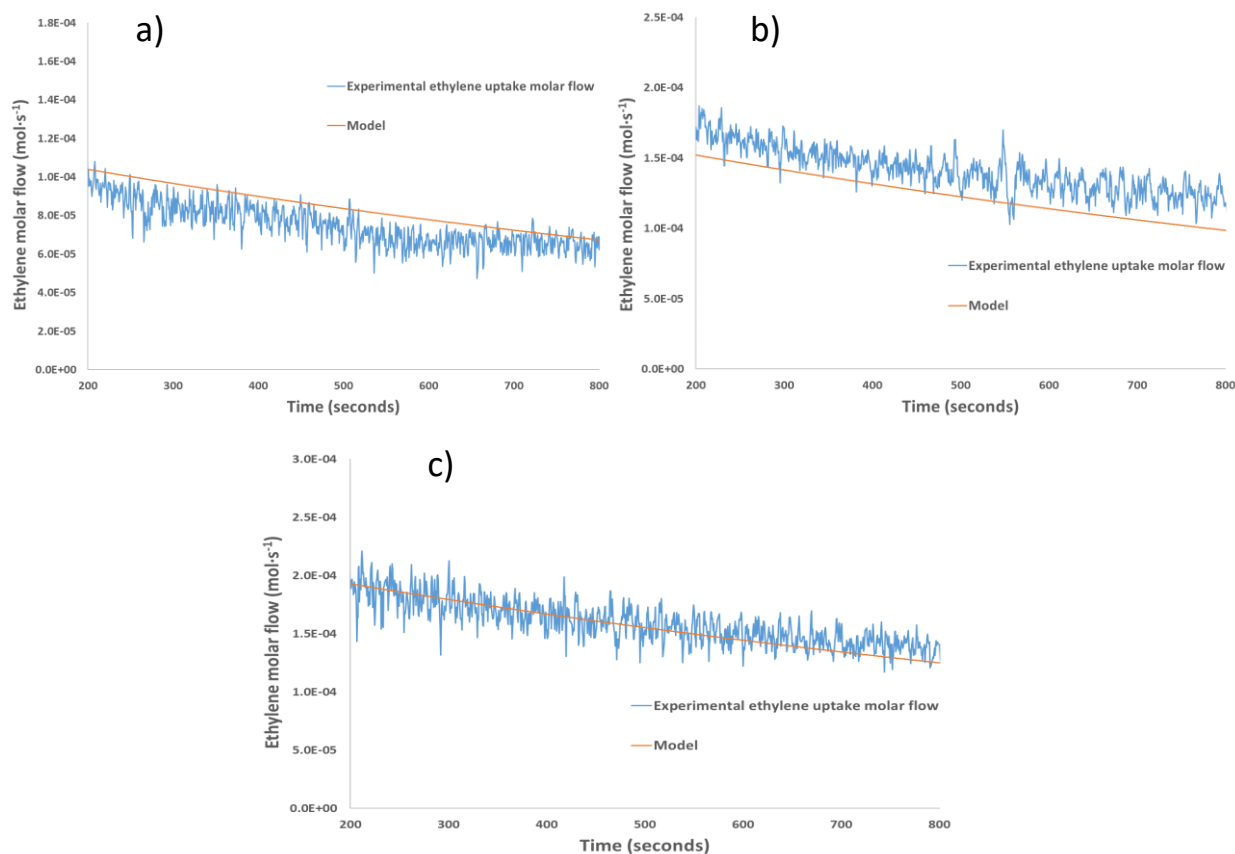


**Figure 3-23.** Validating experimental ethylene uptake curves versus model: a) Copo\_60\_1, b) Copo\_100\_2, and c) Copo\_150\_4.

The complete table with the propagation constants and decay constant for Ethylene/1-hexene copolymerization with  $\text{Cp}_2\text{HfCl}_2$  are showed in Table 3-22.

**Table 3-22.** Ethylene/1-hexene copolymerization kinetic parameters with  $\text{Cp}_2\text{HfCl}_2$

Parameters	Values	SE
$k_{pAA} k_f$ ( $\text{L}^2\text{mol}^{-2}\text{s}^{-1}$ )	17,350	34.9
$k_{pAB} k_f$ ( $\text{L}^2\text{mol}^{-2}\text{s}^{-1}$ )	412	52.1
$k_{pBA} k_f$ ( $\text{L}^2\text{mol}^{-2}\text{s}^{-1}$ )	230.3	0.54
$k_{pBB} k_f$ ( $\text{L}^2\text{mol}^{-2}\text{s}^{-1}$ )	0	0
$k_d$ ( $\text{s}^{-1}$ )	0.000723	$4. \times 10^{-6}$

One observation is that R-squared for the ethylene/1-hexene copolymerization model is lower than ethylene polymerization model proposed in the previous sections. Further analysis indicates that the decay constant has higher variability and has a direct correlation with the amount of 1-hexene added to the reactor: more 1-hexene, higher decay constant (Figure 3-24). A hypothesis of this phenomena is the presence of impurities not removed by the purification system or there are other types of decay reactions that were not considered by the proposed model.

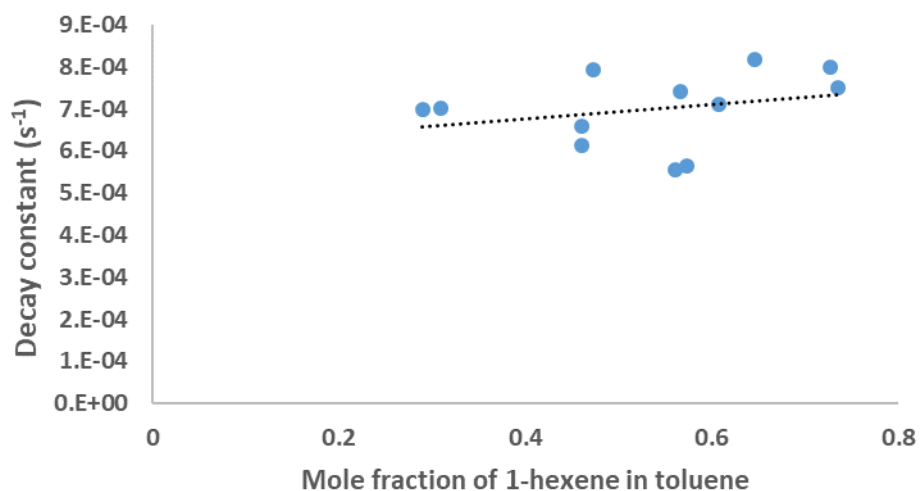


**Figure 3-24.** Decay constant versus mole fraction of 1-hexene in toluene.

### 3.5. Conclusions

The polymerization kinetic constants for the metallocene catalyst bis(cyclopentadienyl) hafnium(IV) dichloride were successfully estimated for ethylene polymerization and ethylene/1-hexene copolymerization. It was identified that the catalyst follows second order kinetics for the propagation and first order for catalyst decay over the range of conditions tested in this thesis. In addition, the pre-exponential factor and the activation energy for the propagation and decay constant were estimated. The results indicate that the models proposed adequately describe the polymerization kinetic, the number average molecular weight, and the average 1-hexene in the polymer made with  $\text{Cp}_2\text{HfCl}_2$  for ethylene polymerization with/without hydrogen and ethylene/1-hexene copolymerization.

The decay constant has higher variability for ethylene/1-hexene copolymerization and correlates with the amount of 1-hexene added to the reactor. Further analysis is required to identify the causes of the higher variability.

## **Chapter 4 : Correlating the Microstructure of Linear High-Density Polyethylene with Mechanical Properties using Cross Fractionation Chromatography**

### **4.1. Introduction**

The production of new high density polyethylene (HDPE) grades with specific mechanical properties in commercial facilities is a challenging task that requires time and resources in lab-scale and commercial plants. The development of quantitative methods to predict mechanical properties of HDPE prior to its commercial production will help save time and money during the development phase of new HDPE grades.

Patel and et al. [51] used the model proposed by Huang and Brown (described in Chapter 2) to correlate mechanical properties with tie molecule concentration. They estimated the tie molecule concentration of homogenous ethylene/octene copolymers over a range of densities and molecular weights, and correlated it with polymer mechanical properties. Crystal lamellae and amorphous region thickness were estimated using values for melting peaks and crystalline fractions of the whole polymer. The authors found a good correlation between Young module and tie molecule concentration for densities lower than  $0.91 \text{ g/cm}^3$ , but could not find an adequate correlation for higher densities. The authors suggested that the Young module was influenced by chain loops at higher densities, which were not considered in the Huang and Brown model.

A different approach was proposed by Paul DesLauriers [3]. He proposed the use of a primary structural parameter to estimate the probability of tie molecule formation. The primary structure parameter is calculated using data on the molecular weight distribution (MWD) and average short chain branching distribution (SBD) across the MWD. This data is collected by connecting a Fourier transform infrared detector (FTIR) to a gel permeation chromatographer (GPC). This technique measures the average SCB frequency of each MWD slice, thus correlating polymer molecular weight to its average SCB frequency. Correlations are used to estimate densities, melting temperatures and lamellar thickness of each molecular weight slice, and these values are then used to calculate the probability of tie chain formation for each slice. In a subsequent step, the probability of each slice summed over the whole MWD, using the weight fraction of each slice,

to get a global value for the probability of tie chain formation, called PSP2. This methodology was applied to a number of polyethylene and ethylene/1-hexene copolymer samples over a range of molecular weights, densities and comonomer contents. The authors found that PSP2 could be adequately correlated with Pennsylvania Notch Test (PENT) and Single Point Notched Constant Tensile Load Test (SP-NCTL) (Figure 4-1).

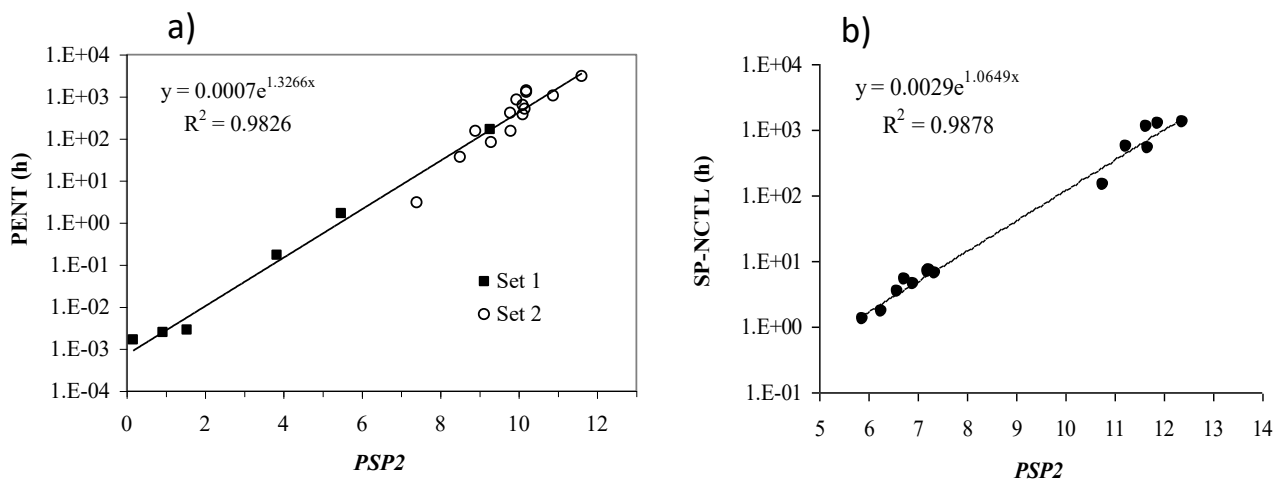


**Figure 4-1.** PENT (a) and SP-NCTL (b) versus PSP2 [3].

In this chapter, DesLauriers method is extended by replacing GPC-FTIR with a cross-fractionation technique. The probability of tie chain formation will be estimated using the values of molecular weight distribution (MWD) and short chain branching distribution (SCBD) from cross fractionation chromatography (CFC). The expected advantage for this approach is that instead of using the average SCB across the MWD to calculate the primary structural parameter, as for the GPC-FTIR case, we can measure the whole SCBD in addition to the MWD. This approach, therefore, may get PSP2 that reflect more polymer microstructural details, and correlate more accurately to the mechanical properties of HPDE.

## 4.2. Experimental Part

Polyethylene samples were provided by Chevron-Phillips. Density measurements were made using ASTM D155, while natural draw ratio (NDR) and strain hardening modulus was measured using ASTM D638 and ISO 18488 standards, respectively.

The samples were analyzed by cross fraction chromatography (CFC) in a fully automated Polymer Char instrument using 1,2,4-trichlorobenzene as a solvent. In the first step, CFC fractionates the polymer according to its crystallizability, using temperature rising elution fractionation (TREF). In a second step, polymer fractions of different crystallizabilities are analyzed by gel permeation chromatography (GPC) to determine their MWDs. This will be explained in more details in section 4.4.2.

## 4.3. PSP2 and PSP2\* Calculations

The core of the proposed method is the calculation of PSP2, proposed by DesLauriers, and PSP2\*, the modified parameter calculated using CFC results. These methods will be explained in this section, following the procedure suggested by DesLauriers [3].

### 4.3.1. Density

The density of polyethylene can be correlated with its molecular weight by the Equation [52]

$$\rho = 1.0748 - (0.0241) \cdot \log MW \quad (4.1)$$

Equation (4.1) is valid for  $MW = 0.7$  to  $1 \times 10^4 \text{ kg} \cdot \text{mol}^{-1}$ . Polyethylenes with  $MW$  values lower than  $700 \text{ g/mol}$  are expected to be 100% crystalline; in this case, a maximum density of  $1.006 \text{ g} \cdot \text{cm}^{-3}$  is assigned to the polymer. Equation (4.1) can be used to estimate densities from  $0.906$  to  $1.01 \text{ g} \cdot \text{cm}^{-3}$ .

The incorporation of 1-olefins to a polyethylene lowers the density of the copolymer as compared to an ethylene homopolymer of same molecular weight. For random ethylene/1-olefin copolymers, DesLauriers and Rohlfiing proposed the following correction [52]

$$\rho_{\text{Copolymer}} = \rho - \Delta\rho \quad (4.2)$$

$$\Delta\rho = C_1(\text{SCB}/\text{PDI}^n)^{C_2} + C_3(\text{SCB}/\text{PDI}^n)^{C_4} \quad (4.3)$$

where  $C_1 = 0.01239302$ ,  $C_2 = 0.49586823$ ,  $C_3 = 0.000345888$ ,  $C_4 = -0.78067392$ ,  $n = 0.318975556$ . SCB is given in frequency per 1,000 carbon atoms, and  $\Delta\rho$  in  $\text{g}\cdot\text{cm}^{-3}$ . These set of constants applies only for ethylene/1-hexene copolymers.

### 4.3.2. Melting Temperature

Empirical equations have been estimated to correlate the HDPE melting temperature to its density. The values of density and melting temperature were taken from Patel [51] and Mirabella [53] studies. A completely amorphous polyethylene has a melting temperature of 23 °C and density of 0.852  $\text{g}\cdot\text{cm}^{-3}$  [37], while a completely crystalline polyethylene has a melting point of 142.5 °C and density of 1.01  $\text{g}\cdot\text{cm}^{-3}$  [33]. For intermediate values between these two extremes, the following equation applies (Figure 4-2)

$$T_m(C) = 20573.60101*\rho^3 - 63771.78675*\rho^2 + 65899.64632*\rho - 22559.77696 \quad (4.4)$$

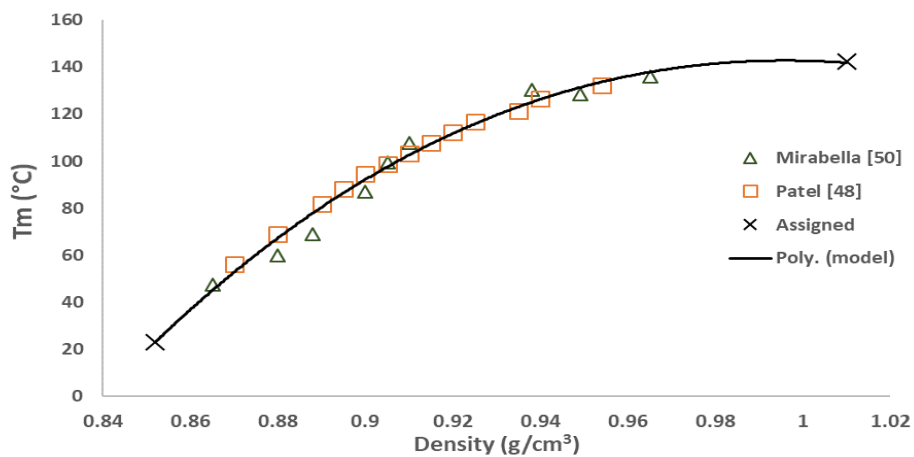


**Figure 4-2.** Correlation of between melting temperature and polyethylene density [3].

### 4.3.3. Crystalline Lamella and Amorphous Layer thickness

The thickness of the crystalline lamella layer ( $l_c$ ) may be approximated by the Gibbs-Thompson equation

$$T_m = T_m^o \left( 1 - \frac{2\sigma_e}{\Delta H_f L_c} \right) \quad (4.5)$$

Using the parameter given by Patel [51], Equation (4.5) simplifies to

$$L_c(\text{nm}) = \frac{0.624 \text{ nm} \cdot T_m^o(\text{K})}{T_m^o(\text{K}) - T_m(\text{K})} \quad (4.6)$$

where  $T_m$  is the actual melting temperature, and  $T_m^o$  is the equilibrium melting point for polyethylene.  $T_m$  is estimated using Equation (4.4) and  $T_m^o$  was assigned as 142.5 °C [3].

The Gibbs-Thompson equation is valid for crystal lamellae of large lateral dimensions, but for polyethylenes with densities lower than 0.89 g·cm<sup>-3</sup> the chains crystallize as fringed micelles [51]. As a result, Equation (4.6) is not applicable. Therefore, the model proposed in this thesis is limited to polyethylenes with densities higher than 0.89 g·cm<sup>-3</sup>.

The amorphous layer thickness is estimated as [51]

$$L_a(\text{nm}) = L_c(\text{nm}) \frac{\rho_c(1 - X_c)}{\rho_a X_c} \quad (4.7)$$

where  $X_c$  is the weight percentage crystallinity,  $\rho_c$  is the density of crystalline polyethylene ( $\rho_c = 1.006 \text{ g}\cdot\text{cm}^{-3}$ ) and  $\rho_a$  is the density of amorphous polyethylene ( $\rho_a = 0.852 \text{ g}\cdot\text{cm}^{-3}$ ).

The weight percentage crystallinity is estimated as [54]

$$X_c = 100 \frac{(V - V_a)}{(V_c - V_a)} = 100 \frac{(1/\rho - 1/\rho_a)}{(1/\rho_c - 1/\rho_a)} = 100 \left( \frac{\rho_c}{\rho} \right) \left( \frac{\rho - \rho_a}{\rho_c - \rho_a} \right) \quad (4.8)$$

where  $V$  is the specific volume and  $\rho$  is the actual polymer density.

#### 4.3.4. Probability of Tie Molecule Formation

Huang and Brown proposed [40], using Gaussian statistic for chain segments during the crystallization process, the probability of the chain for forming a tie-molecules ( $P_{TM}$ ) is given by

$$P_{TM} = \frac{1 \int_L^{\infty} r^2 \exp(-b^2 r^2) dr}{3 \int_0^{\infty} r^2 \exp(-b^2 r^2) dr} \quad (4.9)$$

where,

$L = 2L_c + L_a$  ( $L_c$  is thickness of the crystalline lamella and  $L_a$  is the amorphous layer thickness).

$r$  = end-to-end distance of a random coil.

$b = \frac{3}{2\bar{r}^2}$  ( $\bar{r}$  is the mean square value of the end-to-end distance for random coil conformation chain).

$$\bar{r}^2 = Dnl^2$$

$D =$  Chain extension factor in melt = 6.8 for polyethylene

$n =$  Number of bonds =  $M_w/14$  for polyethylene

$l =$  The bond length = 0.153 nm for polyethylene

Equation (4.9) can be simplified solving the integral in the denominator and re-arranging the integral limits, resulting in the following equation:

$$P_{TM} = \frac{1}{3} \left( 1 - \frac{4b^3}{\sqrt{\pi}} \int_0^L r^2 \exp(-b^2 r^2) dr \right) \quad (4.10)$$

Thus, the highest value of probability of tie-chain formation that can be obtained by Equation (4.10) is 0.33.

#### 4.4. PSP2 and PSP2\* Calculation Methods

##### 4.4.1. PSP2 Estimation

PSP2 was the parameter estimated by DesLauriers to correlate with the mechanical properties of polyethylene using the MWD-SCB data measured with GPC-IR. The following are the steps need to be followed to estimate PSP2:

1. Cut the MWD in several slices of 0.025 units' width and determine its SCB. An example is given in Figure 4-3.

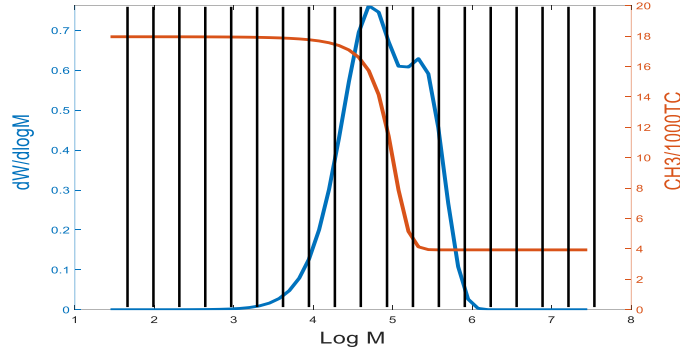


**Figure 4-3.** GPC-IR cut in slice by slice basis.

2. Each slice corresponds to a narrow molecular weight slice within the MWD for the whole polymer. For this molecular weight slice, the following parameters are estimated:
  - 2.a. The density is calculated using Equations (4.1) and (4.2).
  - 2.b. The melting temperature is estimated using Equation (4.4) and the density values (2.a) as input.
  - 2.c. The crystalline lamella and amorphous layer thickness are estimated using Equations (4.6), (4.7) and (4.8), and 2.a. and 2.b. values as inputs.
  - 2.d. The probability of tie chain formation is calculated with Equation (4.10).
3. After the probability of tie chain formation are calculated for each slice, these probabilities are multiplied by the weight fraction of each slice in order to have a single value of the probability of tie chain formation for the whole polymer. This final value, known as PSP2, is expressed in percentage and defined as

$$PSP2 (\%) = 100 \cdot \sum_{i=1}^n w_i P_{TM_i} \quad (4.11)$$

#### 4.4.2. PSP2\* Estimation

The new parameter, PSP2\*, proposed in this thesis, is calculated following a similar procedure used to find PSP2, but the polymer microstructural information is obtained from CFC instead of

GPC-IR. Thus, in addition to the MWD, the complete SCBD is also considered in the novel procedure. Figure 4-4 shows the results of the characterization of an ethylene/1-hexene sample with CFC.

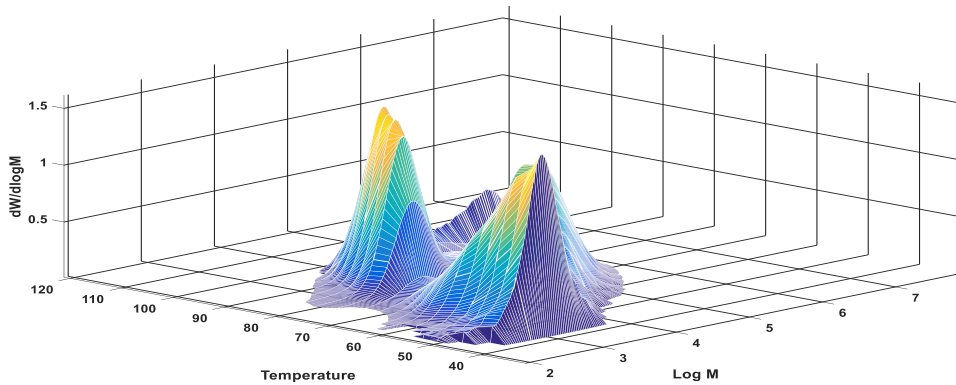


**Figure 4-4.** Cross fractional results for an ethylene/1-hexene sample.

CFC is an analytical instrument where a TREF column is coupled with GPC columns in series. Fractions eluting from the TREF columns over a narrow range of temperatures,  $\Delta T$ , are sequentially analyzed by GPC. This procedure generates multiple MWDs, one for each TREF temperature interval, which are associated with an average comonomer molar fraction (or SCB frequency), which is considered to be constant for each fraction [55]. This process is illustrated in Figure 4-5.

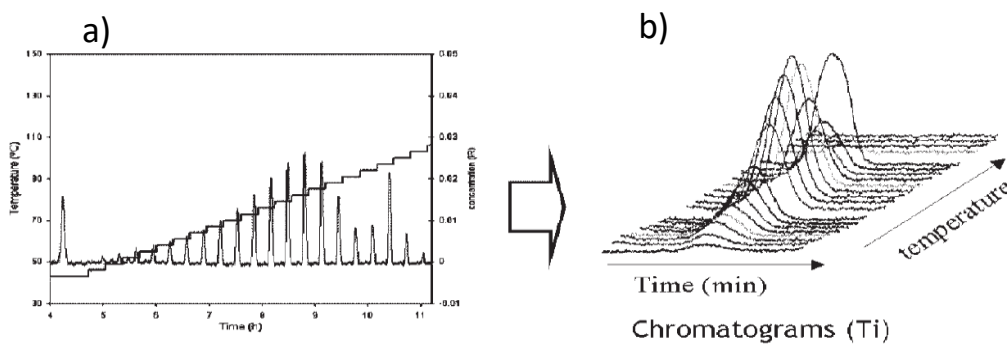


**Figure 4-5.** Continuous raw IR signal (a) and separated chromatograms (b) to process the cross-fractionation raw signals [35]

Based on the operation and the data exported by the CFC, which includes multiple chromatograms (each chromatogram at a specific elution temperature and therefore a specific short chain branching) a Matlab code was developed to estimate the PSP2 for each chromatogram, as explained in Section 4.4.1., and the PSP2 obtained by each chromatogram was multiplied by the weight fraction of the polymer at its respective elution temperatures. The final sum of the weighted PSP2s was called PSP2\* (Equation (4.12)). The expected advantage of PSP2\* over the PSP2 is the inclusion of the SCBD for each molecular weight slice of the polymer.

$$PSP2^*(\%) = \sum_{Temp=30}^n \left( \sum_{Chromatograms=1}^n PSP2_{chrom} \right)_{temp} w_{temp} \quad (4.12)$$

#### 4.5. Results and Discussion

Six polyethylene samples were provided by Chevron-Philips. Their densities and mechanical properties are shown in Table 4-1.

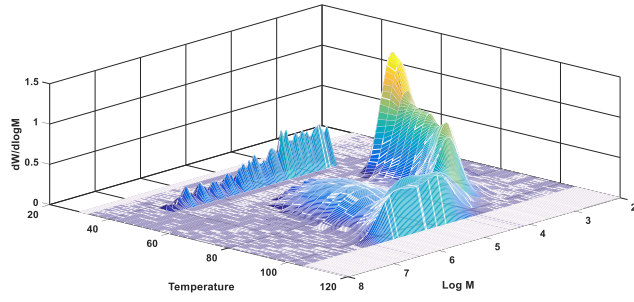
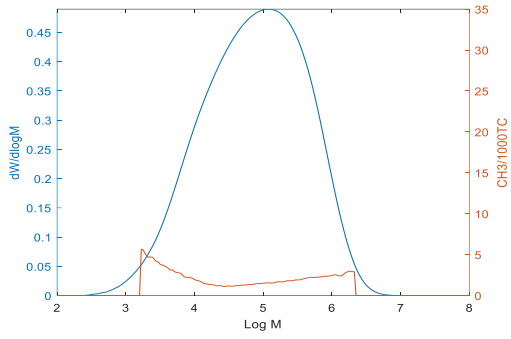
**Table 4-1.** Densities and mechanical properties of polyethylene samples

Samples	Density (g·cm <sup>-3</sup> )	Mw (kg·mol <sup>-1</sup> )	SCB (per 1000 C atoms)	NDR (% strain)	SHM (MPa)
A	0.9471	294	1.75	533	72.7
B	0.9493	266	1.56	573	55.1
C	0.9514	242	1.40	612	50.6
F	0.9527	224	1.29	642	46.3
E	0.9544	215	1.13	666	38.7
G	0.9594	186	0.94	751	27

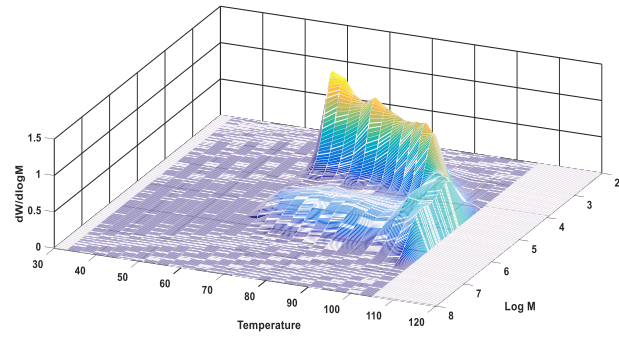
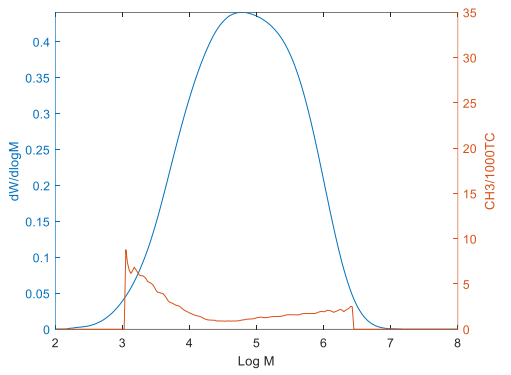
\*NDR is Natural Draw Ratio and SHM is Strain Hardening Modulus.

The samples were analyzed using the CFC. Figure 4-6 shows the results from CFC and GPC.

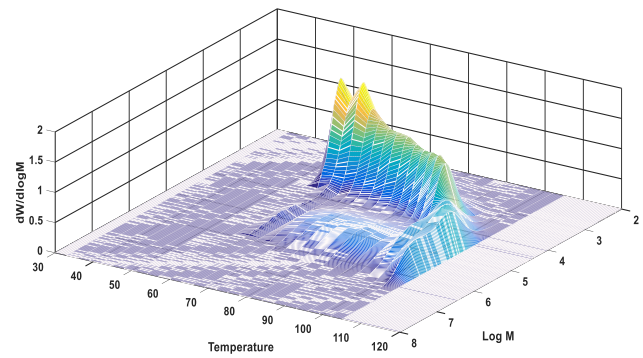
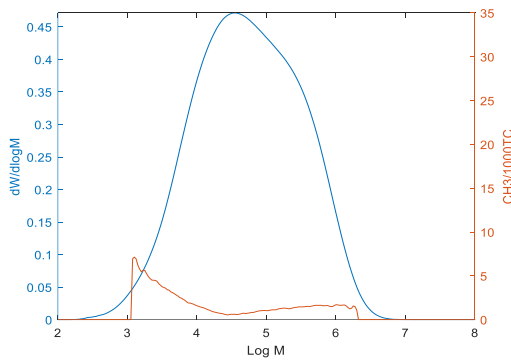
### Sample A



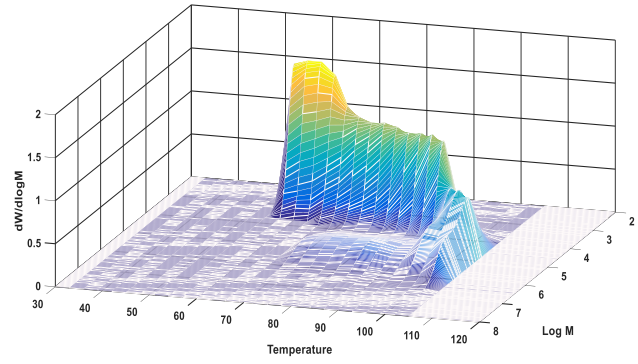
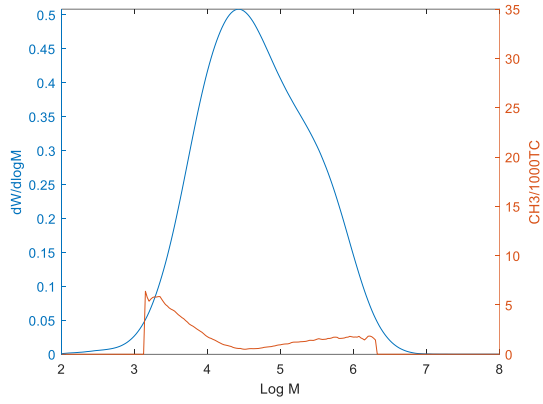
### Sample B



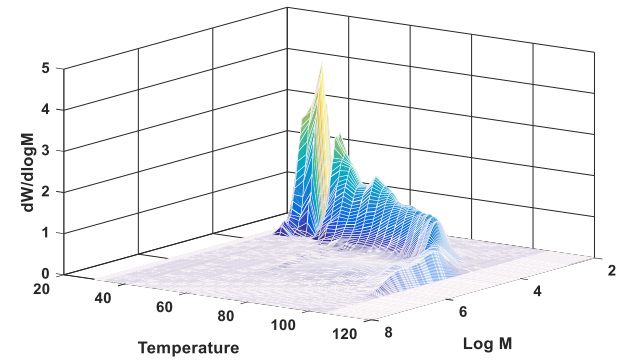
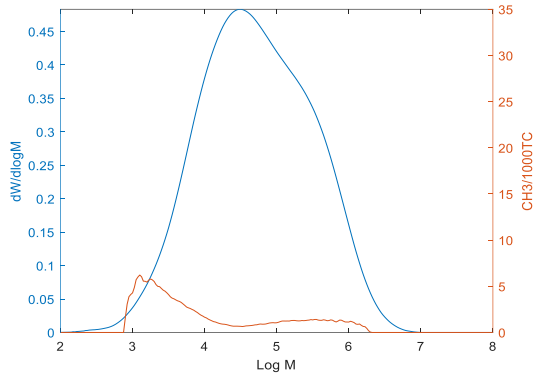
### Sample C



### Sample E



### Sample F



### Sample G

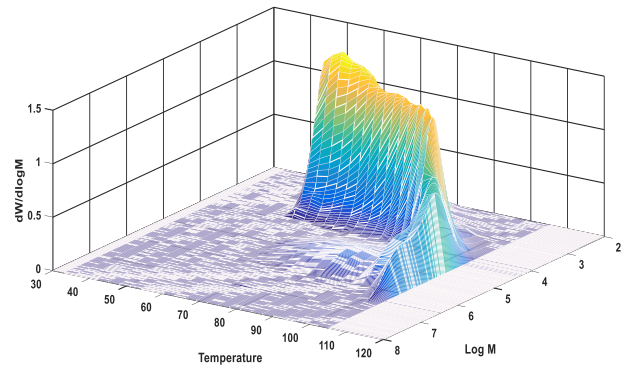
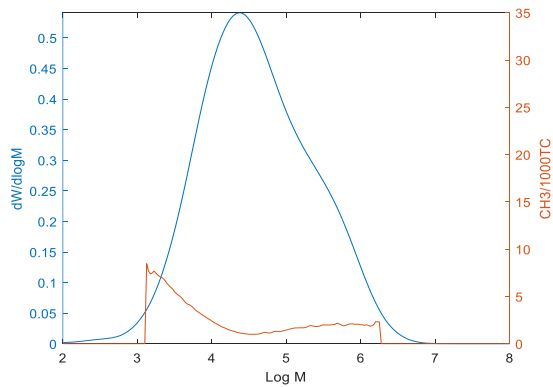


Figure 4-6. Polyethylene characterization by GPC-IR and CFC.

Table 4-2 shows the values for PSP2 and PSP2\* for these samples, while Figure 4-7 correlates these parameters to the mechanical properties of the polymers. The following observations can be deduced from the results:

1. The correlation between the mechanical properties and primary structural parameters follow the expectations: the draw natural ratio decreases with increasing tie molecule probability (or higher PSP values) because they prevent the extension of the chain without breaking [56], while the strain hardening modulus increases due to higher tie molecule density.
2. PSP2\* and PSP2 vales are very similar; PSP2\* is just 1% higher in average than PSP2.
3. The statistical correlation between mechanical properties and primary structure parameters is the same using PSP2 or PSP2\*.

**Table 4-2.** Primary structure parameters, PSP2 and PSP2\*, of polyethylene samples

<b>Samples</b>	<b>Mw (kg·mol<sup>-1</sup>)</b>	<b>SCB (per 1000 C atoms)</b>	<b>NDR (% strain)</b>	<b>SHM (MPa)</b>	<b>PSP2 (%)</b>	<b>PSP2* (%)</b>
A	294	1.75	533	72.7	10.7	10.8
B	266	1.56	573	55.1	9.9	10.0
C	242	1.40	612	50.6	8.5	8.7
F	224	1.29	642	46.3	8.3	8.5
E	215	1.13	666	38.7	7.6	7.6
G	186	0.94	751	27	6.8	6.8

Although PSP2\* can be correlated with the mechanical properties of polyethylene, the proposed new parameter does not bring any important improvement over the existing PSP2 for the samples considered in study. Since CFC is a more time consuming and expensive technique than GPC-IR, it seems that the use of PSP2\* as a predictor of mechanical properties for these samples is unjustified. Although this conclusion is disappointing, it does not mean it would always be the case. In the following paragraphs we will explore some reasons why the values of PSP2 and PSPS\* are so close for these samples.

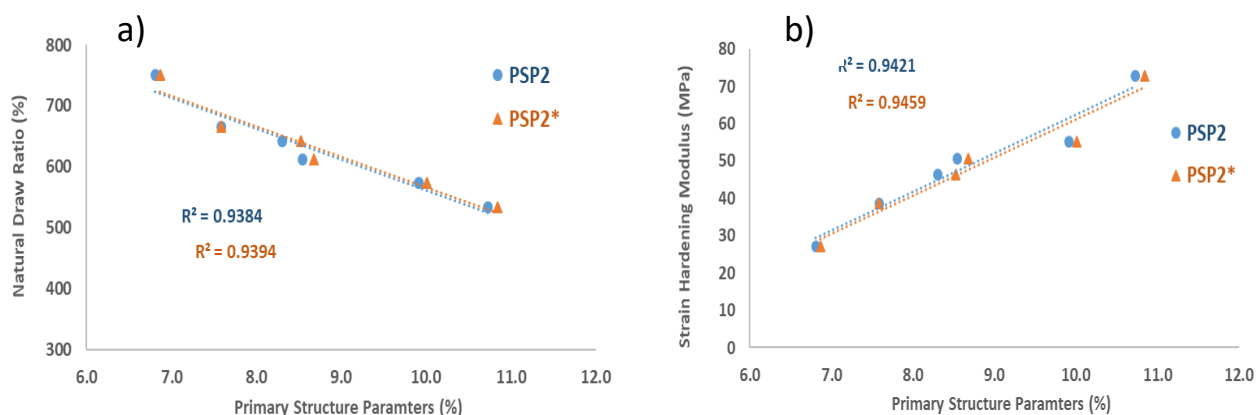


**Figure 4-7.** Primary structural parameters, PSP2 and PSP2\*, versus (a) Natural Draw Ratio and (b) Strain Hardening Modulus.

One reason for the similar values between PSP2\* and PSP2 is the narrow SCBD of the polymers considered in this investigation in the range of molecular weights where tie molecules are more probable to be formed. For instances, Figure 4-8 shows the SCBD across the MWD for each elution temperature for sample A, which is the sample with the highest average 1-hexene content and broader SCBD. In accordance with the method proposed in this study, tie molecules will be formed for sample A, when Log M is higher than 4.7 (chains with molecular weights around 50,000 g/mol). However, for polymer chains with Log M higher than 6 and 0 SCB/1000 C atoms the probability of tie molecule formation is 32% (Being the highest value of probability of tie molecule formation 33%), while the probability of tie formation for polymer chains with Log M higher than 6 and 25 SCB/1000 C atoms is around 32.8%, as a result, the variation of the probability of tie formation for polymer chains with Log M higher than 6 is less than 1%.

On the other hand, for polymer chains with Log M between 4.7 and 6, the SCB varies between 0 and 7 SCB/1000 C atoms, this area is delimited by the red circle in Figure 4-8. For a polymer chain with Log M equal to 5.5, if the SCB is 0 SCB/1000C atoms, the probability of tie molecules formation is 29.5%, while if the SCB is 7 SCB/1000C atoms, the probability of tie molecules formation is 31%. Thus, the variation of probability of tie molecules formation is less than 2%.

In conclusion, the SCBD of the samples analyzed are not broad enough to generate a significant variation in the probability of tie molecule formation.

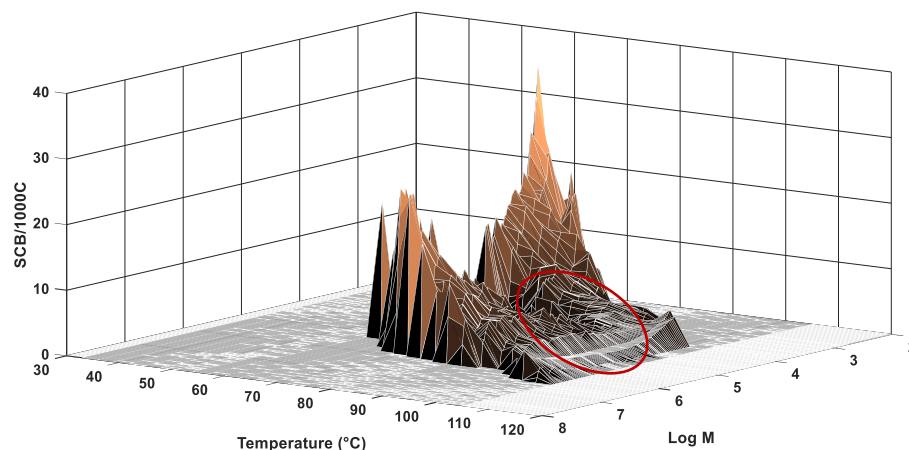


**Figure 4-8.** SCBD over molecular weight of sample A.

To study the effect of the comonomer distribution in the estimation of PSP2 and PSP2\* in more detail, virtual binary polymer blends were created using Flory and Stockmayer distributions for ethylene/1-hexene copolymers. Four blends were analyzed, with the characteristics shows in Figure 4-9. The specification of the polymer populations made on each single site catalyst, and the values estimated for PSP2 and PSP2\* are presented in Table 4-3.

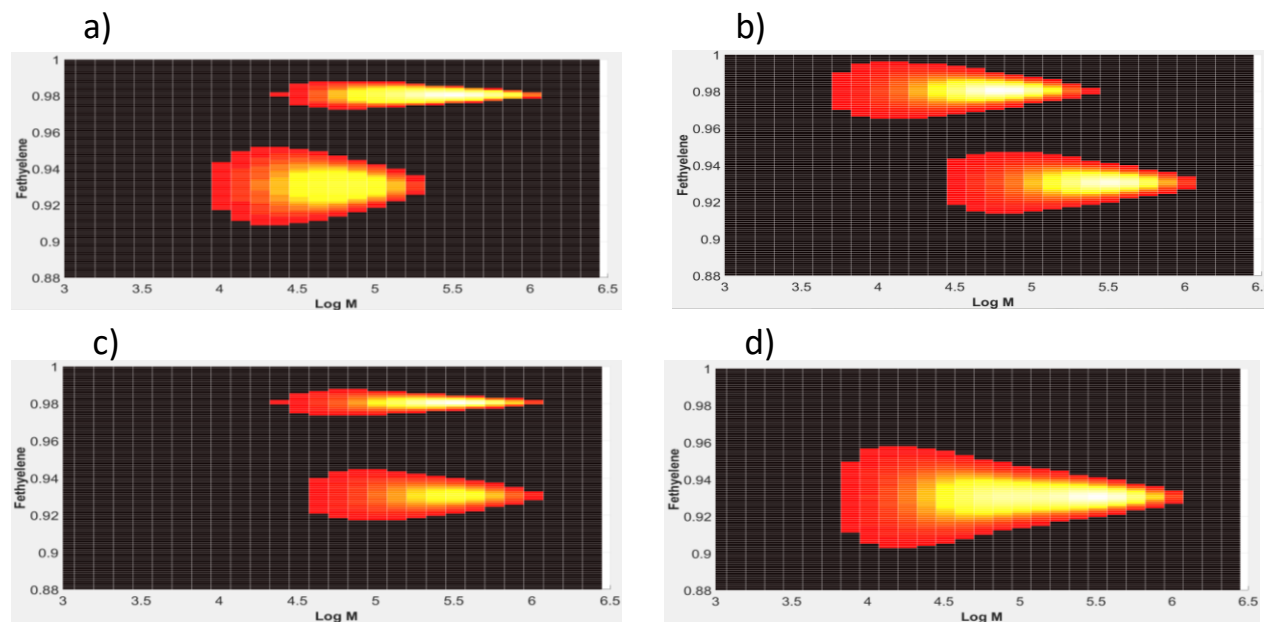


**Figure 4-9.** Virtual binary polymer blends designed to compare PSP2 and PSP2\*: a) Blend 1, b) Blend 2, c) Blend 3, and d) Blend 4.

**Table 4-3.** Virtual polymer blends.

Site Type	Blend 1		Blend 2		Blend 3		Blend 4	
	1	2	1	2	1	2	1	2
<i>m</i>	0.5	0.5	0.5	0.5	0.5	0.5	0.5	0.5
<i>r<sub>n</sub></i>	4 000	800	4000	800	2400	2400	4000	800
<i>F<sub>ethylene</sub></i>	0.992	0.96	0.96	0.992	0.96	0.992	0.976	0.976
<i>r<sub>A</sub>r<sub>B</sub></i>	15	5	15	5	15	5	15	5
<i>c</i>	0.00025	0.00125	0.00025	0.00125	0.00041667	0.00041667	0.00025	0.00125
<i>β</i>	0.0095	0.0488	0.0682	0.0084	0.0682	0.0084	0.0356	0.0275
<i>F<sub>hexene</sub></i>	0.008	0.04	0.04	0.008	0.04	0.008	0.024	0.024
<i>SCB/1000</i>	4	19	19	4	19	4	11	11
<i>M<sub>n</sub> (g·mol<sup>-1</sup>)</i>	112200	22440	112200	22440	67320	67320	112200	22440
<i>PDI</i>	2	2	2	2	2	2	2	2
<i>M<sub>w</sub> (g·mol<sup>-1</sup>)</i>	224400	44880	224400	44880	134640	134640	224400	44880
<i>M<sub>n</sub> blend</i>	37 400		37 400		67320		37400	
<i>M<sub>w</sub> blend</i>	134 640		134 640		134640		134640	
<i>PDI blend</i>	3.6		3.6		2		3.6	
<i>F<sub>ethylene</sub> blend</i>	0.976		0.976		0.976		0.976	
<i>F<sub>hexene</sub> blend</i>	0.024		0.024		0.024		0.024	
<b>PSP2</b>	<b>14.08</b>		<b>14.13</b>		<b>19.02</b>		<b>14.43</b>	
<b>PSP2*</b>	<b>14.64</b>		<b>14.35</b>		<b>17.96</b>		<b>14.85</b>	

*m* is mass fraction of catalyst site, *r<sub>n</sub>* is number average chain length, *F<sub>ethylene</sub>* is average ethylene content in the polymer, *r<sub>A</sub>* and *r<sub>B</sub>* are the reactivity ratios, *c* is  $1/r_n$  and  $\beta = \overline{F}_A(1 - \overline{F}_A)\sqrt{1 - 4\overline{F}_A(1 - \overline{F}_A)(1 - r_A r_B)}$

The polymer populations in all blends are present in a mass ratio of 1:1. In Blend 1, the population with the highest *M<sub>n</sub>* has the highest comonomer fraction (*normal comonomer distribution*). In Blend 2, the population with the highest *M<sub>n</sub>* has the lowest comonomer fraction (*reverse comonomer distribution*). In Blend 3, both populations have the same *M<sub>n</sub>* (*bimodal comonomer distribution*). Finally, in Blend 4, both populations have the same comonomer fraction (*uniform comonomer distribution*). These 4 blends cover all the possible permutations of *M<sub>n</sub>* and *F<sub>ethylene</sub>* for binary polyolefin blends.

Table 4-3 and Figure 4-10 show that PSP2 and PSP2\* follow the same trend for the blends 1, 2 and 4: when PSP2 increases, PSP2\* also increases, and vice-versa, but the trend is different for the blend 3. For these blends, PSP2 values are more spread out than PSP2\* values.

The virtual binary blend 3 has a bimodal comonomer distribution, in this case much broader than the samples analyzed in Table 4-2. Having a broad comonomer distribution, the effect of this

distribution is significant and impact the estimation of the primary structure parameters, in this case, PSP2\* estimates a lower value than the value estimate by PSP2.

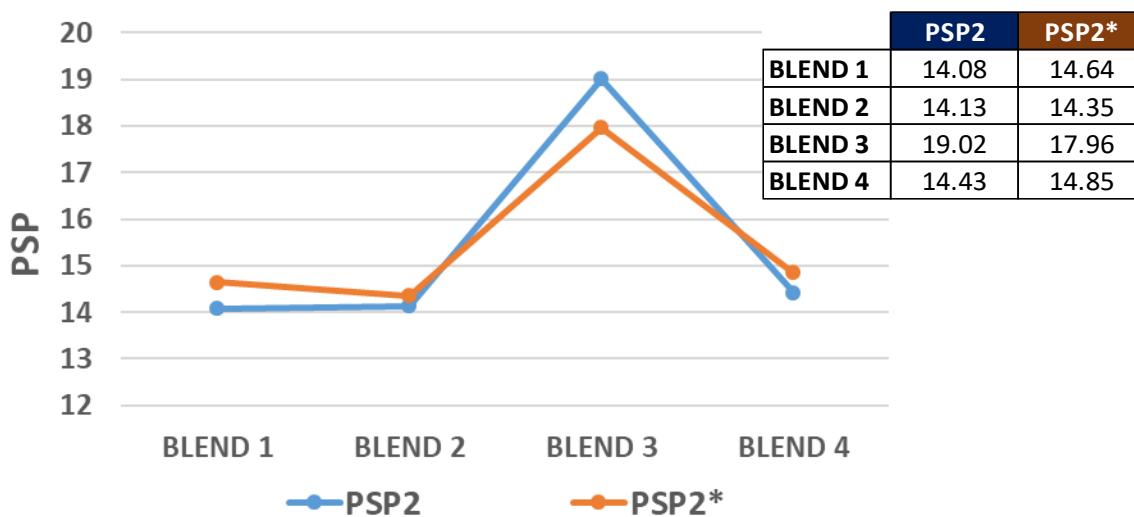


**Figure 4-10.** Comparison of PSP2 and PSP2\*.

We decided to further investigate this phenomenon by generating several binary polymer blends in the range shown in Table 4-4.

**Table 4-4.** Range of properties for polymer blend components.

	Component 1			Component 2		
	Lower Limit	Increment	Higher Limit	Lower Limit	Increment	Upper Limit
$r_n$	1000	1000	4000	1000	1000	4000
$F_{ethylene}$	0.96	0.002	0.98	0.998	-0.002	0.98
$r_a r_b$	15			5		
$m$	0.5			0.5		
<b>Total Number of Combinations: 1,760</b>						

The polymers generate in Table 4-4 have a density between 0.8902 and 0.9647.

From simulation results of Table 4-4, the polymers with the same chain average length in both components but different average ethylene content were analyzed (bimodal comonomer distribution). PSP2\* and PSP2 were estimated for those polymers in order to identify when the divergence between PSP2\* and PSP2 occur. Figure 4-11 show the difference between PSP2\* and PSP2 at varies average ethylene contents for each component and varies average chain average lengths.

As a result, when two polymers are blended, there is a range of average chain length and average ethylene content of each polymer that the resulting polymer blends estimate PSP2\* that diverges from PSP2.

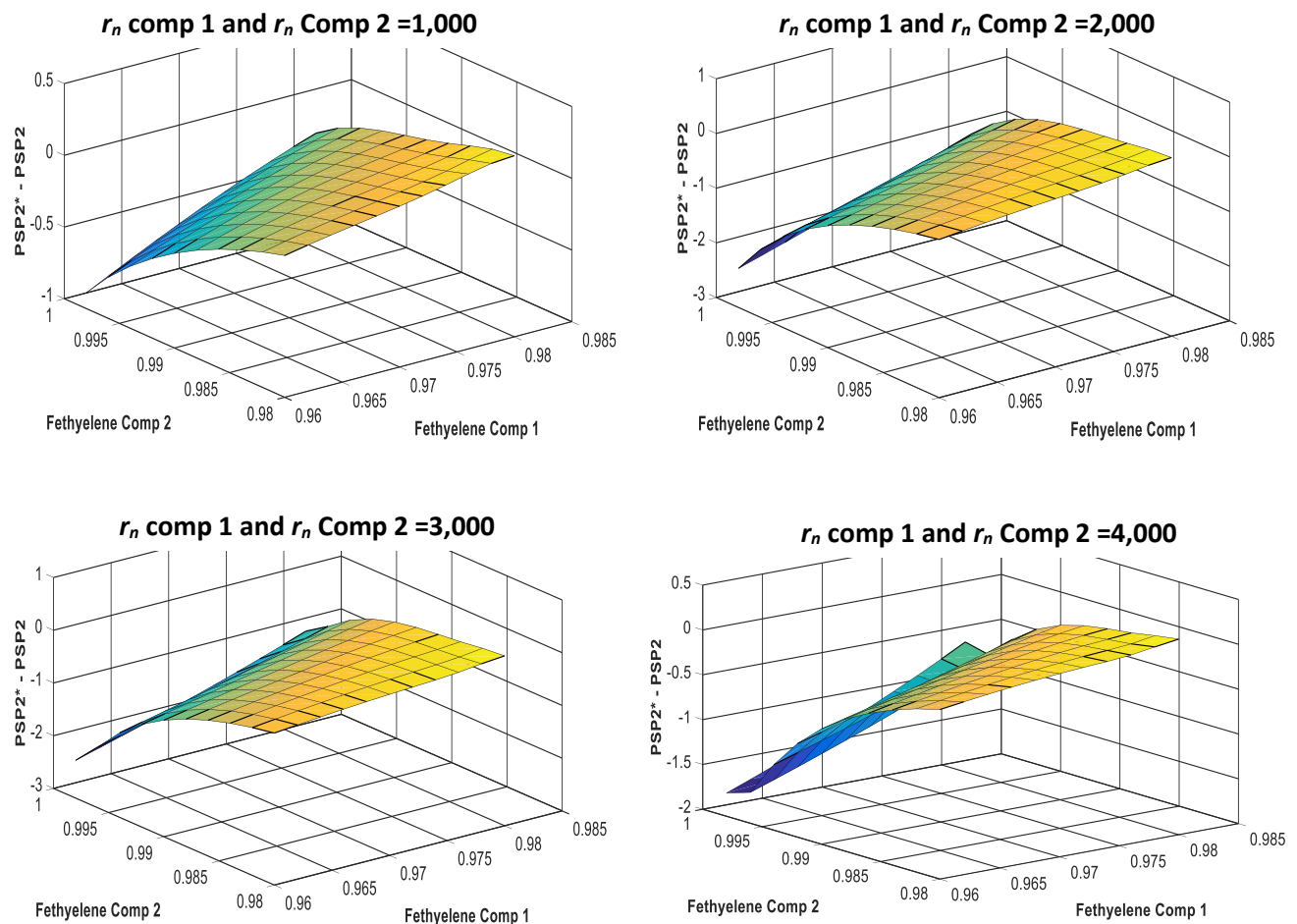


**Figure 4-11.** Behavior of PSP2\*- PSP2 varying ethylene content and chain average length.

The results of figure 4-11 suggests that for a broad comonomer distribution for catalyst sites having the same average chain length, PSP2\* could be up to 3 units apart from the values estimated by PSP2. Another observation is PSP2\* and PSP2 are closer when the average chain length were 1,000 and 4,000 units, and the higher divergences when the average chain length were 2,000 and 3,000. This could be explained by:

1. At average chain length equal to 1,000, only a small fraction of the chains has the length enough to form tie molecules. As a result, the comonomer distribution does not make an important difference between PSP2\* and PSP2.
2. At average chain length 4,000, the comonomer distribution of comonomer is lower respect the other average chain length simulated. This could be explained by the comonomer composition distribution over all chain lengths predict by the Stockmayer distribution [57]:

$$w_{F_A} = \frac{3\tau^2\beta^2}{[2\tau\beta + (F_A - \bar{F}_A)^2]} \quad (4.13)$$

In accordance with Equation (4.13), when average chain length increase ( $\tau$  decreases), and therefore, the comonomer distribution is narrower. Thus, we can expect that when average chain length increases, PSP2\* would be similar to PSP2.

Another interesting result from the simulation is that multiple polymer blends had similar PSP2\* values. Accordingly, if one correlates mechanical properties to either PSP2 or PSP2\*, one would necessarily have to conclude that these different blends had the same mechanical properties, since they share the same PSP2\* values. Table 4-5 shows the property of the 6 blends that have the same PSP2\* of Blend 3 (labeled 3.a to 3.e). Note that the blends with same PSP2\* are different for each other, that is, the requirements for equal PSP2\* are not the same.

In Figure 4-12 we compared blends composed of populations that most differed (in terms of  $r_n$  and  $F_{ethylene}$ ) from those of Blend 3 to understand how blends having populations with different microstructures could still have the same PSP2 or PSP2\*. The blends being compared in Figure 4-12 are highlighted in Table 4-5.

The comparisons of these blends in Figure 4-12 suggest that the criteria to keep the similar PSP2\* of the blend 3.A is to increase the molecular weight but reducing the short chain branching of the blend. The molecular weight distribution and the short chain branching distribution of these blends are shown in Figure 4-13.

**Table 4-5.** Binary blends with same PSP2\* of Blend 3 (Table 3).

Site	1		2		PSP2*	
	$r_n$	$F_{ethylene}$	$r_n$	$F_{ethylene}$	Raw Value	Rounded Value
3	2400	0.96	2400	0.992	17.9592	17.96
3.A	2000	0.976	3000	0.988	17.9740	17.97
3.B	3000	0.98	2000	0.984	17.9920	17.99
3.C	3000	0.98	3000	0.996	17.9707	17.97
3.D	4000	0.972	2000	0.994	17.9866	17.99
3.E	4000	0.98	2000	0.992	17.9510	17.95

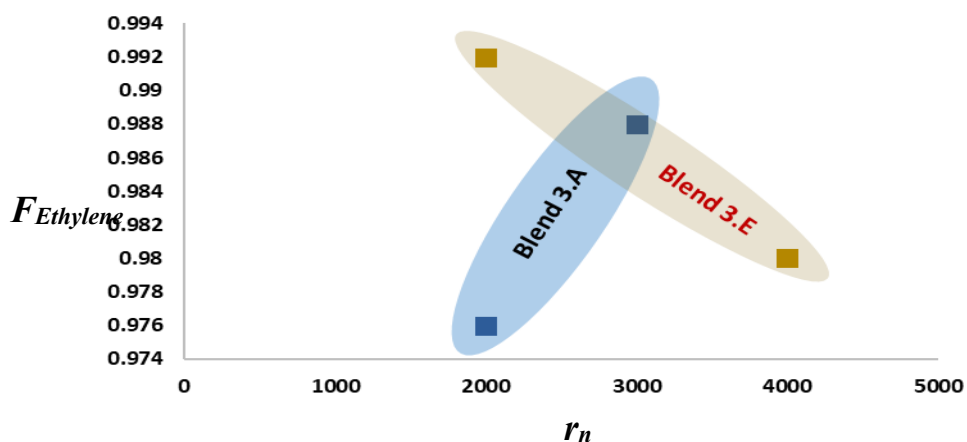


**Figure 4-12.** Comparison of blends with same PSP2\* of Blend 3.

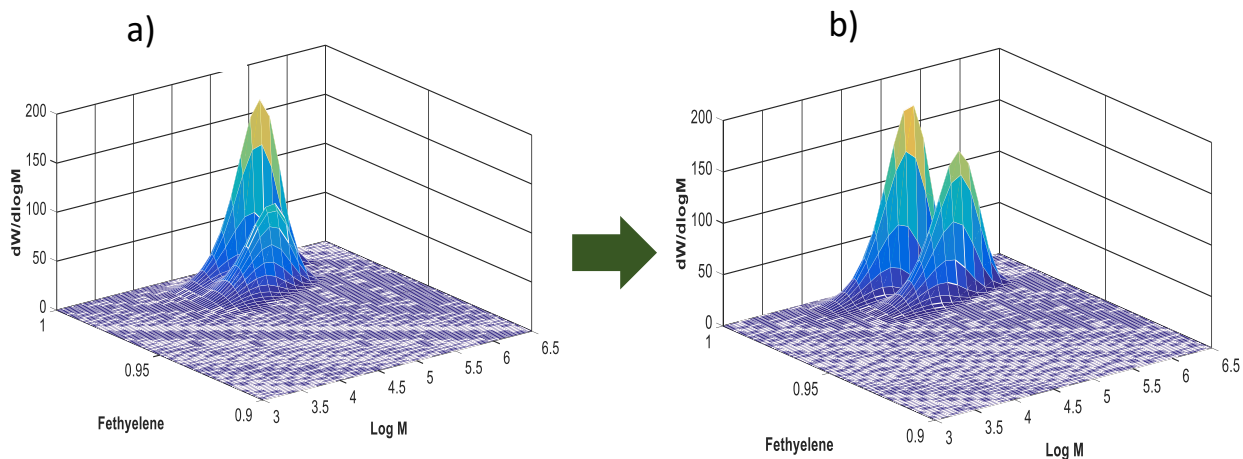


**Figure 4-13.** Molecular weight distribution and short chain branching distributions of blends 3.A (a) and 3.E (b).

Figure 4-14 compares the number of blends with similar PSP2\* in the range specified in Table 4-4. For instance, 20 blends have PSP2\* varying between 15.2 and 15.4. This means 20 blends have similar properties although their polymer structures are different.

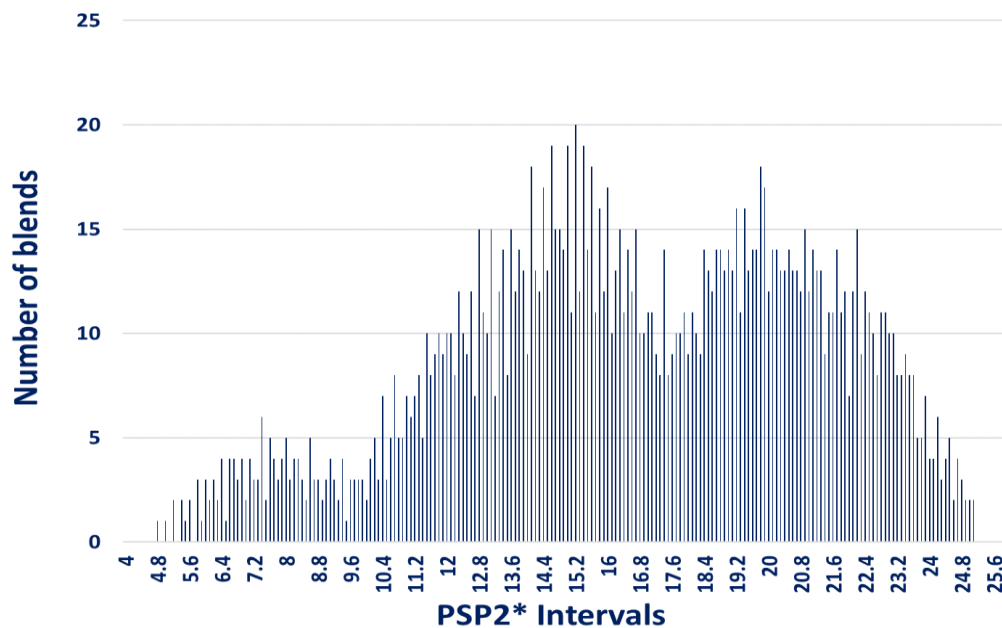


**Figure 4-14.** Distribution of number of blends for PSP2\* intervals of 0.1 units.

#### 4.6. Conclusions

PSP2 is a powerful tool to correlate mechanical properties with the microstructure of the polymer for the copolymer in this study. PSP2 is estimated using the results from GPC – IR, which are faster and cheaper compare with Cross Fraction Technique (CFC). Results from this study suggest that PSP2 is good enough to predict mechanical properties if the comonomer distribution is narrow. For instance, if a single site catalyst is used, PSP2 is good to predict mechanical properties for the whole range of polymer produce.

However, PSP2\* demonstrates that for a specific range of molecular weight and comonomer content, a blend of single sites catalyst could produce a comonomer content broad enough to deviate the value PSP2\* from PSP2 for one more accordance with the polymer structure. Thus, although PSP2 could be enough for more of the cases, PSP2\* could be useful when the correlation of mechanical properties and polymer structure using PSP2 does not work.

In addition, the simulation also helps to identify that it is possible generate blends with similar primary structure parameters, thus, it could be a powerful tool in development of new polyethylene grades.

## Chapter 5 : Integration of Polymerization Kinetics with Polymer Mechanical Properties Prediction

### 5.1. Introduction

Chapter 3 described a polymerization kinetics model for bis(cyclopentadienyl) hafnium(IV) dichloride ( $\text{Cp}_2\text{HfCl}_2$ ). The main model parameters were estimated, and the model could predict the yield and microstructure of polymer produced under specific polymerization conditions. Chapter 4 proposed a model to predict the mechanical properties of polyethylene based on a modification of the DesLauriers approach [3].

In this chapter, these two modelling approaches were integrated so that the mechanical properties of the resulting polymer could be predicted directly from the polymerization conditions. This modeling approach allows the development of new polymer grades, or the optimization of existing ones, with minimal cost and time requirements.

Polymerization kinetics models for bis(cyclopentadienyl)zirconium(IV) dichloride ( $\text{Cp}_2\text{ZrCl}_2$ ), and methyl(6-t-butoxyhexyl) silyl ( $\eta^5$ -tetramethylcyclopentadienyl) (t-butylamido) titanium dichloride (**CGC-Ti**) were also included in the simulations. Models for these catalysts were developed by other members of our group [43]. These 3 catalysts were “virtually blended” in an ideal semi-batch at different proportions and polymerization conditions to analyze the effect on the mechanical properties of the final polymer blend.

### 5.2. Virtual Polymerization Reactor Conditions and Modeling Equations

The following polymerization conditions were adopted for all simulations:

1. Ideal semi-batch with residence time of 1 hour.
2. The reactor volume was assumed in 1 L.
3. Polymerization were in toluene and the reaction temperature was 120°C.
4. The total catalyst concentration in the reactor was 0.2  $\mu\text{mol/L}$ .
5. Ethylene concentration varied from 0.2 to 0.6 mol/L, and 1-hexene concentration from 0 to 0.9 mol/L.
6. Hydrogen was not added to the reactor for the virtual polymerizations.

The polymerization kinetic models for  $\text{Cp}_2\text{ZrCl}_2$  and CGC-Ti were developed in a previous work in our research group [43]. Since the model parameters were estimated in the presence of hydrogen, a proportional factor for polymerizations with and without hydrogen was estimated using catalyst productivity with hydrogen over catalyst productivity without hydrogen. This factor was multiplied by the propagation constants for  $\text{Cp}_2\text{ZrCl}_2$  and CGC-Ti. Table 5.1. summarizes the model parameters for these 2 catalysts. Model parameters for  $\text{Cp}_2\text{HfCl}_2$  were estimated in Chapter 3 of this thesis.

**Table 5-1.** Polymerization kinetics parameters for  $\text{Cp}_2\text{ZrCl}_2$  and CGC-Ti [43].

Parameters	Catalysts	
	$\text{Cp}_2\text{ZrCl}_2$	CGC-Ti
$k_{pAA}$ ( $\text{L}\cdot\text{mol}^{-1}\text{s}^{-1}$ )	190,000	48,400
$k_{pBA}$ ( $\text{L}\cdot\text{mol}^{-1}\text{s}^{-1}$ )	20,000	3,740
$k_{pAB}$ ( $\text{L}\cdot\text{mol}^{-1}\text{s}^{-1}$ )	9,400	5,940
$k_{pBB}$ ( $\text{L}\cdot\text{mol}^{-1}\text{s}^{-1}$ )	0	2,420
$k_{t\beta} + k_{tAl}[Al]$ ( $\text{L}\cdot\text{mol}^{-1}\text{s}^{-1}$ )	86	15
$k_d$ ( $\text{s}^{-1}$ )	$3.70 \times 10^{-4}$	$2.90 \times 10^{-3}$
$k_a$ ( $\text{s}^{-1}$ )	----	$7.70 \times 10^{-4}$
$k_i$ ( $\text{L}\cdot\text{mol}^{-1}\text{s}^{-1}$ )	----	1.00
$r_a$	110	8.10
$r_b$	----	0.06

In order to estimate the amount of polymer produced by each catalyst, the polymerization rate is needed. The following are the equations for the polymerization rates for  $\text{Cp}_2\text{ZrCl}_2$  and CGC-Ti [43]. An expression for the polymerization rate for  $\text{Cp}_2\text{HfCl}_2$  was estimated in Chapter 3.

**$\text{Cp}_2\text{ZrCl}_2$ :**

$$R_p = \widehat{k_p} [A] C_{io} e^{-k_a t} \quad (5.1)$$

$$R_p = \text{Polymerization rate, mol} \cdot \text{s}^{-1} \cdot \text{L}^{-1}$$

$$\widehat{k}_p = k_{pAA} + (k_{pBA} - k_{pAA}) \frac{k_{pABfB}}{k_{pABfB} + k_{pBAfA}}$$

$[A]$  = Ethylene concentration,  $\text{mol} \cdot \text{L}^{-1}$ .

$C_{io}$  = Catalyst concentration,  $\text{mol} \cdot \text{L}^{-1}$ .

$V_R$  = Reactor volume, L.

**CGC-Ti:**

$$R_p = \widehat{k}_p \left( k_i[M]C_{io} \left[ \frac{k_a}{s_1 s_2} \left( \frac{s_1 + k_a}{s_1 (s_1 - s_2)} \right) e^{s_1 t} + \left( \frac{s_2 + k_a}{s_2 (s_2 - s_1)} \right) e^{s_2 t} \right] \right) [A] \quad (5.2)$$

$[M]$  = Ethylene concentration plus 1 – hexene concentration,  $\text{mol} \cdot \text{L}^{-1}$ .

$$s_1 = \frac{-A - \sqrt{A^2 - 4B}}{2}$$

$$s_2 = \frac{-A + \sqrt{A^2 - 4B}}{2}$$

$$A = k_i[M] + k_a + k_d$$

$$B = k_i[M]k_d + k_i[M]k_a + k_a k_d$$

In addition, the model required the estimation of the number average molecular weight ( $M_n$ ), molecular weight distribution (MWD), average comonomer content ( $\overline{F}_A$ ) and comonomer content distribution (CCD) for the estimation of PSP2\*. The equation to estimate  $M_n$  for  $\text{Cp}_2\text{ZrCl}_2$  and CGC-Ti is given by

$$\frac{mw}{M_n} = \frac{(k_{t\beta} + k_{tAl} [Al])}{k_p[M]} \quad (5.3)$$

where  $mw$  is the molecular weight of the repeating unit.

It was assumed that transfer to monomer was negligible for both catalysts. Figure 5.1 compares  $M_n$  estimated by the model (Equation (5.3)) versus experimental values [43].

The results show a good correlation between the model and experimental values. A model to predict  $M_n$  for polymers made with  $\text{Cp}_2\text{HfCl}_2$  was developed in Chapter 3.

The estimation of  $\overline{F}_A$  is given by Mayo-Lewis equation, MWD by Flory distribution, and CCD by the Stockmayer distribution. The equations were explained in Chapter 2.

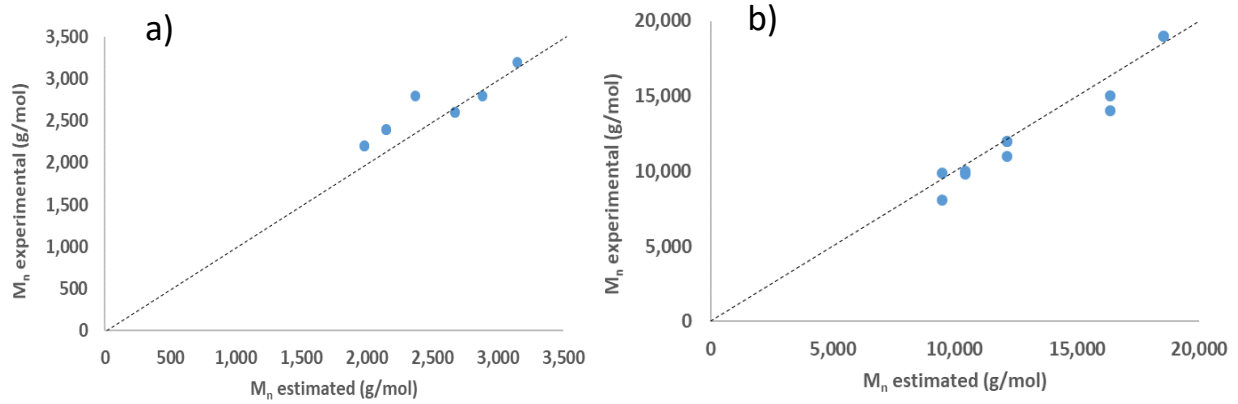


**Figure 5-1.** Comparison between the experimental and estimated  $M_n$  for a)  $Cp_2ZrCl_2$  and b) CGC-Ti

For the simulations, polymerization conditions were kept constant but the amount of polymer made by each catalyst were different due to their own set of kinetic parameters and polymerization rate equations. As a result, the polymer structure for each catalyst would be the same, but the final polymer would be depending on the fraction of polymer made by each catalysts.

The molecular weight distribution of the whole polymer is given by

$$W_{whole\ MW,FA} = f_{Hf} \cdot W_{Hf\ MW,FA} + f_{Zr} \cdot W_{Zr\ MW,FA} + f_{CGC} \cdot W_{CGC\ MW,FA} \quad \text{Eq. 5.4}$$

Where  $f_{Hf}$ ,  $f_{Zr}$  and  $f_{CGC}$  are the mass fractions of polymer made with the catalysts  $Cp_2HfCl_2$ ,  $Cp_2ZrCl_2$  and CGC-Ti, respectively, and  $w_{Hf\ MW,FA}$ ,  $w_{Zr\ MW,FA}$ ,  $w_{CGC\ MW,FA}$  and  $w_{whole\ MW,FA}$  is the Stockmayer bivariate distribution for the catalysts  $Cp_2HfCl_2$ ,  $Cp_2ZrCl_2$ , CGC-Ti and the final polymer blend, respectively.

### 5.3. Integration Model

The integration of the two modelling approaches developed in chapter 3 and chapter 4 was coded in Matlab. Reactor conditions and catalyst fraction were set in accordance with Section 5.2 and both varied to evaluate their impact in PSP2\*. Figure 5-2 shows the logic flowchart for the integration model.

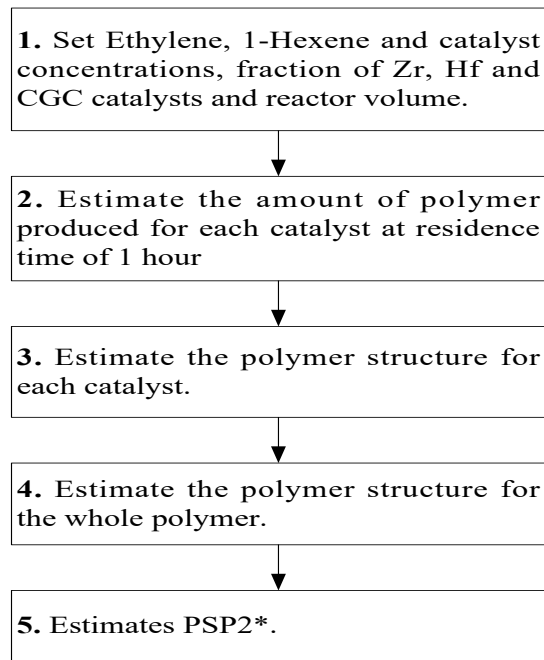


**Figure 5-2.** Logic flowchart for integration model.

## 5.4. Results and Discussion

### 5.4.1 Single Catalysts

Simulations of single type of catalysts were done first to quantify how PSP2\* changed at different polymerization conditions. Since each catalyst (see Table 5-1 and Table 3-22) is characterized with a distinct set of polymerization kinetics parameters, under the same polymerization conditions they will make polymers with different microstructures and PSP2\* values. For instances, Figure 5-3 shows the MWD and CCD of copolymers made with an ethylene concentration of 0.4 mol/L and 1-hexene concentration of 0.1 mol/L with  $\text{Cp}_2\text{HfCl}_2$ ,  $\text{Cp}_2\text{ZrCl}_2$  and CGC-Ti. At these conditions, copolymers made with  $\text{Cp}_2\text{ZrCl}_2$  have the lowest average molecular weight, while CGC-Ti and  $\text{Cp}_2\text{HfCl}_2$  make copolymers with similar average molecular weights (those made with  $\text{Cp}_2\text{HfCl}_2$  have slightly higher molecular weights), but CGC-Ti makes copolymers with the highest average 1-hexene content.

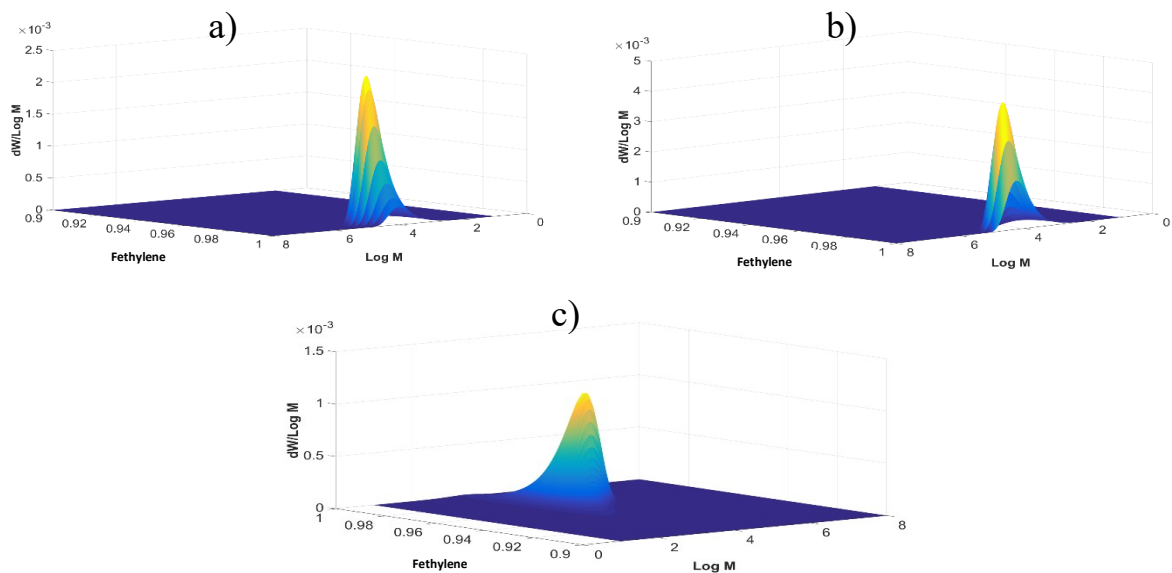


**Figure 5-3.** Molecular weight and comonomer content distribution for ethylene/1-hexene copolymers made with  $\text{Cp}_2\text{HfCl}_2$  (a),  $\text{Cp}_2\text{ZrCl}_2$  (b) and CGC-Ti (c).

Varying ethylene and 1-hexene concentrations, a complete map of number average molecular weight ( $M_n$ ) and the average ethylene content in the polymer ( $F_{\text{Ethylene}}$ ) was generated for polymers made with  $\text{Cp}_2\text{HfCl}_2$ ,  $\text{Cp}_2\text{ZrCl}_2$  and CGC-Ti (Figure 5-4 and Figure 5-5, respectively).

The results show that how  $M_n$  and  $F_{\text{Ethylene}}$  varies with ethylene and 1-hexene concentration is unique for each catalyst. For instance,  $M_n$  of polymer made with  $\text{Cp}_2\text{HfCl}_2$  and CGC-Ti drops significantly when ethylene concentration decreases and 1-hexene concentration increases, while for polymer made with  $\text{Cp}_2\text{ZrCl}_2$ , the  $M_n$  drops more smoothly.

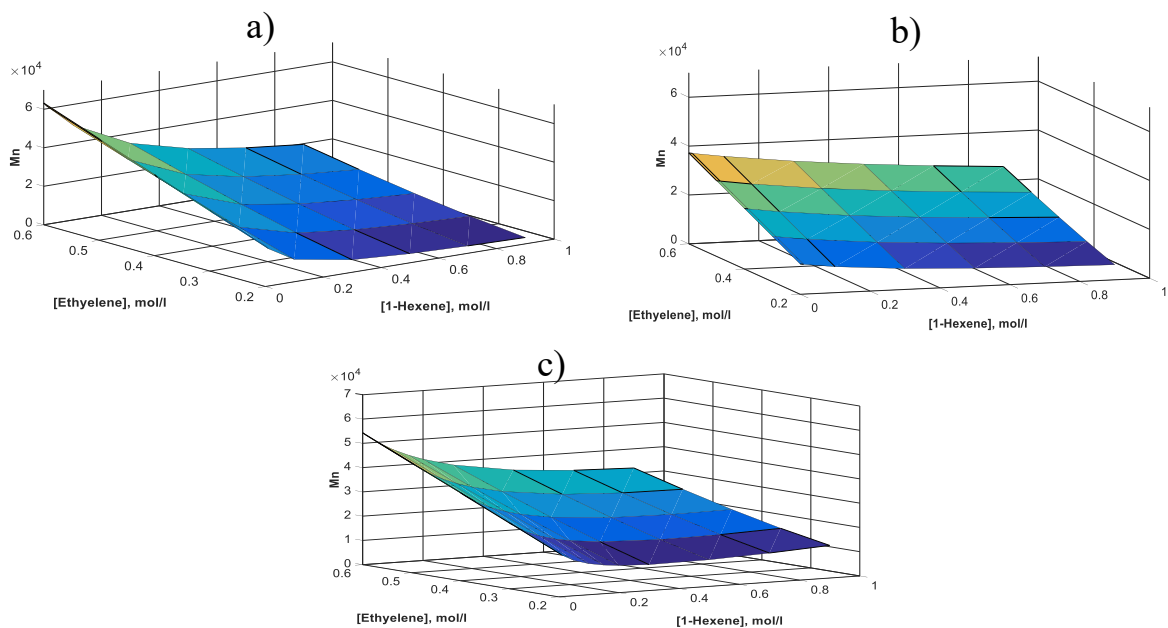


**Figure 5-4.**  $M_n$  versus ethylene and 1-hexene concentrations for ethylene/1-hexene copolymers made with  $\text{Cp}_2\text{HfCl}_2$  (a),  $\text{Cp}_2\text{ZrCl}_2$  (b) and CGC-Ti (c).

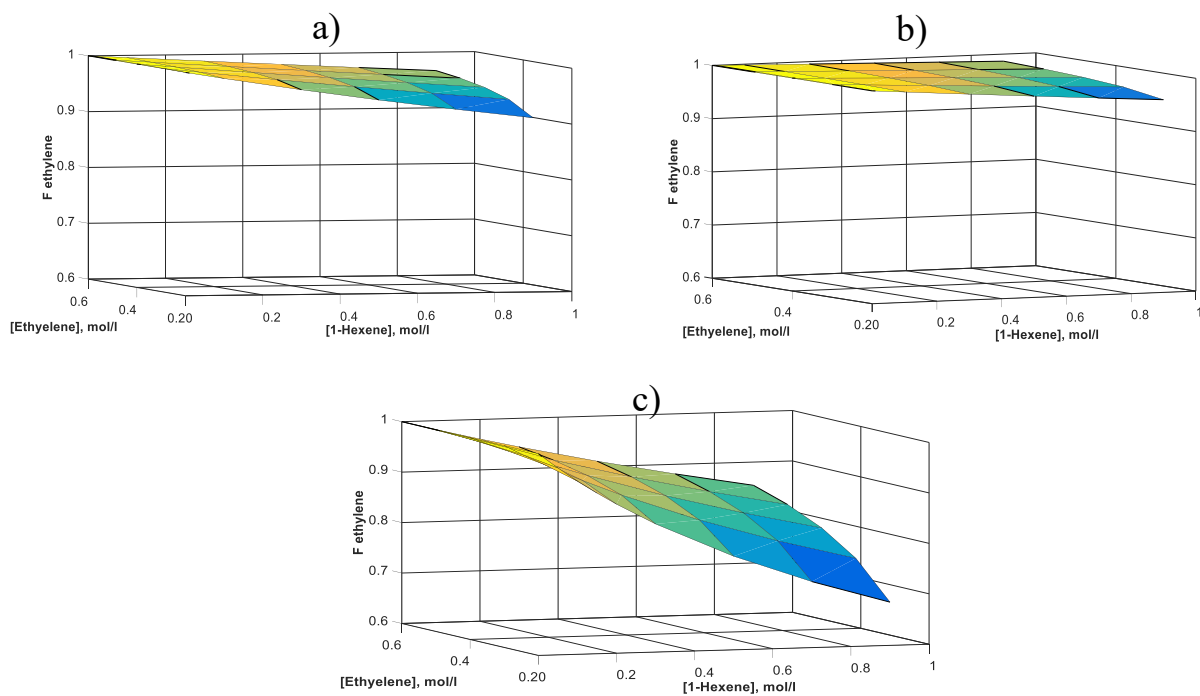


**Figure 5-5.**  $F_{\text{Ethylene}}$  versus ethylene and 1-hexene concentrations for ethylene/1-hexene copolymer made with  $\text{Cp}_2\text{HfCl}_2$  (a),  $\text{Cp}_2\text{ZrCl}_2$  (b) and CGC-Ti (c).

On the other hand,  $\text{Cp}_2\text{HfCl}_2$  incorporates 1-hexene more easily than  $\text{Cp}_2\text{ZrCl}_2$  catalyst, but CGC-Ti has the highest 1-hexene incorporation rate. The unique variation of  $F_{\text{Ethylene}}$  for each catalyst is explained by the different comonomer reactivity ratios of each catalyst.

Higher incorporation of 1-hexene in the copolymer causes a reduction of its crystallinity, reducing the crystal and amorphous layer thicknesses if polymer density moves between 1 and  $0.89 \text{ g/cm}^3$  (Which was one restriction in our simulations) [3]. This lead an increase of tie molecules in the polymer. However, the incorporation of 1-hexene also causes a decrease in the propagation constant of the catalyst, resulting in a decrease in the length of the polymer (or lower molecular weight), which causes a decrease of tie chain molecules formation. As a result, each catalyst has their own tradeoff between lamellae thicknesses and length of the polymer, which makes each catalyst follow different patterns for the formation of tie molecules, and therefore determine the mechanical properties of the polymer.

Figure 5-6 shows how PSP2\* correlates with the ethylene and 1-hexene concentrations in the reactor for each catalyst. PSP2\* for ethylene content lower than 0.96 was not included because the crystallization of the molecules does not follow the spherulites model, and therefore the method used to calculate PSP2\*.

Figure 5-6 show that PSP2\*, which correlates with the concentration of tie molecules in the polymers, differs for each catalyst. For instance, the PSP2\* for  $\text{Cp}_2\text{HfCl}_2$  and  $\text{Cp}_2\text{ZrCl}_2$  decreases when small amounts of 1-hexene are added to the reactor. However, when the concentration of 1-hexene increases in the presence of  $\text{Cp}_2\text{HfCl}_2$ , PSP2\* increases up to a maximum value, but subsequently decreases when 1-hexene concentration decreases. While for  $\text{Cp}_2\text{ZrCl}_2$ , PSP2\* increases steadily when 1-hexene concentration increases. An explanation for  $\text{Cp}_2\text{ZrCl}_2$  behavior it that the length of the polymer decreases in less proportion than the lamellae thickness when 1-hexene concentration increases in the reactor, resulting in an increase of PSP2\*. In case of  $\text{Cp}_2\text{HfCl}_2$ , there is a threshold value where the length of the polymer decreases faster than lamella thickness, resulting in a reduction of PSP2\* when 1-hexene concentration increases.

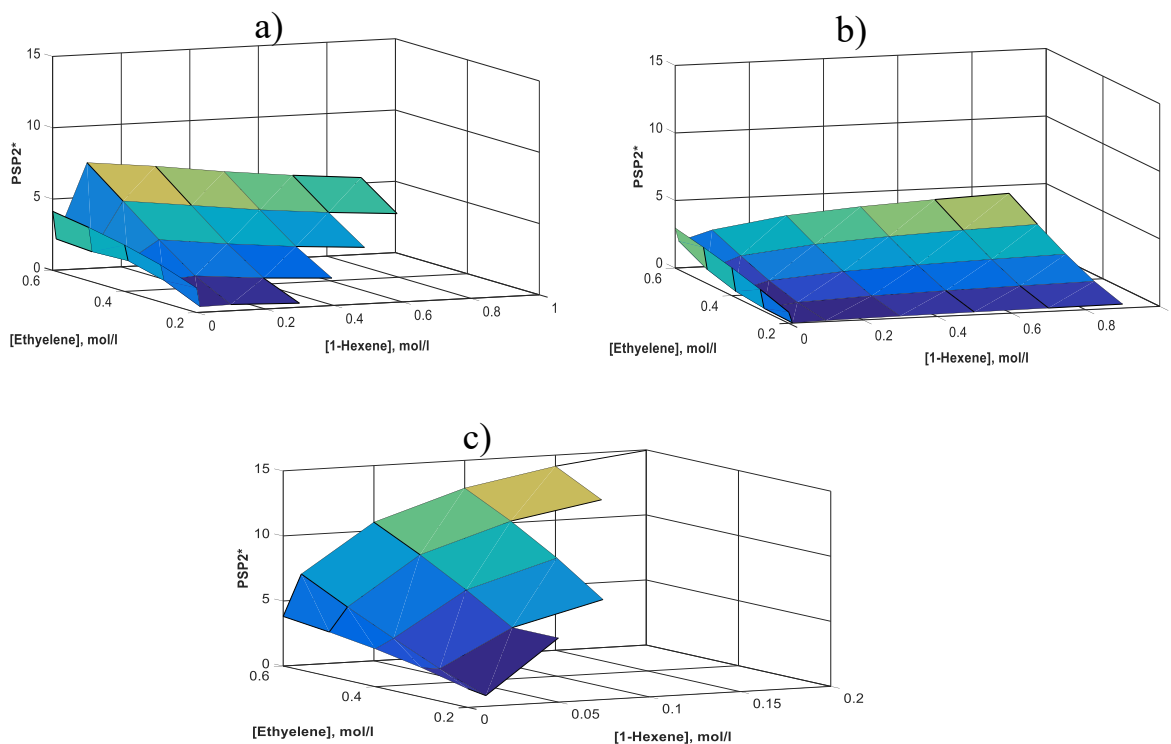


**Figure 5-6.** PSP2\* versus ethylene and 1-hexene concentrations for ethylene/1-hexene copolymer made with  $\text{Cp}_2\text{HfCl}_2$  (a),  $\text{Cp}_2\text{ZrCl}_2$  (b) and CGC-Ti (c).

For CGC-Ti, PSP2\* shows higher values than the other catalyst, which indicates a higher probability of tie molecules formation. In addition, PSP2\* increases continuously when 1-hexene is added to the reactor, except for a region of low ethylene concentration, around 0.2 mol/L, where PSP2\* decreases when a small concentration 1-hexene is added to the reactor, similar behavior of the other catalysts.

These results illustrate that each catalyst has a unique behavior in the tie molecules formation. As a result, the simulation of mixing catalyst and evaluate his impact in PSP2\* could give the starting point to develop tailored polymer more efficiently.

#### 5.4.2 Mix of $\text{Cp}_2\text{HfCl}_2$ , $\text{Cp}_2\text{ZrCl}_2$ and CGC-Ti catalysts

The three catalysts,  $\text{Cp}_2\text{HfCl}_2$ ,  $\text{Cp}_2\text{ZrCl}_2$  and CGC-Ti, were mixed in different proportions to evaluate the effect on PSP2\*, number average molecular weight and average mole fraction of ethylene in the final polymer.

The first step was to estimate the catalyst fraction to be used for each catalyst because the ratio of  $\text{Cp}_2\text{ZrCl}_2$ , CGC-Ti and  $\text{Cp}_2\text{HfCl}_2$  productivities is 12 : 3 : 1, respectively. Thus, if  $\text{Cp}_2\text{ZrCl}_2$  concentration in the reactor is much higher than the others, the amount of polymer produced for CGC-Ti and  $\text{Cp}_2\text{HfCl}_2$  are negligible.

Ethylene and 1-hexene concentrations in the reactor were set to constant values. From results obtained in Section 5.4.1, 1-hexene concentration in reactor was limited to 0.2 mol/L: higher values produce polymer with 1-hexene content higher than 4% for CGC-Ti, invalidating the PSP2\* model. Ethylene concentration varied from 0.2 and 0.6 mol/L. The other conditions were similar to those used in Section 5.2. Table 5-2 summarizes the range of mole fraction for each catalyst used in the simulations.

**Table 5-2.** Simulation conditions for mixing catalysts.

Parameters	Values
$\text{Cp}_2\text{ZrCl}_2$ mole fraction	0 - 0.3
$\text{Cp}_2\text{HfCl}_2$ mole fraction	0 - 1
CGC-Ti mole fraction	0 - 1

Three combinations of ethylene/1-hexene concentrations were used for simulations: 0.2 mol·L<sup>-1</sup> of ethylene and 0.01 mol·L<sup>-1</sup> of 1-hexene, 0.6 mol·L<sup>-1</sup> of ethylene and 0.1 mol·L<sup>-1</sup> of 1-hexene, and 0.6 mol·L<sup>-1</sup> of ethylene and 0.2 mol·L<sup>-1</sup> of 1-hexene.

Simulations results were plotted against  $\text{Cp}_2\text{ZrCl}_2$  and  $\text{Cp}_2\text{HfCl}_2$  mole fractions at a fixed ethylene and 1-hexene concentrations. CGC-Ti fraction can be estimated by subtracting  $\text{Cp}_2\text{ZrCl}_2$  and  $\text{Cp}_2\text{HfCl}_2$  fractions from 1. In the following graph,  $\text{Cp}_2\text{ZrCl}_2$  will be expressed as Zr,  $\text{Cp}_2\text{HfCl}_2$  as Hf and CGC-Ti as CGC.

### 5.4.2.1 Ethylene concentration of 0.2 mol/L and 1-hexene concentration of 0.01 mol/L

For an ethylene concentration of 0.2 mol/L and 1-hexene concentration of 0.01 mol/L, the fraction of polymer made by each catalyst are shown in Figure 5-7.

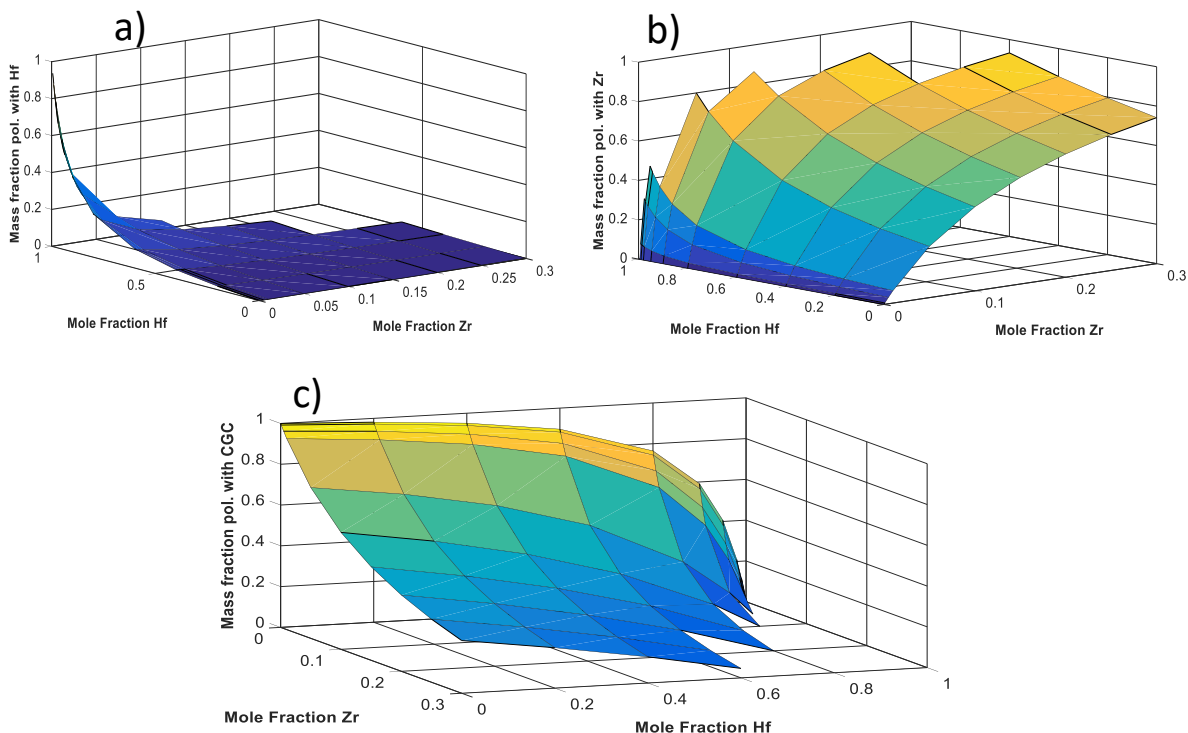


**Figure 5-7.** Fraction of polymer made with  $\text{Cp}_2\text{HfCl}_2$  (a),  $\text{Cp}_2\text{ZrCl}_2$  (b) and CGC-Ti (c).

The results indicate that when the fraction of  $\text{Cp}_2\text{ZrCl}_2$  in the reactor is higher than 0.1, the fraction of polymer produced with  $\text{Cp}_2\text{ZrCl}_2$  is greater than 0.6 (Figure 5.7.b). From Figure 5.7.c, the correlation of the fraction of polymer produced by CGC-Ti with respect to the fraction of  $\text{Cp}_2\text{ZrCl}_2$  and  $\text{Cp}_2\text{HfCl}_2$  are different. For instance, when the fraction of  $\text{Cp}_2\text{ZrCl}_2$  in the reactor increases, the amount polymer produced by CGC-Ti drops significantly, while a large fraction of  $\text{Cp}_2\text{HfCl}_2$  is required to produce the same amount of the polymer produced by CGC-Ti.

Figure 5-8 shows how the number average molecular weight and average ethylene content vary in accordance with the fraction of catalyst in the reactor. Previously, in section 5.4.1, the number average molecular weight produced for each catalyst in the pure state at similar conditions follows

$\text{Cp}_2\text{HfCl}_2 > \text{CGC-Ti} > \text{Cp}_2\text{ZrCl}_2$ . Alternatively,  $\text{Cp}_2\text{ZrCl}_2$  showed the lowest 1-hexene incorporation while CGC showed the highest. As a result,  $F_{\text{Ethylene}}$  follows  $\text{Cp}_2\text{ZrCl}_2 > \text{Cp}_2\text{HfCl}_2 > \text{CGC-Ti}$ . Consequently, the results of Figure 5-8 follow the results obtained in pure state, for instance,  $M_n$  increases when  $\text{Cp}_2\text{HfCl}_2$  fraction increases and reduces when  $\text{Cp}_2\text{ZrCl}_2$  fraction increases.

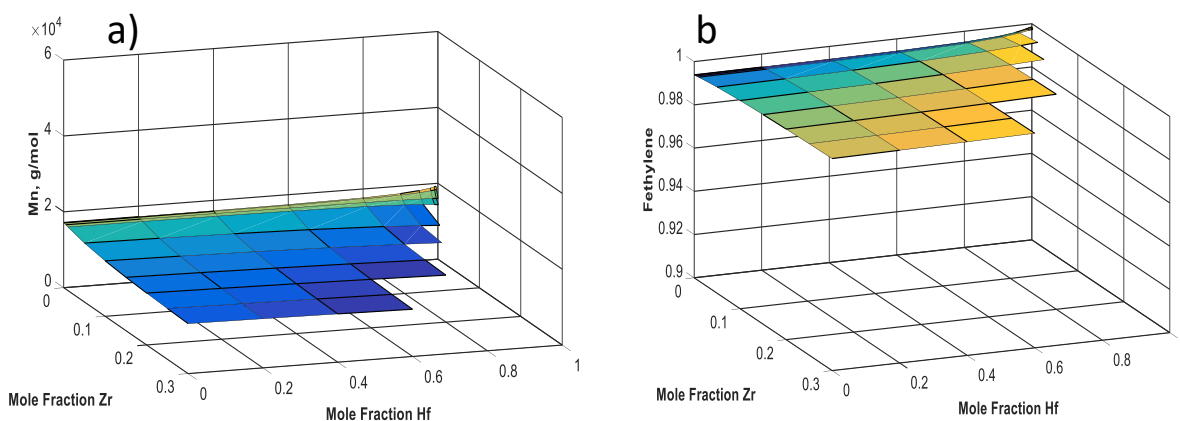


**Figure 5-8.**  $M_n$  (a) and  $F_{\text{Ethylene}}$  (b) for mixing catalyst at ethylene concentration of 0.2 mol/L and 1-hexene concentration of 0.01 mol/L.

For a single site catalyst, the polydispersity index (PDI) is 2, however, when multiple single sites are mixed, PDI increases. PDI is important in the final application because high PDI values make the polymer easier to process during the conversion procedure. Figure 5-9 shows how PDI changes with catalyst fractions in the reactor. The results suggest a small variation of PDI, with the highest value being 2.1. This phenomenon is explained by the number average molecular weight of the three catalyst being similar.

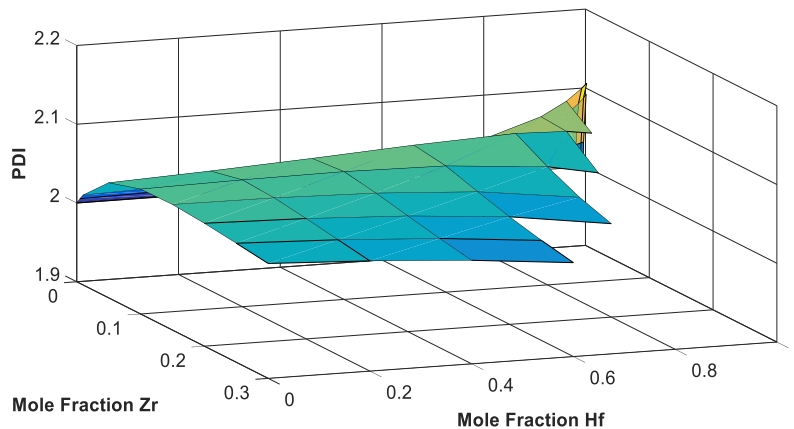


**Figure 5-9.** PDI at ethylene concentration of 0.2 mol/L and 1-hexene concentration of 0.01 mol/L.

Figure 5-10 shows how PSP2\* varies with catalyst fractions in the reactor. For pure catalyst, PSP2\*, in descending order, is given by CGC-Ti > Cp<sub>2</sub>HfCl<sub>2</sub> > Cp<sub>2</sub>ZrCl<sub>2</sub>. This agrees with the result of Figure 5-10, where PSP2\* reduces when Cp<sub>2</sub>ZrCl<sub>2</sub> fraction increases and increases when Cp<sub>2</sub>ZrCl<sub>2</sub> and Cp<sub>2</sub>HfCl<sub>2</sub> fractions decrease.

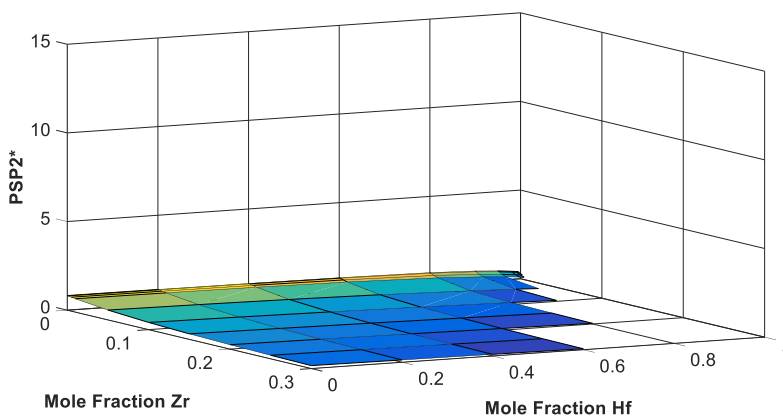


**Figure 5-10.** PSP2\* at ethylene concentration 0.2 mol/L and 1-hexene concentration 0.01 mol/L.

For ethylene concentration of 0.2 mol/L and 1-hexene concentration of 0.01 mol/L, PSP2\* values are small, with the highest PSP2\* value being 0.89.

### 5.4.2.2 Ethylene concentration of 0.6 mol/L and 1-hexene concentration of 0.1 mol/L

For an ethylene concentration of 0.6 mol/L and 1-hexene concentration of 0.1 mol/L, the fraction of polymer made with each catalyst are shown in Figure 5-11.

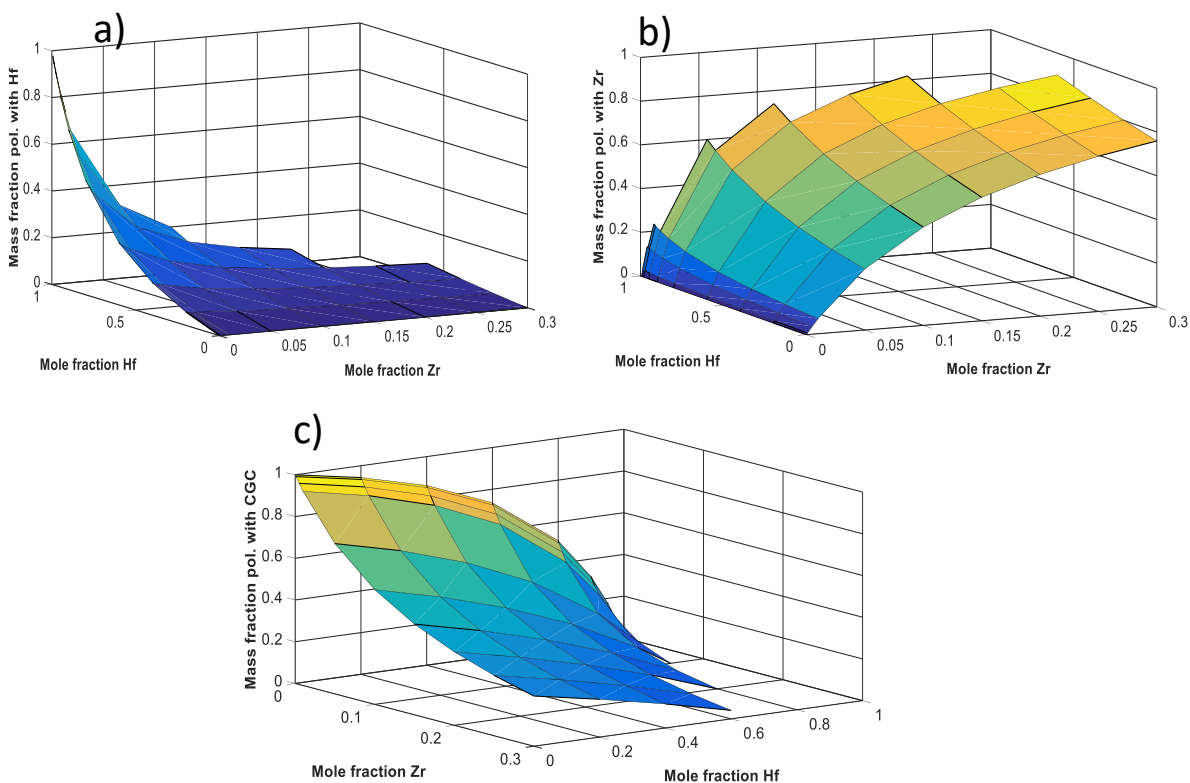
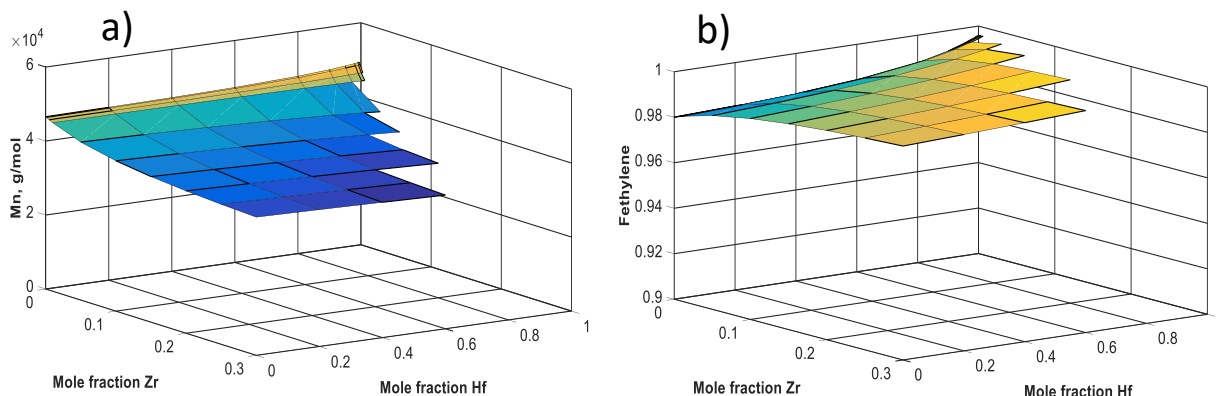


**Figure 5-11.** Fraction of polymer produce with  $\text{Cp}_2\text{HfCl}_2$  (a),  $\text{Cp}_2\text{ZrCl}_2$  (b) and CGC-Ti (c).

The curves are similar to those obtained in Figure 5-7. For instance, when the fraction of  $\text{Cp}_2\text{ZrCl}_2$  is higher than 0.1, the fraction of polymer produced by  $\text{Cp}_2\text{ZrCl}_2$  is greater than 0.6.

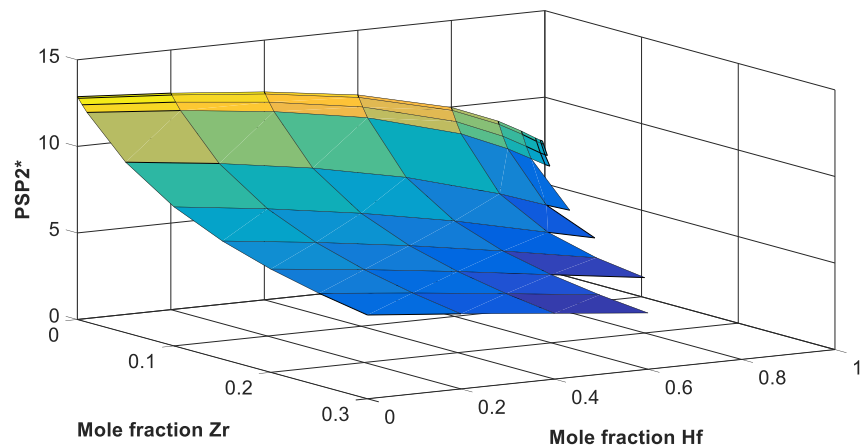
Figure 5-12 shows how number average molecular weight and average mole fraction of ethylene in the polymer vary in accordance with the fraction of catalysts in the reactor. Although the trend is similar to the ones found in Figure 5-8, in this case,  $M_n$  reports higher values which is explained by the higher ethylene concentration in the reactor. Similar analysis is obtained for  $F_{\text{Ethylene}}$ , the average ethylene content is lower with respect to Figure 5-8 due to the higher mole fraction of

1-hexene in the reactor. As a result, lower average ethylene content (or higher average 1-hexene content) incorporates in the polymer when the fraction of CGC-Ti is increased in the reactor; but, the shape of the curve is similar to Figure 5-8.



**Figure 5-12.**  $M_n$  (a) and  $F_{ethylene}$  (b) for mixing catalyst at ethylene concentration 0.6 mol/L and 1-hexene concentration 0.1 mol/L.

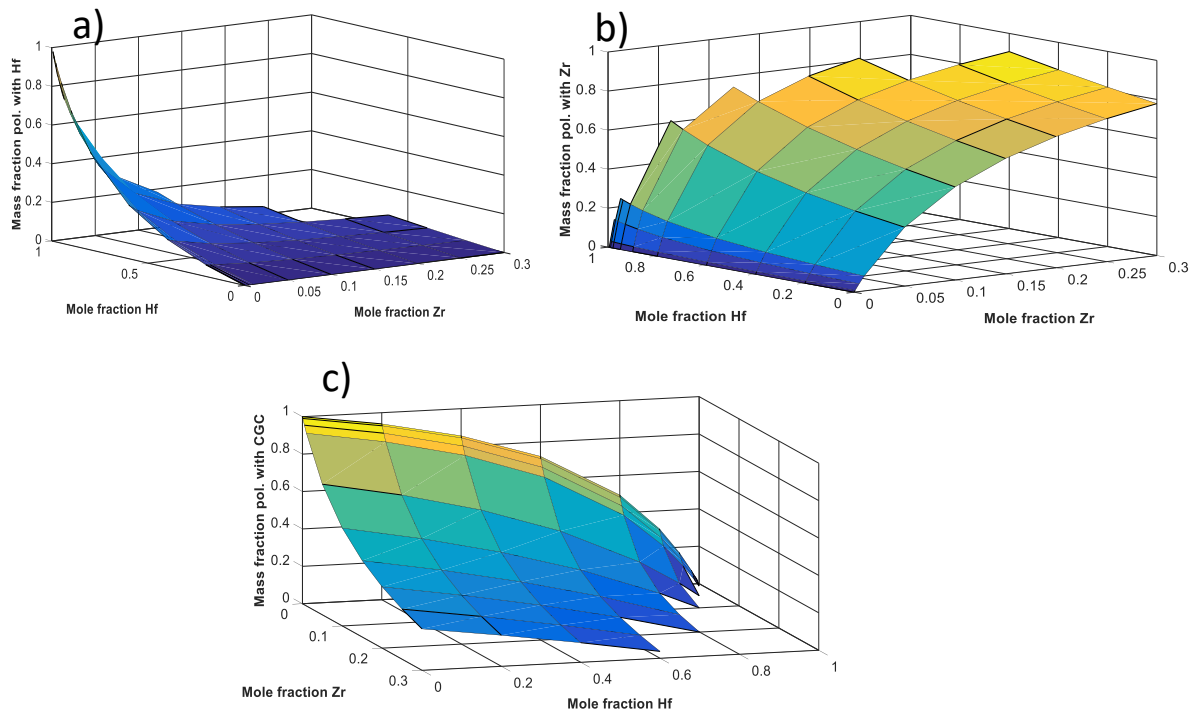
Figure 5-13 shows how PSP2\* varies with catalyst fractions in the reactor. In this case, higher values are reported when compared to Figure 5-10 because higher ethylene concentration causes a higher polymer length while a higher average 1-hexene content causes a shorter lamellae length. Both lead to a higher probability of tie molecules in the polymer. However, the shape of the curve is similar to that obtained in Figure 5-10.



**Figure 5-13.** PSP2\* at ethylene concentration 0.6 mol/L and 1-hexene concentration 0.1 mol/L.

### 5.4.2.3 Ethylene concentration of 0.6 mol/L and 1-hexene concentration of 0.2 mol/L

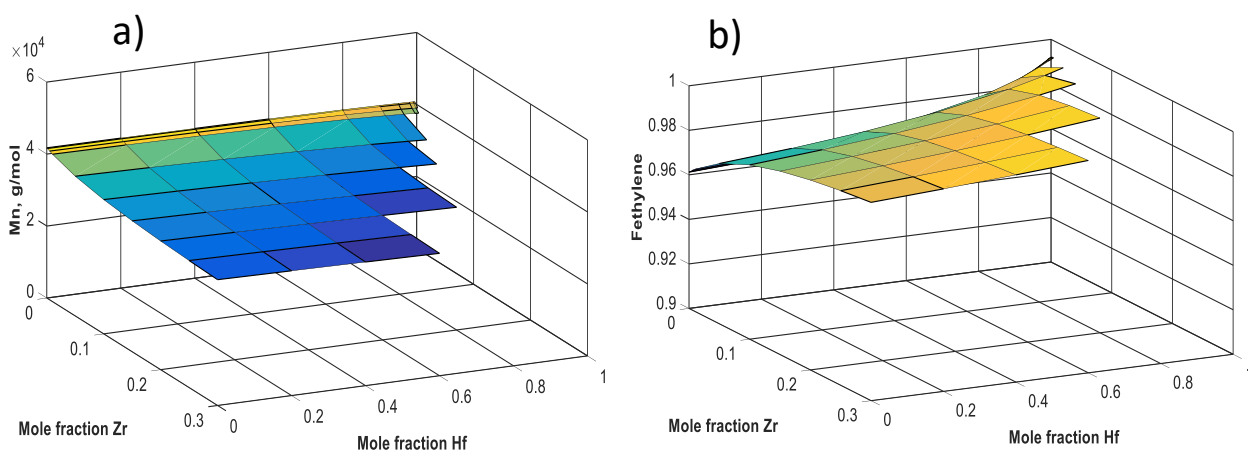
For an ethylene concentration of 0.6 mol/L and 1-hexene concentration of 0.2 mol/L, the fraction of polymer made with each catalyst are shown in Figure 5-14.



**Figure 5-14.** Fraction of polymer produce with  $\text{Cp}_2\text{HfCl}_2$  (a),  $\text{Cp}_2\text{ZrCl}_2$  (b) and CGC-Ti (c).

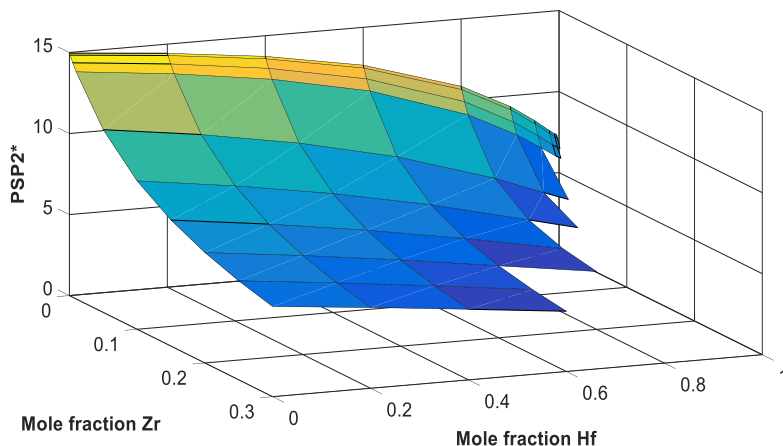
The results are similar to those obtained in Figure 5-7 and Figure 5-11. As a result, there is no significant variation of the fraction of polymer made by mixed catalysts at different ethylene and 1-hexene concentrations.

Figure 5-15 shows how the number average molecular weight and ethylene content vary in accordance with the fraction of catalyst in the reactor. The reduction of  $M_n$  compared to Figure 5-12 is expected due to the higher 1-hexene concentration in the reactor. Higher 1-hexene concentration causes a reduction of propagation constant and therefore a reduction of length of the polymer chain. Higher comonomer content is expected and consequently lower  $F_{Ethylene}$  values. However, the curves of Figure 5-15 are similar to Figure 5-8 and Figure 5-12.



**Figure 5-15.**  $M_n$  in g/mol and  $F_{Ethylene}$  for mixing catalyst at ethylene concentration 0.6 mol/L and 1-hexene concentration 0.2 mol/L.

Figure 5-16 shows how PSP2\* varies with catalyst fractions in the reactor. In this case, higher values are reported when compared to Figure 5-13. This is due to a higher 1-hexene fraction in the reactor and therefore a reduction of lamellae length in the polymer in major proportion than the molecular weight, causing an increase in the probability of entanglements of the polymer. However, the shape of the curve is similar to Figure 5-10 and Figure 5-13.



**Figure 5-16.** PSP2\* at ethylene concentration of 0.6 mol/L and 1-hexene concentration 0.2 of mol/L.

## 5.5. Conclusions

The fraction of polymer produced by each catalyst when  $\text{Cp}_2\text{HfCl}_2$ ,  $\text{Cp}_2\text{ZrCl}_2$  and CGC-Ti are mixed is very similar at different ethylene and 1-hexene concentrations. Although the productivity drops for each catalyst in different proportion, the significant difference between productivities is large enough that it doesn't affect the fraction of polymer produced for each catalyst used.

The number average molecular weight is affected by ethylene concentration and the fraction of 1-hexene in the reactor, as discussed in section 5.4.1. However, the contour of  $M_n$  versus  $\text{Cp}_2\text{HfCl}_2$  and  $\text{Cp}_2\text{ZrCl}_2$  fractions is not affected by ethylene and 1-hexene concentration. The trend slightly shifts to upper values when ethylene concentration increases and 1-hexene concentration decreases. The edges of the contour are given by  $M_n$  of the polymers produced by each catalyst in pure state.

Ethylene content is also affected by the fraction of 1-hexene in the reactor, as discussed in section 5.4.1. The contour of  $F_{\text{Ethylene}}$  versus  $\text{Cp}_2\text{HfCl}_2$  and  $\text{Cp}_2\text{ZrCl}_2$  fractions is not affected significantly by ethylene and 1-hexene concentrations. The edges of the contour are given by  $F_{\text{Ethylene}}$  of polymers produced by each catalyst in pure state.

The Polydispersity Index (PDI) of the whole polymer at different ethylene and 1-hexene concentrations didn't result in values greater than 2.1 because  $M_n$  values of each catalyst were similar in magnitude at similar monomer concentrations.

Finally, PSP2\* shows similar contour at different ethylene and 1-hexene concentrations. The contour shifted to upper if the conditions favored the formation of tie molecules. If the conditions did not favor the formation of tie molecules, the contour shifted to lower values. The edges of the curve are given by PSP2\* values of polymer produced by each catalyst in pure state.

An interesting result in the analysis of PSP2\* is when  $Cp_2HfCl_2$  was mixed with CGC-Ti. Noting the data given by Figure 5-10, 5-13 and 5-16, and comparing them with the result in pure state, mixing catalysts could be an efficient solution to increase the properties and comonomer content for  $Cp_2HfCl_2$ . This can be seen through two examples:

1. At an ethylene concentration of 0.6 mol/L and 1-hexene concentration of 0.1 mol/L, Table 5-3 shows the properties of the polymer produced by  $Cp_2HfCl_2$ , while the properties of a mixture of  $Cp_2HfCl_2$  and CGC-Ti in a proportion of 0.8 / 0.2, respectively, are shown in Table 5-4:

**Table 5-3.** Polymer properties of  $Cp_2HfCl_2$  at Ethylene concentration of 0.6 mol/L and 1-hexene concentration of 0.1 mol/L.

<b><math>Cp_2HfCl_2</math> Pure</b>	
<b>Parameters</b>	<b>Values</b>
<b>[Ethylene]</b>	0.6 mol·L <sup>-1</sup>
<b>[1-hexene]</b>	0.1 mol·L <sup>-1</sup>
<b><math>M_n</math></b>	49,452 g ·mol <sup>-1</sup>
<b>PDI</b>	2
<b><math>F_{Ethylene}</math></b>	0.996
<b>PSP2*</b>	<b>7.4</b>

**Table 5-4.** Polymer properties of mixed  $\text{Cp}_2\text{HfCl}_2$  / CGC-Ti at Ethylene concentration of 0.6 mol/L and 1-hexene concentration of 0.1 mol/L.

<b>Mix <math>\text{Cp}_2\text{HfCl}_2</math> / CGC-Ti</b>	
<b>Parameters</b>	<b>Values</b>
<b>Mole Fraction Hf</b>	0.8
<b>Mole Fraction CGC</b>	0.2
<b>[Ethylene]</b>	$0.6 \text{ mol}\cdot\text{L}^{-1}$
<b>[1-hexene]</b>	$0.1 \text{ mol}\cdot\text{L}^{-1}$
<b><math>M_n</math></b>	$48,110 \text{ g}\cdot\text{mol}^{-1}$
<b>PDI</b>	2.002
<b><math>F_{\text{Ethylene}}</math></b>	0.988
<b>PSP2*</b>	<b>9.7</b>

The mixed catalysts produced a polymer with a similar number average weight to that of the polymer produced by  $\text{Cp}_2\text{HfCl}_2$ . However, an important characteristic to note is an increase of PSP2\*, and therefore an increase in mechanical properties due to the higher incorporation of 1-hexene in the polymer.  $F_{\text{Ethylene}}$  decreases from 0.996 ( $\text{Cp}_2\text{HfCl}_2$  Pure) to 0.988 (Mixed catalyst).

2. The incorporation of 1-hexene content in the polymer also creates deformation in the crystallization of the polymer, increasing the amorphous content and therefore improving the optical properties [32]. If a commercial plant is limited to operate with a fraction of 1-hexene in the reactor of 0.25, mixing catalysts in the correct proportion could be a solution to control the 1-hexene content in the polymer. For a 1-hexene fraction of 0.25 (Ethylene concentration 0.6 mol/L and 1-hexene concentration 0.2 mol/L), Table 5-5 shows the ethylene content in the final polymer at various mixing catalyst ratio.

From table 5-5, mixing  $\text{Cp}_2\text{HfCl}_2$  with CGC-Ti in a proportion of 0.9 / 0.1 causes an increase of 1-hexane content in the polymer from 0.8% using purely  $\text{Cp}_2\text{HfCl}_2$  to 1.7% when mixing  $\text{Cp}_2\text{HfCl}_2$ /CGC-Ti.

Therefore, the integration model is a useful tool to estimate a starting point when mixing different catalysts and subsequently predicts its impact in the polymer mechanical properties.

**Table 5-5.** Ethylene content at various mixing catalyst ratio for a 1-hexene fraction of 0.25.

<b>Mole Fraction Catalyst</b>		<b>F<sub>Ethylene</sub></b>	<b>PSP2*</b>	<b>M<sub>n</sub> (g·mol<sup>-1</sup>)</b>
<b>Cp<sub>2</sub>HfCl<sub>2</sub></b>	<b>CGC-Ti</b>			
0	1	0.961	15.0	41,730
0.2	0.8	0.963	14.3	41,663
0.4	0.6	0.967	13.5	41,571
0.6	0.4	0.971	12.3	41,437
0.8	0.2	0.979	10.4	41,226
0.9	0.1	0.984	8.9	41,066
0.95	0.05	0.988	8.1	40,964
0.98	0.02	0.990	7.6	40,894
0.99	0.01	0.991	7.4	40,868
0.995	0.005	0.991	7.3	40,855
1	0	0.992	7.2	40,842

## Chapter 6 : Conclusion and Recommendations

### 6.1. Conclusions

The main objective of this dissertation was to propose a global model to predict the mechanical properties of the polymer using its molecular weight distribution and comonomer content distribution from its reaction conditions. In order to achieve this goal, this thesis and its conclusion is divided into three main sections:

First, the polymerization kinetic constants for the metallocene catalyst bis(cyclopentadienyl) hafnium(IV) dichloride were successfully estimated for ethylene polymerization and ethylene/1-hexene copolymerization. It was identified that the catalyst follows second order kinetics for the propagation and first order for catalyst decay over the range of conditions tested in this thesis. In addition, the pre-exponential factor and the activation energy for the propagation and decay constant were estimated. The results indicate that the models proposed adequately describe the polymerization kinetic, the number average molecular weight, and average 1-hexene content in the polymer made with  $\text{Cp}_2\text{HfCl}_2$  for ethylene polymerization with/without hydrogen and ethylene/1-hexene copolymerization. The decay constant has higher variability for ethylene/1-hexene copolymerization and correlates with the amount of 1-hexene added to the reactor. Further analysis is required to identify the causes of the higher variability.

Second, a methodology to calculate the primary structure parameter (PSP2\*) based on the probability of the polymer to make tie molecules using the molecular weight distribution and comonomer content distribution was successfully tested for copolymers with 1-hexene content lower than 1.5%. This methodology was compared with the primary structure parameter (PSP2) proposed by Paul Deslaruries. The results indicate a good correlation between the mechanical properties and PSP2\*. However, PSP2\* is very similar to the values obtained by PSP2. PSP2 can be obtained using the results from GPC – IR, which are faster and cheaper compared to the analysis required for the estimation of PSP2 using Cross Fraction Technique (CFC). Results from this study suggest that PSP2 is good enough to predict mechanical properties if the comonomer distribution is narrow.

However, PSP2\* demonstrates that for a specific range of molecular weight and comonomer content, a blend of single site catalysts can produce a comonomer content broad enough to derive the value of PSP2\* from PSP2. Although PSP2 could be used for more generalized cases, PSP2\* could be useful when the correlation of mechanical properties and polymer structure using PSP2 doesn't work. In addition, the simulation also helps to identify that it is possible to generate blends with similar primary structure parameters. Therefore, it can be a powerful tool in the development of new polyethylene grades.

Finally, the kinetic models for three metallocene catalysts, one estimated in this thesis and the others from previous work [43], were integrated successfully in the model for the estimation of mechanical properties, PSP2\*. Thus, the integrated model can predict the mechanical properties of the resulting polymer directly from the polymerization conditions. The integrated model can successfully predict the number average molecular weight, the weight average molecular weight, polydispersity index, average comonomer content, molecular weight distribution, comonomer content distribution and PSP2\* of the resulting polymer from different mixing proportions of the three catalysts in an ideal semi-batch reactor. One interesting finding is that when  $Cp_2HfCl_2$  is mixed with a small fraction CGC-Ti, PSP2\* increases significantly. The results are a starting point to develop new polymer from mixing catalysts in the reactor.

## 6.2. Recommendations

In chapter 3, it was mentioned that the noise of ethylene flow measured by the ethylene flowmeter was higher when the ethylene pressure in the reactor increases (Figure 3.7) Several actions were taken before and during polymerization, such as tuning temperature control, reducing cooling water temperature, etc., but the noise remained constant.

In addition, it was also noticed that the noise increases when the catalyst concentration varies at similar reaction conditions. For instance, Figure 6.1 shows the ethylene uptake curves at 0.79 MPa. Temperature and stir speed are the same for the three curves. The gray and blue curves display greater noise than green curve.

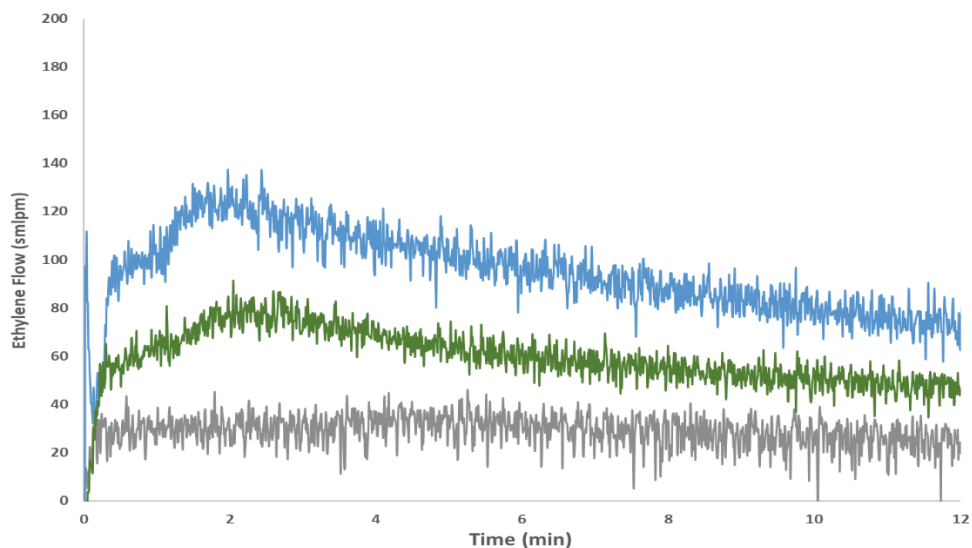


**Figure 6-1.** Ethylene uptake curves at different catalyst concentration.

Further analysis suggests that one probable cause for the generation of the noise is the current pressure control system for ethylene in the reactor. Figure 6-2 illustrates the current installation. Ethylene comes in from cylinders, so the first regulator (PCV-1) drops the ethylene pressure from 15.27 MPa to 3.55 MPa and the second regulator (PCV-2) further drops the ethylene pressure to the value used in the reaction. The pressure is monitored by a local manometer.

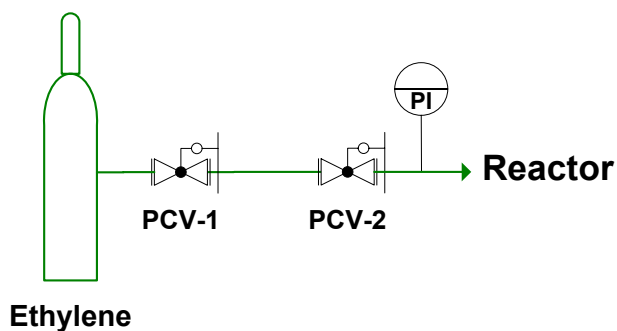


**Figure 6-2.** Current installation for ethylene pressure control.

In our case, PCV-2 is a Swagelok, model KPRCGJC411A20000. This regulator controls the pressure in a range of 0-1.82 MPa and has a flow characteristic (Cv) of 0.002. Figure 6-3 shows the flow data of regulator PCV-2 [58].

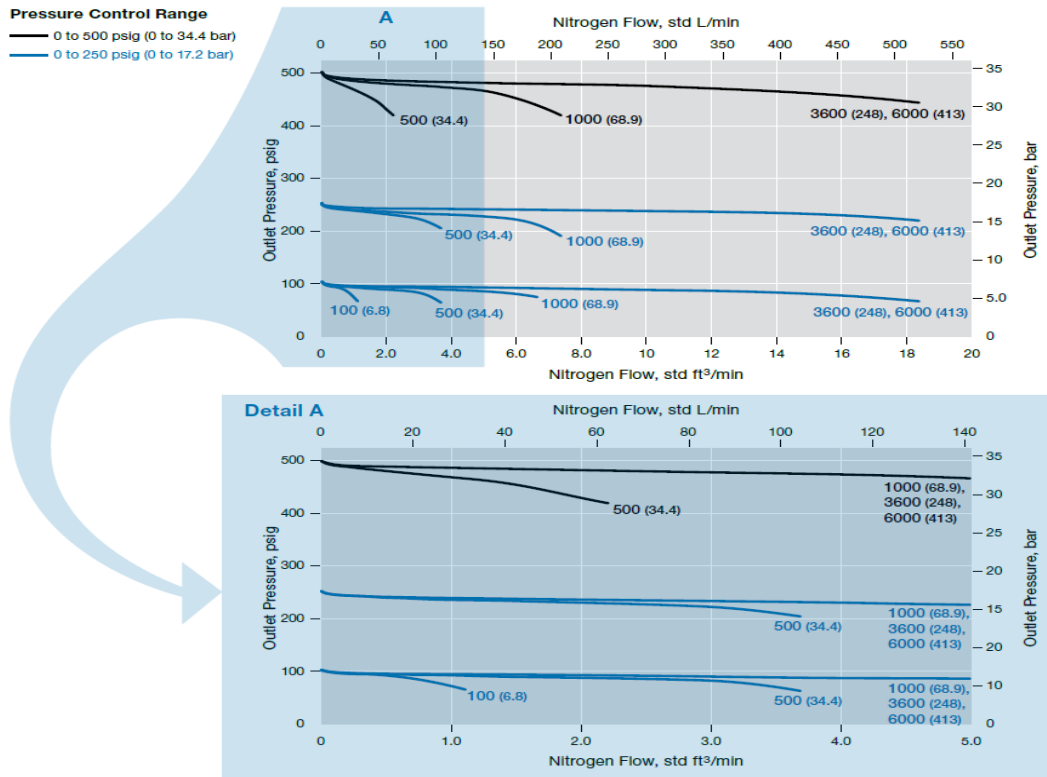


**Figure 6-3.** Flow data of regulator PCV-2 [58].

Our interest are the blue lines in Figure 6-3, which correspond to an operation range between 0 to 1.82 MPa. The first interesting thing to note is that the flow curve changes with the inlet pressure of regulator, the top figure shows curves with inlet pressures at 24.92, 7, 3.6 and 0.79 MPa. The y axis is the outlet pressure; this is the pressure set downstream of regulator. The recommendation by the supplier is to operate the regulator valves at the flat region in the curve. When it operates far right of a curve, it is called “Choked flow” and at this point the flow demand has exceeded the pressure-controlling capabilities of the regulator [58].

During the polymerization, the demand of ethylene flow is given by the reactions taking place inside the reactor, which depends on many factors such as catalyst concentration, reactor

temperature, ethylene pressure, etc. In addition, the ethylene flow usually decreases through time due to catalyst decay. However, as it can be seen in Figure 6-3, for the same inlet pressure, the regulator is capable to control the pressure set for the reaction at a specific range of flow, and when the outlet pressure is modified (or ethylene pressure for the reaction is modified), the flow range controlled by the regulator is also changed. It could be the case that when the ethylene pressure is controlled at 1.14 MPa, the regulator operates in the choked region, as a result, its capability to control the pressure is limited.

In addition, the cylinder pressure also decreases the ethylene pressure below 3.6 MPa due to the ethylene consumption for the polymerization, resulting in different controlled flow ranges by the regulator for similar outlet pressures (or reaction pressures),

Consequently, if the flow required by the reaction doesn't match with the flow range controlled by the regulator at the pressure set, higher ethylene flow is required. Therefore, the regulator is trying to overcompensate for the lack of pressure generated inside the reactor causing instabilities in the reactions and subsequently producing a large amount of noise during data retrieval as seen in Figure 6-2.

As a result, a more flexible reactor pressure control should be considered to reduce the noise in the ethylene flow. Figure 6-4 shows the proposal for a new installation. The proposal consists of an automated pressure control. The regulator would be replaced by a control valve and the local manometer by a pressure transmitter. The logic control will be set up and controlled by LabView. The benefits will be an accurate monitoring of reactor pressure and more flexibility for controlling the ethylene flow to the reactor at different pressures.

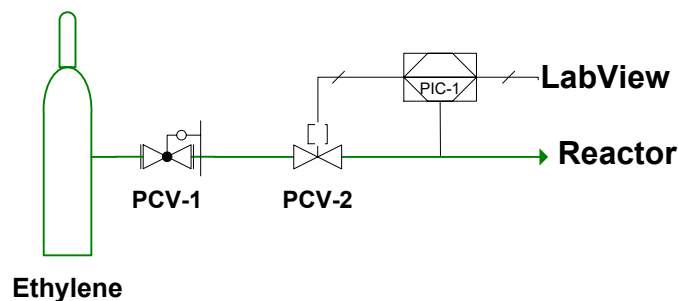


**Figure 6-4.** Proposal for new ethylene pressure control.

In chapter 3, Arrhenius constants were estimated at a reaction pressure of 0.79 MPa. However, to make more robust the results, Arrhenius constants should be estimated at another reaction pressures. Also, the decay constant has higher variability for ethylene/1-hexene copolymerization and correlates with the amount of 1-hexene added to the reactor. One hypothesis for the higher variability is the purity of 1-hexene, thus, it is recommended to investigate if others purification steps are required for 1-hexene.

In chapter 4 and chapter 5, interesting results were obtained by simulating virtual blends. However, these findings should be validated with real polymer blends. Therefore, for chapter 4, binary blends should be polymerized with broad comonomer distribution and then perform mechanical property tests and compare the correlation of PSP2\* and PSP2 with its mechanical properties. Simulation results suggest PSP2\* deviates from PSP2, so it should be verified what parameter offers better correlation.

In addition, in chapter 4 identified the different virtual binary blends that has similar PSP2\*. Following the criteria found in the simulation, polymerizing and blending polymers should be done to ensure that binary blends with same PSP2\* have similar mechanical properties. This will be a great contribution for the design of tailored polymer, because it would be possible to design polymers with better processability while keeping its mechanical properties.

Finally, in chapter 5, virtual blends using kinetic information from metallocene catalysts estimated in this thesis and previous work [43] were simulated at various reaction conditions. It is recommended to perform the reactions mixing the catalyst at several reactions conditions and characterize the final polymer and its mechanical properties to validate the findings obtained by simulations.

## References

- [1] Z. M. Research, "globenewswire," 24 May 2018. [Online]. Available: <https://globenewswire.com/news-release/2018/05/24/1511282/0/en/Global-Polyethylene-Market-Will-Reach-USD-215-Billion-by-2024-Zion-Market-Research.html>. [Accessed 31 July 2018].
- [2] S. Stevenson, "Slate," 19 June 2012. [Online]. Available: [http://www.slate.com/articles/business/operations/2012/06/poland\\_spring\\_s\\_new\\_bottles\\_why\\_are\\_they\\_so\\_thin\\_and\\_flimsy\\_.html](http://www.slate.com/articles/business/operations/2012/06/poland_spring_s_new_bottles_why_are_they_so_thin_and_flimsy_.html). [Accessed 31 July 2018].
- [3] P. J. Deslauriers and D. C. Rohlffing, "Estimating slow crack growth performance of polyethylene resins from primary structures such as molecular weight and short chain branching," *Macromolecular Symposia*, vol. 282, pp. 136-149, 2009.
- [4] P. Europe, "ISO.org," [Online]. Available: <https://committee.iso.org/files/live/sites/tc61/files/The%20Plastic%20Industry%20Berlin%20Aug%202016%20-%20Copy.pdf>. [Accessed 15 05 2018].
- [5] R. Patel, "Types and Basics of Polyethylene," in *Handbook of industrial polyethylene and technology*, Bervily, Scrivener Publishing, 2017, pp. 105-138.
- [6] J. Soares, T. McKenna and C. Cheng, "Coordination Polymerization," in *Polymer reaction engineering*, Malaysia, Blackwell Publishing Ltd, 2007, pp. 29-117.
- [7] A. Peacock, *Handbook of Polyethylene: Structure, Properties, and Applications*, New York: Marcel Dekker, 2000.
- [8] D. Malpass, "An overview of industrial polyethylene processes," in *Introduction to Industrial Polyethylene: Properties, Catalysts, Processes*, Scrivener Publishing, 2010, pp. 85-97.

- [9] Y. Kissin, "Catalyst for the manufacture of polyethylene," in *Handbook of industrial polyethylene and technology*, Beverly, Scrivener publishing, 2017, pp. 25-60.
- [10] D. Malpass, "Chapter 2 - Free Radical Polymerization of Ethylene," in *Introduction to Industrial Polyethylene: Properties, Catalysts, and Processes*, John Wiley & Sons., 2010.
- [11] R. Seymour and T. Cheng, *History of Polyolefins*, Dordrecht: Springer, 1986.
- [12] D. Malpass, "Chapter 5 - Chromium Catalysts," in *Introduction to Industrial Polyethylene: Properties, Catalysts, and Processes*, John Wiley & Sons, 2010.
- [13] D. Malpass, "Chapter 3 - Ziegler-Natta Catalysts," in *Introduction to Industrial Polyethylene: Properties, Catalysts, and Processes*, John Wiley & Sons, 2010.
- [14] J. Soares and A. Hamielec, "Metallocene/Aluminoxane catalysts for olefin polymerization. A review.," *Polymer Reaction Engineering*, vol. 3, no. 2, pp. 131 - 200, 1995.
- [15] W. Kaminsky, "Highly active metallocene catalysts for olefin polymerization," *Journal of the Chemical Society*, pp. 1413-1418, 1998.
- [16] S. Mehdiabadi and J. Soares, "Ethylene Homopolymerization Kinetics with a Constrained Geometry Catalyst in a Solution Reactor," *Macromolecules*, no. 45, p. 1777–1791, 2012.
- [17] A. Razavi, L. Peters and L. Nafpliotis, "Geometric flexibility, ligand and transition metal electronic effects on stereoselective polymerization of propylene in homogeneous catalysis," *Macromolecular catalyst A: Chemical*, no. 115, pp. 129-154, 1997.
- [18] C. Dobbin, "An Industrial Chronology of Polyethylene," in *Handbook of Industrial polyethylene and technology*, Beverly, John Wiley & Sons, Inc., 2017, pp. 3-24.

- [19] J. Soares and T. McKenna, "Polymerization Catalyst and Mechanism," in *Polyolefin reaction engineering*, Boschstr., Wiley, 2012, pp. 53 - 86.
- [20] E. Zurek and T. Ziegler, "Theoretical studies of the structure and function of MAO (methylaluminoxane)," *Progress in Polymer Science*, vol. 29, no. 2, pp. 107-148, 2004.
- [21] D. Malpass, "Chapter 6 - Single Site Catalysts," in *Introduction to Industrial Polyethylene: Properties, Catalysts, and Processes*, John Wiley & Sons, 2010.
- [22] L. D'Agnillo, J. Soares and A. Penlidis, "Controlling molecular weight distributions of polyethylene by combining soluble metallocene/MAO catalysts," *Journal of Polymer Science: Part A: Polymer Chemistry*, vol. 36, pp. 831-840, 1998.
- [23] F. P. Alt, L. Böhm, H. Enderle and J. Berthold, "Bimodal polyethylene – Interplay of catalyst and process," *Macromolecular*, no. 163, pp. 135-143, 2001.
- [24] S. Mehdiabadi, *Synthesis, Characterization and Polymerization Kinetic Study of Long Chain Branched Polyolefins Made with Two Single-Site Catalysts*, Waterloo, 2011.
- [25] S. Mehdiabadi, J. Soares, D. Bilbao and J. Brinen, "A Polymerization Kinetics Comparison between a Metallocene Catalyst Activated by Tetrakis(pentafluorophenyl) Borate and MAO for the Polymerization of Ethylene in a Semi-batch Solution Reactor," *Macromolecular*, no. 5, pp. 418 - 430, 2011.
- [26] J. Soares and T. McKenna, "Polymerization Kinetics," in *Polyolefin Reaction Engineering*, Boschstr., Wiley, 2012, pp. 131-186.
- [27] P. Flory, *Principles of polymer chemistry*, Ithaca: Cornell University Press, 1953.
- [28] A. Hameliec and J. Soares, "Polymerization reaction engineering — Metallocene catalysts," *Progress in Polymer Science*, vol. 21, no. 4, pp. 651 - 706, 1996.

- [29] P. Mueller, J. Richards and J. Congalidis, "Polymerization Reactor Modeling in Industry," *Macromolecular*, no. 5, pp. 261-277, 2011.
- [30] J. Soares and A. Hameliec, "Analyzing TREF data by Stockmayer's bivariate distribution," *Macromolecular*, no. 4, pp. 305-324, 1995.
- [31] J. Soares and T. Mckenna, "Polyolefin Microstructural Modeling," in *Polyolefin Reaction Engineering*, Boschstr., Wiley, 2012, pp. 187-270.
- [32] P. Painter and M. Coleman, *Essentials of Polymer Science and Engineering*, Lancaster: Destech Publication, Inc, 2009.
- [33] A. Argon, "Structure of solid polymers," in *The Physics of Deformation and Fracture of Polymers*, Cambridge, Cambridge University Press, 2013, pp. 40-76.
- [34] E. Fischer, "Studies of structure and dynamics of solid polymers by elastic and inelastic neutron scattering", *Pure and Applied Chemistry*, vol. 50, pp. 1319-1341, 1978.
- [35] R. Seguela, "Critical Review of the Molecular Topology of Semicrystalline Polymers: The Origin and Assessment of Intercrystalline Tie Molecules and Chain Entanglements," *Journal of polymer science, part B: Polymer physics*, vol. 43, pp. 1729-1748, 2005.
- [36] G. Meiner and A. Peterlin, "Plastic deformation of polyethylene - III Mechanical properties and morphology of drawn low density polyethylene," *European polymer journal*, vol. 7, pp. 657 - 670, 1971.
- [37] P. Smith, P. J. Lemstra and A. P. L. PIJPERS, "Tensile Strength of Highly Oriented Polyethylene. II. Effect of Molecular Weight Distribution," *Journal of Polymer Science: Polymer Physics Edition*, vol. Vol. 20, pp. 2229-2241, 1982.

- [38] P. Vincent, "A correlation between critical tensile strength and polymer cross-sectional area," *POLYMER*, vol. 13, no. December, pp. 558 - 560, 1972.
- [39] G. Capaccio and I. M. Ward, "Effect of molecular weight on the morphology and drawing behaviour of melt crystallized linear polyethylene," *POLYMER*, vol. 16, no. April, pp. 239 - 243, 1975.
- [40] Y.-L. Huang and N. Brown, "Dependence of Slow Crack Growth in Polyethylene on Butyl Branch Density: Morphology and Theory," *Journal of Polymer Science: Part B: Polymer Physics*, vol. 29, pp. 129-137, 1991.
- [41] J. Soares and T. Mckenna, "Polyolefin Microstructural Characterization," in *Polyolefin Reaction Engineering*, Boschstr., Wiley, 2012, pp. 15-52.
- [42] M. Chanda, "Chain Copolymerization," in *Introduction to Polymer Science and Chemistry*, Boca Raton, Taylor & Francis Group, 2013, pp. 383-428.
- [43] S. Saadat, *Polymerization Kinetics of Ethylene/1-Hexene Copolymers Made with Two Metallocene Catalysts*, Edmonton: University of Alberta, 2018.
- [44] E. Adisson, M. Ribeiro, A. Deffieux and M. Fontanille, "Evaluation of the heterogeneity in linear low-density polyethylene comonomer unit distribution by differential scanning calorimetry characterization of thermally treated samples," *Polymer*, vol. 33, no. 20, pp. 4337-4342, 1992.
- [45] G. Hohne, W. Hemminger and H.-J. Flammersheim, *Differential Scanning Calorimetry and introduction for practitioners*, Berlin: Springer-Verlag, 1996.
- [46] S. Mehdiabadi and J. Soares, "In-Depth Investigation of Ethylene Solution Polymerization Kinetics With  $\text{rac-Et(Ind)}_2\text{ZrCl}_2/\text{MAO}$ ," *Macromolecular*, pp. 246-262, 2013.

- [47] S. Mehdiabadi and J. Soares, "Quantifying the Copolymerization Kinetics of Ethylene and 1-Octene Catalyzed with  $\text{rac-Et(Ind)}_2\text{ZrCl}_2$  in a Solution Reactor," *Macromolecules*, vol. 49, p. 2448–2457, 2016.
- [48] G. Seber and C. Wild, *Nonlinear regression*, Hoboken: Wiley-Interscience, 2003.
- [49] A. Barton, *Handbook of solubility parameters and other cohesion parameters*, Second ed., Boca Raton, Fl: CRC Press, Inc, 1991.
- [50] M. Rubenstein and R. Colby, "Thermodynamic of Mixing," in *Polymer Physics*, New York, Oxford University Press Inc, 2003, pp. 137 - 170.
- [51] R. M. Patel, K. Sehanobish, P. Jain, S. P. CHUM and G. W. Knight, "Theoretical prediction of Tie-Chain concentration and its characterization using postyield response".
- [52] P. J. Deslauriers and D. C. Rohlfing, "System and method for estimating density of a polymer". USA Patent US 2011 0035193A1, 7 August 2009.
- [53] F. M. MIRABELLA and A. BAFNA, "Determination of the Crystallinity of Polyethylene/Olefin Copolymers by Thermal Analysis: Relationship of the Heat of Fusion of 100%Polyethylene Crystal and the Density," *Journal of Polymer Science: Part B: Polymer Physics*, vol. 40, p. 1637–1643, 2002.
- [54] P. C. Hiemenz and T. P. Lodge, *Polymer Chemistry*, Boca Raton: Taylor & Francis Group, 2007.
- [55] A. Ortin, B. Monrabal and J. Sancho-Tello, "Development of an Automated Cross-Fractionation Apparatus (TREF-GPC) for a Full Characterization of the Bivariate Distribution of Polyolefins," *Macromolecular symposia*, vol. 257, p. 13–28, 2007.

- [56] A. Rudin and P. Choi, "Mechanical Properties," in *The Elements of Polymer Science & Engineering*, Waltham, Academic Press, 2013, pp. 149-229.
- [57] J. B. Soares and T. F. Mcknenna, "Polyolefin Reaction Engineering," in *Instantaneous Distribution*, Boschstr., Wiley, 2012, pp. 188-251.
- [58] Swagelok, "Pressure Regulator Flow Curves Technical Bulletin," AGS, USA, 2017.